

TECHNISCHE UNIVERSITÄT MÜNCHEN

Lehrstuhl für Experimentelle Genetik

Implementation and optimization of a large-scale ENU mouse mutagenesis screen and
characterisation of five ENU-induced limb mutant lines

Dian Agustina Michel

Vollständiger Abdruck der von der Fakultät Wissenschaftszentrum Weihenstephan für Ernährung,
Landnutzung und Umwelt der Technischen Universität München zur Erlangung des akademischen
Grades eines

Doktors der Naturwissenschaften

genehmigten Dissertation

Vorsitzender:

Univ.-Prof. Dr. A. Gierl

Prüfer der Dissertation:

1. Univ.-Prof. Dr. M. Hrabé de Angelis

2. Univ.-Prof. Dr. E. Wolf

(Ludwig-Maximilians-Universität München)

Die Dissertation wurde am 25. Mai 2009 bei der Technischen Universität München eingereicht und
durch die Fakultät Wissenschaftszentrum Weihenstephan für Ernährung, Landnutzung und Umwelt
am 30. Juli 2009 angenommen.

Danksagung

Mein besonderer Dank geht an Prof. Dr. Martin Hrabé de Angelis, dem Betreuer dieser Arbeit, der mir die Möglichkeit gegeben hat, in einem so einzigartigen, spannenden wie auch herausfordernden Großprojekt wie dem ENU Maus-Mutageneseprojekt teilzunehmen. Ohne seine uneingeschränkte Unterstützung hätte ich meine Arbeit nicht in dieser Weise durchführen können.

Bedanken möchte ich mich auch bei Prof. Dr. Rudi Balling, der sein Vertrauen in mich setzte und an die GSF Neuherberg/ Institut für Säugetiergenetik geholt hat, was für mich der Einstieg in das spannende Gebiet der Mausgenetik und der ENU Mutagenese war.

Ich danke meinen Kollegen am Institut für Experimentelle Genetik für die gute Zusammenarbeit, insbesondere Véronique Blanquet, Sybille Wagner und Isabel Rubio Aliaga für ihre Hilfe, Geduld, die wissenschaftlichen Gespräche wie auch ihre moralische Unterstützung gerade während turbulenter Phasen des Projektes. Dank gilt auch den „Streifenhörnchen“ aus dem B-Streifen, ohne die dieses Großprojekt sicherlich nicht so erfolgreich geworden wäre.

Nicht zuletzt geht mein Dank auch an Geert, meinem Mann, der mich gerade zum Ende der Arbeit hin mit viel Verständnis, klug-sanftem Druck, Humor und kulinarischen Erlebnissen großartig unterstützt hat.

1	SUMMARY	4
2	INTRODUCTION	5
2.1	AIM OF PHD WORK	5
2.2	FORWARD AND REVERSE GENETICS IN FUNCTIONAL GENE STUDIES	6
2.3	SPONTANEOUS AND IRRADIATION MUTANTS	7
2.4	CHEMICAL MUTAGENESIS	8
2.4.1	<i>Chemical mutagenesis experiments in model organisms</i>	8
2.4.2	<i>Previous mutagenesis experiments in the mouse</i>	8
2.4.3	<i>ENU is the most powerful mutagen in mouse male germ cells</i>	9
2.4.4	<i>The biochemical action of ENU</i>	9
2.4.5	<i>Mutation frequency of ENU</i>	10
2.4.6	<i>Pathogenic mutations</i>	10
2.5	PHENOTYPING PROTOCOLS	11
2.5.1	<i>Specific locus test</i>	11
2.5.2	<i>Multiple end point approach</i>	11
2.5.3	<i>SHIRPA protocol</i>	13
2.6	STRUCTURE OF THE MUNICH ENU MOUSE MUTAGENESIS PROJECT	14
2.7	CURRENT ENU MUTAGENESIS SCREENS	14
2.8	INHERITED LIMB PATTERNING DEFECTS IN HUMANS AND THEIR MOLECULAR MECHANISMS	16
2.8.4	<i>Fibroblast growth factor (Fgf) pathway and PD patterning</i>	17
2.8.5	<i>Sonic hedgehog pathway and AP patterning</i>	18
2.8.6	<i>Wnt pathway and DV patterning</i>	19
2.8.7	<i>T-box genes and limb identity</i>	19
2.8.8	<i>Hox genes and determinants along the PD axis</i>	20
3	MATERIALS AND METHODS	23
3.1	ANIMALS	23
3.1.1	<i>Husbandry</i>	23
3.1.2	<i>Strains</i>	23
3.1.3	<i>Preparation of animals</i>	23
3.2	ENU ADMINISTRATION	24
3.2.4	<i>Preparation of ENU</i>	24
3.2.5	<i>Quality control</i>	24
3.2.6	<i>ENU injection</i>	24
3.2.7	<i>Precautions for ENU handling and quality control</i>	24
3.2.8	<i>Implementation of an injection schedule</i>	24
3.3	IMPLEMENTATION OF BREEDING SCHEMES	27
3.3.1	<i>Sterility testing</i>	27
3.3.2	<i>F1 breeding for the dominant screen</i>	27
3.3.3	<i>Dominant confirmation cross and maintenance breeding</i>	27
3.3.4	<i>G3 breeding for the recessive screen</i>	28
3.3.5	<i>Recessive confirmation crosses and maintenance breeding</i>	28
3.3.6	<i>SLT test</i>	31
3.4	WORKFLOW MANAGEMENT	31
3.4.1	<i>Breeding management</i>	31
3.5	PRIMARY SCREENING AND PHENOTYPING	34
3.5.1	<i>Phenotyping workflow</i>	34
3.5.2	<i>Screens</i>	35
3.5.2.1	<i>Biochemical Metabolites</i>	35
3.5.2.2	<i>Dysmorphology</i>	36
3.5.2.3	<i>Sex Reversal</i>	36
3.5.2.4	<i>Behaviour</i>	37
3.5.2.5	<i>Clinical Chemistry</i>	37
3.5.2.6	<i>Hemostasis</i>	38
3.5.2.7	<i>Immunology/ Allergy</i>	38
3.5.2.8	<i>Lysosomal Enzymes</i>	40
3.5.2.9	<i>Mitochondrial screen</i>	40
3.5.3	<i>Recording system</i>	40
3.5.4	<i>Interaction Core Facility/ Screeners</i>	41
3.6	MAPPING OF THE ENU INDUCED MUTATION	42
3.6.1	<i>Strategies for genetic mapping of dominant and recessive mutations</i>	42
3.6.2	<i>DNA isolation from mouse tissue</i>	43

3.6.3	<i>Linkage analysis – Candidate gene approach</i>	43
3.6.4	<i>Sequencing</i>	46
3.6.5	<i>Sequence analysis software</i>	47
3.7	PHENOTYPIC CHARACTERIZATION.....	47
3.7.1	<i>X-ray analysis</i>	47
3.7.2	<i>Skeletal preparation</i>	47
3.7.3	<i>Sperm analysis</i>	48
3.7.4	<i>Histology</i>	48
3.7.5	<i>Immunohistochemistry</i>	48
3.8	EXPRESSION ANALYSIS	49
3.8.1	<i>Genotyping ALI037</i>	49
3.8.1.1	Generation of mouse embryos.....	49
3.8.1.2	DNA extraction from mouse embryonic yolk-sacs	50
3.8.1.3	RNA extraction.....	50
3.8.1.4	cDNA synthesis	50
3.8.2	<i>Working with bacteria</i>	50
3.8.2.1	Media for bacterial culture.....	50
3.8.2.2	Bacterial stocks and their maintenance.....	50
3.8.2.3	Generation of chemically competent E.coli cells.....	51
3.8.2.4	Transformation of competent E. coli cells.....	51
3.8.2.5	Cloning of PCR products.....	52
3.8.2.6	Plasmid maxi preparation.....	52
3.8.3	<i>Whole mount in situ hybridisation</i>	52
3.8.3.1	Labelling the riboprobe.....	52
3.8.3.2	Hybridization	53
3.8.3.3	Removal of unbound probe and antibody.....	53
3.8.3.4	Staining	54
3.8.3.5	Solutions.....	54
3.9	DATABASES	55
3.9.1	<i>MouseNet</i>	55
3.9.2	<i>Map viewer</i>	56
3.9.3	<i>ClustalW for homology studies. Domain studies</i>	56
3.9.4	<i>PhosphoSite</i>	56
3.10	CHEMICALS AND REAGENTS.....	56
4	RESULTS – PART I DEVELOPMENT, IMPLEMENTATION AND OPTIMIZATION OF A LARGE-SCALE ENU MUTAGENESIS SCREEN	59
4.1	SCREENING OUTCOME.....	59
4.1.1	<i>Data sets used</i>	59
4.1.2	<i>Screening numbers and mutant recovery rates (MRR)</i>	60
4.2	COMPARISON: DOMINANT VERSUS RECESSIVE SCREEN.....	61
4.2.3	<i>Evaluation of the individual screens</i>	63
4.2.4	<i>Evaluation of individual phenotype categories</i>	63
4.2.5	<i>Evaluation of ENU regimes</i>	66
5	RESULTS - PART II CHARACTERIZATION OF ALI MUTANTS (ALI3, ALI9, ALI12, ALI19 AND ALI037).....	68
5.1	CHARACTERIZATION OF ALI3/9/12/19	68
5.1.1	<i>Phenotype description of ALI3/9/12/19</i>	68
5.1.2	<i>Molecular characterization of the ALI3/9/12/19 mutation</i>	71
5.2	CHARACTERIZATION OF ALI037	74
5.2.1	<i>Phenotype description of ALI037</i>	74
5.2.1.1	Limb and other skeletal phenotypes of ALI037	74
5.2.1.2	Fertility phenotype of male ALI037 mutants.....	77
5.2.2	<i>Molecular characterization of the ALI037 mutation</i>	80
5.2.3	<i>Functional analysis of the Zfp145^{ALI037/ALI037} mutation</i>	83
5.2.3.1	Zfp145 expression in E 11.5 mouse embryos.....	83
5.2.3.2	Influence of ALI037 mutation on the expression pattern in E 11.5 mouse embryos and limbs	84
5.2.3.3	Immunohistochemistry of testes.....	87
6	DISCUSSION.....	89
6.1	IMPLEMENTATION OF A LARGE-SCALE GENOME-WIDE GENETIC SCREEN IN THE MOUSE.....	89
6.1.1	<i>Improvement of ENU treatment QC</i>	89
6.1.2	<i>Optimization of breeding schemes</i>	90
6.1.3	<i>Workflow management</i>	91

6.1.4	<i>The mutation recovery rate is actually higher</i>	93
6.2	DOMINANT VERSUS RECESSIVE SCREEN	94
6.2.1	<i>Considerations about mutant recovery rates and external limiting factors</i>	94
6.2.2	<i>Dominant and recessive strategy across the screens</i>	95
6.2.3	<i>Some phenotype categories show a higher prevalence in dominant or recessive strategy</i>	96
6.2.4	<i>Impact of the ENU regime on the strategy</i>	100
6.3	CHARACTERIZATION OF ABNORMAL LIMB MUTANTS	101
6.3.1	<i>ALI3/ ALI9/ ALI12/ ALI19 mutations affect the Sonic hedgehog pathway</i>	101
6.3.2	<i>ALI3/ ALI9/ ALI12/ ALI19 as new animal models for Greig syndrome and Pallister-Hall syndrome</i>	102
6.3.3	<i>The effect on downstream targets of ALI3/ ALI9/ ALI12/ ALI19 mutations</i>	105
6.3.4	<i>ALI037 mutation revealed a putative new regulatory domain of Plzf</i>	105
6.3.5	<i>ALI037 is a hypomorphic allele with a null effect</i>	107
6.4	MORE MOUSE MODELS FOR INHERITED DISEASES IN HUMAN	109
6.5	OUTLOOK AND PERSPECTIVES	110
7	REFERENCES	111
8	APPENDIX PUBLISHED LITERATURE	122
	CURRICULUM VITAE	123

1 Summary

Aim of the project and this PhD work was the implementation, development and optimization of a systematic large-scale ENU mutagenesis using the mouse as an animal model for inherited human disease by elucidating the phenotype-genotype correlation and to obtain a deeper insight into the function of genes and their role in the patho-mechanism of diseases. The first part of this work demonstrated that the core facility of a comprehensive systematic and large-scale ENU mouse mutagenesis screen was successfully implemented and optimized with regard to (a) the reliability and quality of ENU administration, (b) the efficiency and effectiveness of breeding schemes, and (c) the management of coordinated workflow processes. These efforts resulted in the efficient and effective systematic generation of mutant mouse models that comprise a broad spectrum of genetic diseases. More than 400 isolated mutant lines serve as a starting point for the elucidation gene function studies and for the dissection of human inherited diseases on the molecular level as well as new entry points for novel therapeutic strategies.

The results and comparison of dominant versus recessive strategy revealed, beside the quality and efficiency of the participating groups in the screen, considerable indications for the setup of future mouse genetic screens regarding the prevalence of certain phenotypes and the effectiveness of parameters used. In order to choose the appropriate strategy and estimate the scale of future genetic screens, the screen-specific mutant recovery rate (i.e. clinical chemistry, dysmorphology) and the mutant recovery rate of more specific and functional parameter groups (i.e. blood count, renal parameters, body size etc.) have to be considered (as discussed in section 5.2.3). In the end of the first part, the work compared the two different ENU regimes used (3x80mg/kg, 3x90mg/kg b.w.) and came to the result that there is no significant difference with regard to the mutant recovery rate. However, the more conservative regime of 3x80mg/kg body weight is preferable due to the higher stability of parameters such as viability and sterility period of ENU treated males, which are essential for the reliable management of an ENU breeding colony.

The characterization of five mutant lines, in the second part of this thesis, underlined proof-of-principle for the chosen forward genetics approach using ENU mutagenesis in the mouse. In addition to the generation of novel alleles by ENU mutagenesis, it was demonstrated by the analyses of five mutant phenotypes that were displaying dysmorphological abnormalities in the limbs, named as ALI3, ALI9, ALI12, ALI19, and ALI037, that also known genes can be affected and even several time. The investigations included the determination of the chromosomal localisation by classical linkage analysis and the application of the candidate gene approach. Candidate gene approach represents a strategy in positional cloning comprising of cross checking for known alleles and phenotypes in the chromosomal region of interest, after which potential candidate genes are confirmed by DNA sequencing of coding, non coding or regulatory regions. Consequences of the molecular alterations are elucidated by phenotype analysis of skeletal elements (x-ray, skeletal preparation) in different developmental stages, and the investigation of the molecular alteration on other interaction partners of the same signalling pathways by *in situ* hybridisation and immune

histochemistry. In the case of ALI037, the induced mutation was moreover analysed by phylogenetic comparison and by modelling of the induced alteration *in silico*. The mutant lines ALI3, ALI9, ALI12, and ALI19 represented in fact an allelic series of *Gli3*, a transcription factor and member of the Sonic hedgehog-signalling pathway, which plays an essential role in limb development, determination of digit identity, and pathogenesis of human polydactyly. The mutated gene in ALI037 was identified as *Plzf*, another zinc finger protein, which plays a central role in early spermatogenesis in male mice and in limb development by regulative interaction of *Hoxd11*. *Hoxd11* a member of the 5' Hox gene family of homeobox genes that regulate the architecture of the body plan and determine the proximal-distal axis. The interesting aspect and novelty of this allele is the localisation of its mutation at the C-terminus, downstream beyond the DNA-binding zinc finger domain, which gives a hint for a putative novel regulatory domain for *Plzf* and, thus, a presumably new molecular basis for human polydactyly and infertility in men.

2 Introduction

2.1 Aim of PhD work

Aim of the project and this PhD work was the implementation, development and optimization of a systematic large-scale ENU mutagenesis using the mouse as an animal model for inherited human disease by elucidating the phenotype-genotype correlation and to obtain a deeper insight into the function of genes and their role in the patho- mechanism of diseases. To date, approximately 1700 genes, or 8% out of the estimated 21.000 protein-coded transcription units are described as monogenic inherited human diseases. Of these, only about 10% consist of single nucleotide polymorphisms with suggestive phenotypic consequences (Brinkman et al., 2006). Hence, the molecular basis for the majority of genetic diseases is still unknown; a phenomenon also described as the “phenotype gap” (Brown and Peters, 1996).

Two main strategies in functional gene studies, generally known as “reverse” and “forward” genetics, are used to close this gap. Whereas reverse genetics starts from a defined gene, which is modified or depleted using transgenic or gene trap technology, to study the consequences in the phenotype. In contrast, forward genetics starts from a mutant phenotype, which either occurred spontaneously or was physically or chemically induced, to study the molecular basis of the phenotypic alteration. The use of chemical mutagenesis in other organisms such as *Drosophila melanogaster*, *Caenorhabditis elegans*, and *Danio rerio* already demonstrated the strength and impact of forward genetics strategies, which profoundly improved the understanding of molecular principles of signalling pathways in developmental biology or physiology. Since the alkylating agent ethylnitrosourea (ENU) is known to induce mainly point mutations in proliferating pre-meiotic germ cell stages, it is therefore predestined for an unbiased generation of large numbers of mutant animal models ranging from loss of function as hypomorphs, or null alleles to hypermorphs with gain of function alleles.

This study applied the phenotype-driven strategy of ENU mutagenesis in the mouse, which has a high similarity in its genome, biochemical pathways and patho-mechanism compared to the human

system. The new aspect of this study was the focus on the systematic generation of mouse models for monogenic inherited human diseases using ENU as a large scale and genome-wide approach. Due to the principle of an explorative and non hypothesized-driven approach, the first challenging aspect was the adaptation of a comprehensive clinical examination and diagnostics for human for the mouse with phenotyping procedures appropriate for a large-scale application to cover the, as possible, broadest spectrum of disease phenotypes. Mutant phenotypes were assessed for specific monogenic traits and postnatal abnormalities comprising congenital malformations, clinical chemical, biochemical, haematological, immunological defects, and complex traits such as allergy and behaviour, which data was evaluated and analysed by the cooperation partners of the scientific consortium. The second challenge - and the first main part of this PhD work - was the organisation and optimization of a large-scale mutagenesis project in the core facility with regard to the efficiency of mutant production, the number of research groups involved and the number of animals that were systematically assessed for mutant phenotypes. In order to address dominant and recessive mutations, both breeding schemes had been realised, which also raised the aspect of a comparison between the dominant and recessive screen regarding mutant recovery and occurrence of specific mutant phenotypes. The outcome of the statistical analysis might have further implications for the optimization of future mouse genetic screens with regard to strategy and assessing parameters.

The second part of this thesis demonstrated proof-of-principle by the molecular analyses and phenotypic characterization of selected mouse mutant phenotypes in order to uncover (a) the molecular alteration of the gene and subsequently (b) its function in the context of the disease. In addition to the generation of novel phenotypes and alleles by ENU mutagenesis, it was shown by the analyses of five mutant phenotypes that were displaying dysmorphological abnormalities in the limbs, named as ALI3, ALI9, ALI12, ALI19, and ALI037. The investigations included the determination of the chromosomal localisation by classical linkage analysis and the application of the candidate gene approach. Candidate gene approach represents a strategy in positional cloning comprising of cross checking for known alleles and phenotypes in the chromosomal region of interest, after which potential candidate genes are confirmed by DNA sequencing of coding, non coding or regulatory regions. Consequences of the molecular alterations are elucidated by phenotypic analysis of skeletal elements (x-ray, skeletal preparation) in different developmental stages, and the investigation of the molecular alteration on other interaction partners of the same signalling pathways by *in situ* hybridisation and immune histochemistry. In the case of ALI037, the induced mutations was moreover analysed by phylogenetic comparison and by modelling of the induced alteration *in silico*.

2.2 Forward and reverse genetics in functional gene studies

Even though the sequences of the human and mouse genomes are available since a number of years and were approved several times, only about 10% of the 21.000 genes of the entire mouse genome have been functionally characterised yet (Venter et al., 2001). Two different and complementary

approaches are predominantly used to tackle this challenge, which are commonly known as forward and reverse genetics. During the last thirty years of progress in biomedical sciences, the analysis of gene function was mainly focused on transgenic techniques and the use of mouse embryonic stem cells, which was introduced in the 1980s (Thomas and Capecchi, 1987) and that made it possible to manipulate the mouse genome by homologous recombination and to design mouse mutants for every gene of interest. This strategy was extended by the gene trap technology through the construction of genome-wide libraries of embryonic stem cells in which every gene in the mouse is inactivated and can be recovered through the generation of chimeras (Zambrowicz et al., 1998). The main prerequisite for this approach is knowledge of the gene before the mutant phenotype is generated and characterised. For this reason, this approach is also known as the gene-driven approach or reverse genetics. The reverse strategy is the classical phenotype-driven approach, also called forward genetics, and aims at the isolation of a mutant phenotype of interest in the first step without knowing the molecular basis of the mutation. In this approach, the mutant phenotypes are generated by random mutagenesis either using irradiation or chemicals; the animals are then systematically screened for a phenotype of interest; if a mutant phenotype occurs, the inheritance of the phenotype and the nature of the trait have to be confirmed in a testcross. The second step is the identification and molecular characterisation of the causative mutation for the mutant phenotype using standard genetic and molecular tools for positional or candidate cloning, which was the rate-limiting step so far. The increasing number of micro-satellite markers, the development of high-throughput polymerase chain reaction (PCR) and automated mutation detection systems in the last couple of years have made the phenotype-driven strategy more and more interesting for the dissection of complex traits that underlie the pathogenesis of human diseases.

2.3 Spontaneous and irradiation mutants

The lack of information about mutant phenotypes, their causative genes and their function had been the driving force for extensive efforts of mouse geneticists since decades, which originally started in the beginning of the 20th century with the search for spontaneous mutations in mouse colonies of the mouse fanciers. In 1905, Cuénot had reported that the mouse mutant Agouti yellow is a Mendelian trait (Cuénot, 1905; Silver, 1995). To date, a collection of approximately 1200 spontaneous mutations in the mouse are available, which are maintained and disseminated by the Jackson Laboratory. Due to the low rate of spontaneous mutations of 1×10^{-6} , the number of relevant mutant mouse lines was restricted; for this reason different compounds such as x-radiation and a battery of chemicals were systematically tested for their efficacy to induce mutations at a higher frequency. Muller and colleagues showed in 1927 that the exposure of mouse germ cells to ionizing radiation (x-radiation) induced heritable mutations in the offspring. It has been shown under different protocols of exposure, that x-irradiation induces mutations in mouse spermatogonia at a rate of 0.5 to 13.3×10^{-5} per locus, which is one magnitude higher than the spontaneous mutation frequency (Favor, 1999; Silver, 1995). This was the basis for systematic research on the effects of radiation on mutation frequencies at the

research centres in Oak Ridge, Tennessee, USA, and Harwell, England by systematically producing new mouse mutants with radiation (Davis and Justice, 1998; Lyon and Renshaw, 1986; Russell et al., 1988). It was shown that x-radiation induces mainly large deletions or other lesions such as translocations or complex rearrangements within the genome. Beside the production of a large number of new mouse mutants the researchers generated a first valuable region-specific chromosome map of the mouse. In addition to ionizing radiation, a large number of natural and synthetic chemicals were assessed for their ability to induce mutations in germ cells of different model organisms. The frequencies and types of mutations induced by chemical mutagens have been analysed by conducting the specific locus test (SLT) that was developed by W. L. Russel and published in 1951. In 1956, Oakberg determined the duration of the different stages of spermatogenesis in the mouse, which formed the basis for breeding schemes in mutagenicity tests. Chemical mutagens were then characterized by their differential spermatogenic response (Ehling et al. 1972) and are described in the next section in more detail.

2.4 Chemical mutagenesis

2.4.1 Chemical mutagenesis experiments in model organisms

Genome-wide chemical mutagenesis experiments were successfully conducted in other species, i.e. in *Drosophila melanogaster* (Nusslein-Volhard and Wieschaus, 1980; Wieschaus et al., 1984) in *Ceanorhabditis elegans* (Brenner, 1974), and in *Danio rerio* (Haffter et al., 1996; Weinstein et al., 1996). Fundamental biochemical pathways processes were found that were similar to vertebrates such as pattern formation (anteroposterior and dorsoventral axis, patterning of the nervous system), organogenesis and other processes in developmental pathways. Signalling pathways such as for Ras and Notch are found to be homolog in yeast, flies, worm, and humans. Nonetheless, the mouse has become the prominent animal model due to its genetic and physiological properties. Beside the high degree of homology between the mouse and human genomes to an extent of approximately 98 %, both genomes are organised and structured in syntenic regions. Humans carry about 22-25000 genes and have a direct mouse counterpart that can be physically matched to mouse chromosomal regions. Moreover, due to its similarity in biochemical pathways and its physiology to humans, the mouse has obtained an important role in the elucidation of molecular pathways underlying general biological processes and especially the pathogenesis of human diseases.

2.4.2 Previous mutagenesis experiments in the mouse

In the 1980s, Bode and Justice carried out the first saturation mutagenesis of a specific chromosomal region in the mouse, which was defined by induced deletions of the albino locus and the t-complex (Justice and Bode, 1988a; Justice and Bode, 1988b), and created a valuable genetic map of 6- to 11-cM segment of mouse chromosome 7. The same strategy was later carried out for a 1 to 2cM segment of mouse chromosome 7 surrounding the pink-eyed-dilution locus (Rinchik et al., 2002). A few screens for specific dominant mutations (cataracts, blood enzymes) were launched (Ehling, 1986;

Ehling et al., 1985; Ehling et al., 1982; Pretsch and Charles, 1984), after having recognized the advantage of ENU-induced mutations for studying gene function also in mammals. In some cases, a number of allelic series of a single locus were isolated and used to study the fine structure of protein function (Graw et al., 2002b; Klopp et al., 1998). Nevertheless, it became obvious that huge efforts were needed to obtain a saturation of the genome in which at least a mutant for each single gene, and even more for each informative allele is generated. In 1996, two large-scale and genome-wide ENU mouse mutagenesis projects were launched at the MRC Harwell, England (Nolan et al., 2000b) and this Munich ENU mouse mutagenesis project (Hrabe de Angelis et al., 2000) in the framework of the German Human Genome Project (DHGP) for a systematic production of mouse models for human inherited diseases aiming at the elucidation of gene function and molecular pathways underlying the pathogenesis of diseases in humans.

2.4.3 ENU is the most powerful mutagen in mouse male germ cells

In 1979, Russel and colleagues demonstrated and postulated ENU to be the most potent mutagen in mouse spermatogonial stem cells (Russell et al., 1979); ENU is a synthetic alkylating compound initially generated in order to study mutagenicity mechanisms. A number of studies showed that post-spermatogonial stem cells and female germ cells yield mutation rates that are one order of magnitude below that of male stem cells (Ehling and Neuhauser-Klaus, 1988; Favor et al., 1990). The basis of this cell-specific sensitivity for ENU is poorly understood; however, cell type specific differences in cell division (mitosis, meiosis), repair mechanisms and/ or accessibility of chromatin due to histones or protamines are most likely involved (Favor, 1998).

2.4.4 The biochemical action of ENU

The alkylating effect of ENU does not need any metabolic activation, and its ethyl group can be transferred to nucleophilic sites of nucleic acids, i.e. N¹, N³ or N⁷ groups of adenine, O⁶, N³ or N⁷ of guanine, O², O⁴ or N³ of thymine, and the O² or N³ of cytosine. If these DNA adducts are not repaired, they result in mispairing of the two DNA strands and base pair substitutions during the next cycle of DNA replication. ENU induces predominantly point mutations, namely base pair substitutions such as A-T transversions and A-G transitions based on the mispairing after alkylation at O⁴ and O² thymine (Popp et al., 1983) that covers about 82% of all induced ENU mutations (Barbaric et al., 2007; Justice et al., 1999), or small deletions. Due to the point mutations, ENU can induce different types of alleles from null alleles, hypomorphs, antimorphs, or hypermorphs that can range from loss-of-function to gain-of-function mutations. New alleles or allelic series of known genes already demonstrated to be extremely useful to define the function of a gene like in the example of allelic series of the quaking locus in different tissues ((Davis and Justice, 1998; Sidman et al., 1964), or different new functions of quaking alleles during embryogenesis (Justice and Bode,

1988b; Shedlovsky et al., 1988). Finally, new genes can be isolated that underlie the mechanisms of diseases.

2.4.5 Mutation frequency of ENU

Early publications suggested that, with the administration of optimal ENU doses, mutation frequencies of $6-1.5 \times 10^{-3}$, can be yielded using the specific locus test (SLT), which equals to one mutation per gene in every 175 to 655 gametes (Hitotsumachi et al., 1985). The specific locus test represents a phenotype-based test system focusing on seven specific coat colour loci and will be described later in more detail under section 2.5.1.

Favor and colleagues (1998) demonstrated a co-linear relation between ENU concentration and specific locus mutations up to a dose of 400mg/kg bodyweight ENU and determined a threshold dose of 38.75mg/kg body weight ENU at which intracellular repair processes seem to reach their saturation (Favor, 1998). One of those DNA repair systems is O6-alkylguanine-DNA alkyltransferase (AGT) that was initially studied in hamster spermatogonial cells (Seiler et al., 1997) AGT efficiently repairs alkylated guanine adducts by transferring the alkyl group from the affected nucleotide to its own cysteine (Lindahl et al., 1988). Hence, only 13% G to C transversions were detected among all reported ENU induced DNA lesions (Justice et al., 1999). Recent sequence-based studies on ENU induced mutations revealed a mutation frequency of one point mutation in every 1 to 2.5 megabases per genome resulting in 1000-2500 point mutations, which include silent as well as functionally relevant changes. Considering that 1-3% of the genome cover coding regions, only 10-25 potential functional mutations per genome can be expected.

2.4.6 Pathogenic mutations

Pathogenic mutations can occur at three different types of DNA sequences: the coding sequence of a gene locus, at the intragenic noncoding sequences, and at regulatory sequences outside the exons.

- Base pair substitutions in coding sequences can be again divided into three groups: 1. Silent mutations do not cause any amino acid exchange; these substitutions affect predominantly the third base of a codon, also called the wobble-position. 2. Non-sense mutations represent base pair exchanges that lead to a premature stop codon, which leads in most cases to a hypomorphic or a loss-of-function mutation. 3. Missense mutations are caused by base pair exchanges at the first or second position of a codon resulting in an amino acid exchange. This exchange can be a conservative substitution by a chemically similar amino acid, which has a neutral or only a subtle effect on protein function. Whereas, a non-conservative substitution results in an amino acid replacement with a dissimilar side chain that introduces a charge difference.
- Base pair substitutions in non-coding sequences are most sensitive at the conservative splice-acceptor sites of introns leading to splicing failures (transcription of intronic sequences, skipping of exonic sequences, fusion proteins). Substitutions in conservative elements of 5' or 3'

untranslated regions can have an effect on the transcription level of a gene or on its mRNA stability.

- Base pair substitutions in regulatory elements are the third type of mutations that can occur in promoter regions upstream of the first exon or with a certain distance to the gene of interest.

2.5 Phenotyping protocols

The main interest of a phenotype-driven strategy is the implementation of appropriate procedures to assess mutant phenotypes of interest either to receive the mutation frequency or to obtain animal models and thus an insight into the gene function.

2.5.1 Specific locus test

Early phenotyping protocols, such as the specific locus test (SLT) of W.L. Russel, were initially developed to assess compounds for their mutagenic effects by yielding specific mutation rates, and to study the mechanisms of mutation induction in mouse germ cells. The Tester-stock carried seven recessive mutations affecting visible external traits such as coat/ eye colour, and ear shape: a (non-agouti, Chr. 2), b (brown, Chr. 4, tyrosine-related protein 1 Tyrp1b), cch (chinchilla at albino, Chr. 7, tyrosinase Tyrc-ch, d (dilute, Chr. 9, myosin Va Myo5ad), p (pink-eyed dilution, Chr. 7), s (piebald spotting, Chr. 14, endothelin-B receptor Ednrbs), and se (short ear, Chr. 9, bone morphogenetic protein 5 Bmp5se). In Russell's SLT, untreated T-stock females are mated to mutagen-treated wild-type males and to another set of untreated wild-type males as a control group. In the absence of any mutation, offspring derived from this cross will display the wild-type phenotype. An induced mutation to a recessive allele in a germ cell of the treated wild-type male will generate an offspring homozygous for the respective recessive allele resulting in an immediately visible specific locus phenotype among the otherwise wild-type progeny. This approach allows the calculation of mutation rates by simply scoring the number of mutant phenotypes per offspring. All mutants are subjected to allelism tests to confirm the mutation.

2.5.2 Multiple end point approach

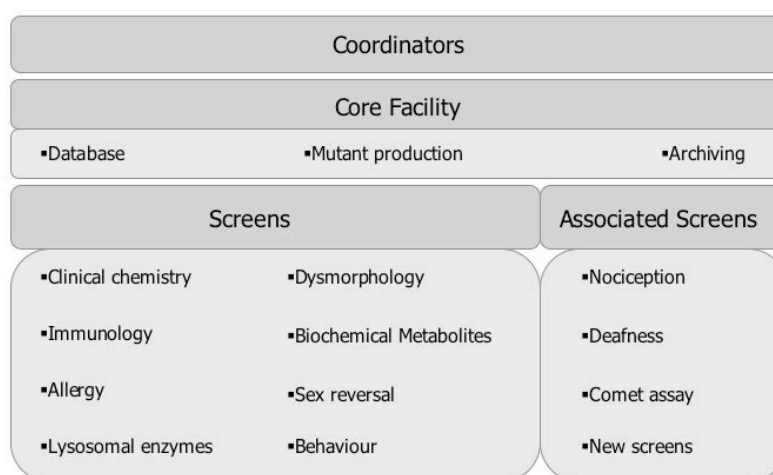
In the early 1980s, Ehling developed a phenotypic assay for dominant cataract mutations in mice (Ehling et al., 1982). At the age of 4 to 6 weeks, F1 offspring of mutagen-treated males were examined biomicroscopically, with the aid of a slit lamp, for lens opacities. The alterations in the lens were categorized into seven phenotypic classes: total opacity, nuclear and zonular cataract, nuclear cataract, anterior pyramidal cataract, anterior polar cataract, anterior capsular cataract, and vacuolated lens. Variants exhibiting lens opacity were bred further to confirm the genetic nature of its variant phenotype. Additionally, biochemical methods have been established to detect and quantify dominant mutations in erythrocyte enzyme activities (Charles and Pretsch, 1987; Pretsch and Charles, 1984). In this assay, ten enzymes from the glycolytic, pentose phosphate pathways and the citric acid cycle, which represent a set of structural, regulatory and operating loci, controlling the activity of each particular enzyme, were analysed. The enzymes included LDH (Lactate dehydrogenase), TPI

(Triosephosphate isomerase), MDH (Malate dehydrogenase), GPI (Glucosephosphate isomerase), PGK (3-phospho-glycerate kinase), PGAM (Phosphoglycero mutase), GAPDH (Glyceraldehyde-3-phosphate dehydrogenase), G6PD (Glucose-6-phosphate dehydrogenase), PK (Pyruvate kinase) and GR (Glutathione reductase). The three endpoints - specific recessive genes, dominant cataracts and enzyme activity mutations - were combined in the multiple endpoint approach to increase the number of loci tested from 7 to 70 and to compare the mutability of different loci (Ehling et al., 1985). This combination of three endpoints represented a big step forward in mutagenesis and toxicological studies of chemical compounds. Nevertheless, the number of phenotypes was restricted to the endpoint loci still leaving a large number of mutant phenotypes that are valuable for the functional analysis of genes.

2.5.3 SHIRPA protocol

New assays and protocols such as the SHIRPA protocol were developed to recover novel phenotypes with neuropathological and behavioral abnormalities (Rogers et al., 1997). SHIRPA (for Smith Kline Beecham; Harwell, MRC Mouse Genome Centre and Mammalian Unit; Imperial College School for Medicine at St. Mary's; Royal London School of Medicine; Phenotype Assessment) uses a combination of standardized protocols for behavioural and functional assessment that provide a sensitive measure for quantifying phenotype expression in the mouse. SHIRPA includes three stages of assessment: The primary screen provides a behavioural and functional profile by observational assessment indicating defects in gait or posture, motor control and coordination, changes in excitability and aggression, salivation, lacrimation, piloerection, defecation, muscle tone, and temperature. The secondary screen involves a comprehensive behavioural and functional battery and pathological analysis including the measurement of spontaneous locomotor activity, food and water intake, quantification of balance and coordination using an accelerating rota-rod, perception of pain (hot-plate assay) and biochemical examination by measuring serum urea, electrolyte and blood glucose. The tertiary screen includes the assessment of existing or potential models of neurological disease. Anxiety is measured by open-field activity, the elevated plus maze or the light-dark box; memory is assessed by the Morris water maze. These assessments are complemented by well-established methods in the analysis of structural and functional abnormalities in

Figure 1 Original structure of the ENU mouse mutagenesis project set up in the framework of the German Human Genome Project (DHGP).



the nervous system such as electromyography, electroencephalography, nerve conduction, and magnetic resonance imaging techniques.

2.6 Structure of the Munich ENU mouse mutagenesis project

Aim of the Munich ENU mouse mutagenesis project was the systematic and large-scale production of mouse models for inherited diseases in human, which was too difficult to be performed by a single research centre. For this purpose, in 1996, nine research groups from the Ludwig-Maximilian University (LMU), the Technical University Munich (TU Munich), the University Freiburg, the Max-Planck-Institute of Psychiatry (MPI) and the GSF National Research Centre (GSF) were associated in a scientific consortium in the framework of the German Human Project headed by the coordinators Prof. Hrabé de Angelis, Prof. Wolf, and Prof. R. Balling (Figure 1). The core facility was the central platform for breeding, mutagenesis of males, sample taking and distribution from offspring of mutagen-treated mice to all participating research groups. Moreover, the data and workflow management, and the archiving of all mutant mouse phenotypes, was managed by the core facility. The screens were responsible for the analysis of samples as well as for the isolation of specific mutant phenotypes that included abnormal phenotypes in clinical chemistry, dysmorphology, immunology and allergy, in sex reversal, in lysosomal enzymes, biochemical metabolites, and in behaviour. The pool of F1 / G3 animals were openly accessible to external research groups that requested to screen for additional parameters, and as long as the additional assessment procedures could be integrated into the workflow without affecting the main parameters those groups were associated to the project.

2.7 Current ENU mutagenesis screens

Nowadays, the impact and role of mouse ENU mutagenesis in gene function studies is reflected in the increasing number of genetic screens of different scales during the last couple of years. Despite the fact that predominantly large research centres are economically and structurally capable of performing systematic genome-wide screens for a broad variety of phenotypes a remarkably increasing number of smaller and more focused projects have addressed their genetic screens either to particular phenotypes (Graw et al., 2001a; Klopp et al., 1998), to certain developmental stages (Garcia-Garcia et al., 2005; Kasarskis et al., 1998; Zarbališ et al., 2004) or specific pathways (Hoebe and Beutler, 2008; Mohan et al., 2008; Rubio-Aliaga et al., 2007) to defined chromosomes (Kile et al., 2003) or chromosomal regions (Rinchik et al., 2002; Rinchik et al., 1990). In Table 1 a selection of current phenotype- and genotype-driven ENU mutagenesis projects are listed in alphabetical order. However, the table does not claim to be complete.

Table 1. Overview of current phenotype- and gene-driven ENU mouse mutagenesis projects.

Due to the increasing numbers of smaller screens focusing on specific phenotypes, pathways as well as modifiers and sensitized screens the table does not claim to be complete. (Modified after (Brown and Balling, 2001))

Mutagenesis Project	Strategy	Phenotype	Gene-driven approach	URL
Australian Phenomics Facility	genome-wide recessive	immunity and tolerance, deafness, male fertility	F1 archive	http://www.apf.edu.au/
Baylor Mouse Mutagenesis for Developmental Defects	Chr. 11 balancer recessive	birth defects, patterning defects, growth and endocrine defects, neurological anomalies, blood defects		http://www.mouse-genome.bcm.tmc.edu/ENU/ENUhome.asp
Genomics Institute of the Novartis Research Foundation	genome-wide dominant and recessive	immunology, neurobiology, vision, metabolic disorders, and hearing		http://www.gnf.org/technology/organimal/mammalian-genetics-phenotyping.htm
Harwell Mutagenesis Programme	genome-wide dominant, recessive and sensitized	EmPress phenotyping pipeline modifier and sensitized screens (diabetes)	F1 archive	http://www.har.mrc.ac.uk/research/mutagenesis/
Harvard's Mutation Mapping and Developmental Analysis Project	genome-wide recessive	late embryonic development affecting organogenesis		http://www.brighamandwomens.org/research/genetics/moran.asp
The Jackson Laboratory Neuroscience Mutagenesis Facility	genome-wide recessive	neurological, behavioural and sensory disorders; age-related disorders	EMS/ ENU treated ES cells	http://nmf.jax.org/
The Jackson Laboratory HLBS Mutagenesis Program	genome-wide recessive	Heart, Lung, Blood and Sleep Disorders	EMS/ ENU treated ES cells	http://pga.jax.org/index.html
The Jackson Laboratory Reproductive Genomics Program	genome-wide recessive	infertility mutations	EMS/ ENU treated ES cells	http://reproductivegenomics.jax.org/
McLaughlin Institute Mouse Mutagenesis Program	genome-wide recessive and sensitized	neurological and behavioural mutations		http://www.montana.edu/mri/enump.html
Munich ENU Mouse Mutagenesis Project	genome-wide dominant and sensitized	bone and cartilage disorders	F1 archive	http://www.helmholtz-muenchen.de/en/ieg/group-genome-project/enu-screen/index.html
Northwestern University Center for Functional Genomics	genome-wide	neuroendocrinology and stress, learning and memory, psychostimulant response, circadian rhythmicity, vision		http://www.genome.northwestern.edu/
RIKEN ENU mutagenesis project	genome-wide dominant and recessive	neurology, hematology, bone; late onset phenotypes: fundus image, blood pressure, hearing, tumorigenesis	F1 archive	http://www.gsc.riken.jp/Mouse/
The Sloan Kettering Mouse Project	genome-wide recessive	embryonic patterning of spinal chord, urogenital system, limb development		http://www.mskcc.org/mskcc/html/10173.cfm
Toronto's Center for Modeling Human Disease	genome-wide dominant	cardiovascular, diabetes, renal hemtopoietic, neurological and skeletal systems		http://www.cmhd.ca/enu_mutagenesis/index.html

Beside the group of mutant phenotypes that revealed new functions of a gene, as for example for *Notch* in early ear development (Kiernan et al., 2001) or even completely novel genes such as *Tmc1* involved in progressive deafness (Kurima et al., 2002; Vreugde et al., 2002) also a part of phenotypes were isolated which genes were already known. Moreover in some cases, ENU induced multiple hits in the same gene, which affect the phenotype in a various manners and intensities as described for *Pax6* (Favor et al., 2001; Graw et al., 2005; Thaug et al., 2002), the kit ligand gene (Rajaraman et al., 2002a; Rajaraman et al., 2002b), *Smad2/ Smad4* (Vivian et al., 2002), the *quaking* locus (Noveroske et al., 2005), or recently the *Thoc1* gene (Wang et al., 2007). These mutant phenotypes represent allelic series of a single gene that are one of the main important aspects and advantages in forward genetics regarding the dissection of gene function. In contrast, reverse genetics aims at the complete depletion of a gene and its function resulting in a null allele in order to reveal general consequences on phenotype levels. But only subtle changes in important functional DNA sequences in a gene can lead to the identification of functional domain with enzymatic activity, domains that bind to other proteins or represent a domain that regulates the transcription of a gene by modification through phosphorylation or acetylation.

2.8 Inherited limb patterning defects in humans and their molecular mechanisms

Today, known human inherited diseases are collected and described in McKusicks book of Mendelian inherited diseases in man, which is available online and meanwhile better known as the OMIM (**O**nline **M**endelian **i**n **M**an) database (McKusick, 2007). To date, more than 6000 entries of Mendelian traits are available, in 2429 cases the phenotype-genotype correlation is described and known but from more than 1500 phenotype descriptions even the molecular basis is still unknown (OMIM website <http://www.ncbi.nlm.nih.gov/Omim/mimstats.html>). Considering the assumed number of 21.000 genes of the human genome approximately 11.000 genes, are annotated yet.

In humans, approximately one newborn in a thousand displays a malformation in the limbs (Manouvrier-Hanu et al., 1999). Previously, two different schemes were mainly applied to classify human limb malformations: the first scheme, called Temtamy and McKusick classification, based on a purely clinical description (Temtamy and McKusick, 1978), the second, called Winter and Tickle classification, distinguished limb anomalies which derived from embryological patterning defects of the axial and appendicular skeleton from those which are not (Winter and Tickle, 1993). Nowadays, the knowledge about the underlying molecular mechanisms has increased, which resulted in a classification of limb anomalies according to their genetic defect. But still, only a smaller part of genotype-phenotype correlation underlying limb anomalies is known.

A limb can be divided into three segments: the stylopodium, a proximal segment, which consists of a single bone (humerus/ femur), the zeugopodium, a medial segment consisting of two bones (radius/ulna and tibia /fibula), and the autopodium, which represents the distal and more complex segments (hand/ foot) consisting of carpal/tarsal bones, metacarpals/-tarsals, proximal, middle and

distal phalanges. As for all outgrowing structures, limb development and the connected molecular pathways being responsible for the first patterning are divided into three axes, the proximal-distal (PD), dorsal-ventral (DV) and anterior-posterior (AP) axis. The progenitor cells that form the limb bud derive from the lateral plate mesoderm (Cohn and Tickle 1996). The initiation of limb bud development depends on the so called apical epidermal ridge (AER) a stripe of specialized epithelial cells at the most distal part of the limb bud (Gilbert, 2000) defining the P-D axis. This is interconnected with the A-P limb bud polarization that is under the control of the posterior zone of polarizing activity (ZPA). In addition, these complex processes are interlinked with a constant equilibrium of proliferation and apoptotic processes during the generation of the zeugopodium and interdigital spaces forming individual fingers and digits. Therefore, a highly coordinated regulation of several molecular processes is required for a correct formation of these limb segments where numerous genes are included. By using the same principles for all parts of the body as well as during organogenesis, similar molecular pathways are activated during different stages of development, which, in case of a genetic defect, can result in multiple phenotypes. Mutations in early patterning genes cause disorders called dysostoses affecting only specific skeletal elements whereas the rest of the skeleton remains large unaffected. In contrast, mutations in genes that are primarily involved in organogenesis causing disorders called osteochondrodysplasias; they affect the development and growth of most skeletal elements in a pleiotropic manner (Hall, 2002). The main signalling pathways involved in limb development will be briefly presented following the molecular pathways of the axes of a limb. An overview of limb patterning syndromes and underlying genetic bases is summarized in (Kalff-Suske et al., 1999; Roscioli et al., 2005; Vortkamp et al., 1991).

2.8.4 Fibroblast growth factor (Fgf) pathway and PD patterning

Members of the fibroblast growth factor family (Fgfs) play a major role in the outgrowth of the limb bud. Limb bud outgrowth is initiated by Fgf10 secretion in the lateral plate mesoderm that triggers Fgf8 in the ectoderm, which in turn induces proliferation and Shh expression in the mesoderm (Capdevila and Izpisua Belmonte, 2001; Martin, 2001; Tickle and Munsterberg, 2001). Null mutation of Fgf10 in mice leads to limb bud initiation but results in a complete lack of limb growth since neither the AER nor the ZPA are formed (Manouvrier-Hanu et al., 1999; Sekine et al., 1999). When Fgf8 is inactivated limb bud outgrowth is initiated but the limbs lack several skeletal elements. Other members of the Fgf family have been identified in the AER such as Fgf2, Fgf4, and Fgf8 that are believed to maintain Shh in the ZPA (Lewandoski et al., 2000; Moon and Capecchi, 2000). Conditional gene inactivation of Fgf4 and Fgf8 in mice showed that early inactivation results in a complete lack of limb formation. However, when inactivation takes place at a later stage the limb buds grow out but display abnormal skeletal patterning including missing skeletal elements or reduced size, which was believed to be regulated by the number of chondrocyte progenitors for later condensation (Sun et al., 2002). The Fgfs themselves have not yet been associated to human limb malformations, but mutations of genes encoding the respective FGF receptors (FGFR) have been

identified in certain chondrodysplasias, and craniostenoses associated with limb malformations (Table). Four Fgf receptor genes have been described so far (Fgfr1-4), their structure consist of a hydrophobic leader sequence, three Ig-like domains, an acidic box, a transmembrane region, and a tyrosin kinase domain. A number of isoforms are generated by Fgfr1-3 among which the b and c isoforms of Fgfr2 are best studied. These isoforms bind specifically to their ligands and are regulated in a tissue-specific manner. Fgfr2b expression is confined to epithelial lineages and can only be activated by Fgf7 and Fgf10, whereas Fgfr2c expression is restricted to mesenchymal lineages and can only be activated by Fgf 2,4,6,8,9 (Coumoul and Deng, 2003; Peters et al., 1992; Xu et al., 1999; Xu et al., 1998). Heparin stimulation is needed for complete activation of Fgf pathways after which FGF-FGFR complexes are internalized and trigger other signalling pathways in the nucleus (Coumoul and Deng, 2003) . Inactivation of both isoforms of Fgfr2 in mice resulted in a failure of limb induction displaying mutant embryos that miss fore- and hind limbs. Although the presumptive limb region displayed initial thickening Fgf8 was not detected in the mesoderm; and Fgf10, which was initially expressed in the mesenchyme, gradually disappeared. Xu and colleagues therefore proposed that limb induction is dependent on a positive regulatory loop involving Fgfs and the two isoforms of Fgfr2. Inactivation of either one of the isoforms of Fgfr2 did not block limb bud initiation (Coumoul and Deng, 2003; Revest et al., 2001) but in Fgfr2b deficient mice *Shh* and *Fgf4* expression were not detected. Moreover, apoptotic processes in the limb bud ectoderm and mesenchyme at E 10 to E10.5 provided evidence that Fgfr2b-mediated Fgf-signals function as survival factors for limb bud maintenance and growth (Revest et al., 2001).

2.8.5 Sonic hedgehog pathway and AP patterning

Sonic hedgehog (*Shh*) is a secreted protein, which is believed to regulate the patterning mechanisms along the AP axis. *Shh* functions by binding to a receptor called Patched (*Ptch*), which is associated to a signal transducer *Smoothened* (*Smo*). In the absence of *Shh* binding *Ptch* functions as a repressor of *Smo*, and the *Gli3* protein is tethered via *Fused* (*Fu*) and *Cos2* (suppressor of *Fu*) to the microtubules of the responding cell. In this status, *Proteinkinase A* (*PKA*) cleaves a part of *Gli3* transforming it into *Gli3R*, which enters the nucleus and acts as an inhibitor of transcription. When *Shh* is binding to *Ptch* its repressive effect on *Smo* is abolished. *Smo* releases *Gli3* from the microtubules by phosphorylating *Fu* and *Cos2* and prevents further cleavage of *Gli3* by inhibiting *PKA*. In this conformation *Gli3A* can act as a transcriptional activator of the same genes it used to repress (Gilbert, 2000; Niswander, 2003). Shortly after limb bud initiation the AP axis is determined by a mutual antagonistic equilibrium between *Gli3R* and *Hand2*, two genes encoding transcription factors. *Gli3R* is expressed anteriorly in its truncated and repressive form, and *Hand2* that is expressed in the posterior mesenchyme of the forelimb where it is believed to induce *Shh* expression (Charite et al., 2000; Fernandez-Teran et al., 2000; te Welscher et al., 2002). In early limb development *Shh* expression is confined to the ZPA of the limb bud (Riddle et al. 1993) where it regulates the level of *Gli3R* in a graded manner by repressing *Gli3* at the transcriptional level and by preventing the transformation of the full-length form *Gli3A* in to the truncated form *Gli3R*. Complete

inactivation of *Shh* in mice embryos results in severe limb phenotype with missing digits at the fore limbs, a single bi-phalangeal digit at the hind limbs, and a fore limb zeugopod with a single bone (Chiang et al., 1996). *Shh* conveys its influence at a distance by initiation and maintenance of a *Bmp2* expression, which also possess a polarizing activity (Duprez et al., 1996; Francis et al., 1994). Among the known target genes of *Shh* are the 5' *Hoxd* genes which expression coincides in the posterior ZPA. More evidence were given with transplantation experiments of the ZPA or *Shh*-secreting cells to the anterior part of the limb bud that leads to the formation of mirror-image patterns of *Hoxd* gene expression and digit patterns (Izpisua-Belmonte et al., 1991). Heterozygous *Xt* mouse mutants carrying a deletion in the 3' end of *Gli3* displayed craniofacial malformations and preaxial polydactyly (Hui and Joyner, 1993). In parallel, mutations in the human *GLI3* gene are associated to congenital skeletal malformation in the skull and limbs (Kalff-Suske et al., 1999; Kang et al., 1997; Roscioli et al., 2005; Vortkamp et al., 1991).

2.8.6 Wnt pathway and DV patterning

A member of the *Wnt* family of growth factors, *Wnt7a*, has been shown to play an essential role in dorso-ventral patterning in limb development. *Wnt7a* expression is strictly confined to the dorsal ectoderm of the limb bud (Dealy et al., 1993; Parr et al., 1993), and homozygous *Wnt7a* knockout mice displayed paws with a double ventral phenotype (sole pads on both sides). In contrast, *Engrailed1* (*En1*) a homeodomain-containing transcription factor expressed in embryonic ventral limb ectoderm, is essential for ventral limb patterning. Loss of *Engrailed-1* function in mice results in dorsal transformations of ventral paw structures, and in subtle alterations along the proximal-distal limb axis. *Engrailed-1* seems to act in part by repressing dorsal differentiation induced by *Wnt-7a*, and is essential for proper formation of the apical ectodermal ridge (Cygan et al., 1997; Loomis et al., 1996). *Wnt7a* induces and maintains expression of the LIM-homeodomain protein *Lmx1b* in mesenchymal cells of the dorsal limb. Earlier *Wnt7a* signalling in limb bud stages also seems to maintain *Shh* expression, since in homozygous *Wnt7a* knockout mice the most posterior digit is often missing (Parr and McMahon, 1995). In humans, a number of mutations in *LMX1B* are associated with the Nail-patella syndrome displaying anomalies of the nails, patella, elbows and renal parenchyma (Vollrath et al., 1998).

2.8.7 T-box genes and limb identity

The T-Box transcription factor family is involved in the P-D determination of limb and digit identity during embryonic development including the genes *T*, *Tbx2*, *Tbx3*, *Tbx4*, *Tbx15*, and *Tbx18*. Mutations of T-box genes are associated with a number of congenital malformations effecting the axial skeleton, craniofacial and limb development. T-Box genes had been first described in 1927 in heterozygous mutant mice, carrying a genetic defect at the *Brachyury* or *T* locus and that displayed a short tail. Homozygous mutations had been embryonic lethal due to complete lack of axial development (Kispert and Hermann, 1993; Wilkinson et al., 1990). Complete inactivation of *T* had lead to embryonic lethality at E10.5 whereas misexpression of T was shown to affect the formation of

a mature, organized AER, which can lead to disturbances of *Shh* expression and thus changes in skeletal limb patterning of the most distal elements such as digit duplications, antero-posterior transformations, or changes in tarsal bones (Liu et al., 2003). *Tbx2* and *Tbx3* are normally expressed along the anterior and posterior edges of the limb buds in fore- and hindlimbs and required for patterning processes of the posterior digits (Suzuki et al., 2004). Null mutations of *Tbx2* in mice were embryonic lethal between E10.5 and E14.5 due to cardiac malformations with digit duplications at the hindlimbs (Harrelson et al., 2004; Suzuki et al., 2004). Also inactivation of *Tbx3* resulted in embryonic lethality by mid gestation due to yolk sac defects with abnormal hand- and footplates (Suzuki et al., 2004). *Tbx4* and *Tbx5* are both predominantly responsible for the specification of hind limb and fore limb, respectively. *Tbx4* null mutants die at stage E10.5 due to dysfunction of the allantois (Naiche and Papaioannou, 2003). While limb bud initiation did not seem to be disturbed but maintenance of *Fgf10* expression in the mesenchyme failed and thus limb bud outgrowth. Conditional inactivation experiments showed in addition that *Tbx4* and *Tbx5* interaction with *Wnt* and *Fgf* signalling pathways are needed in a critical time window in order to have normal limb development (Takeuchi et al., 2003). *Tbx5* had been demonstrated to be essential for forelimb formation in vertebrates (Agarwal et al., 2003; Ahn et al., 2002; Takeuchi et al., 2003). *Tbx5* is required for the induction and maintenance of the AER by activating *Fgf10*, which leads to *Fgf8* expression in the AER and limb bud outgrowth. Misexpression experiments of *Tbx5* in chick wings at later stages showed immaturity of the AER and decreased *Fgf8* expression in the AER (Rallis et al., 2003). *Tbx15* and *Tbx18* seem to have redundant functions in limb development and both expressed the limb mesenchyme. *Tbx15* is additionally expressed in the pharyngeal and the craniofacial region (Agulnik et al., 1998; Candille et al., 2004; Singh et al., 2005). Complete inactivation leads to a relatively mild phenotype such as decreased bone length and alterations in bone shape due to deregulation in endochondral bone development (Singh et al., 2005). Null mutants of *Tbx18* die perinatally with severe malformation of the vertebral column (Kraus et al., 2001). Since a 93% sequence homology of *Tbx15* and *Tbx18* and co-expression had been detected compensation effects of *Tbx18* are discussed (Singh et al., 2005). Mutations in human *TBX3*, *TBX4* and *TBX5* are associated to limb defects.

2.8.8 Hox genes and determinants along the PD axis

Hox genes encode a family of transcription factors that are essential for the architecture of the body plan and patterning processes during embryonic development from *Drosophila* (Gehring et al. 1993), zebrafish (Sordino et al., 1995), to higher vertebrates. (Favier and Dolle, 1997; van der Hoeven et al., 1996; Zakany et al., 1997). *Hox* proteins are characterised by a highly conserved sixty amino acids DNA-binding motif called homeodomain that is encoded by a homeobox element and located in the second exon of all *Hox* genes (Fraenkel and Pabo, 1998; Gehring, 1993). The majority of *Hox* genes are believed to interact with specific DNA-binding partners forming a multi-meric protein complex that control transcriptional activation or suppression of their target genes (Mann and Affolter, 1998). Especially the *Hoxa* and *Hoxd* clusters are mainly involved in the control of structure formation along

the PD axis and patterning of secondary axes of the limbs in a sequential and concerted manner, which was shown by systematic gene inactivation of the *Hox* clusters (Beckers et al., 1996; Davis and Capecchi, 1996; Zakany et al., 2004). Corresponding to the three parts of a limb, expression of *Hoxa* and *Hoxd* follow three successive phases. Inactivation studies in chick and mouse have demonstrated that *Hoxa9/ Hoxa10* and *Hoxd9/Hoxd10* are expressed during specification and formation of the stylopods (upper arm/ leg); *Hoxa11* and *Hoxd9* to *Hoxd13* are predominantly expressed during zeugopod formation (lower arm/leg); and *Hoxa13* and *Hoxd10* to *Hoxd13* are active in the formation and patterning of the autopods (hand/ foot) (Favier and Dolle, 1997; Nelson et al., 1996; Zakany and Duboule, 1999). Targeted inactivation or over-expression of 5' *Hoxa* and *Hoxd* genes in chick and mouse resulted in size reduction and shape alterations of specific skeletal elements such as shortening, fusion, webbing and duplication of the digits, associated with delays in chondrification and ossification (Favier and Dolle, 1997; Zakany and Duboule, 1996). These outcomes have lead to the conclusion that, during early limb development, the 5' *Hox* clusters control the recruitment of mesenchymal cells into the area of precartilaginous condensation and their subsequent growth and maturation, and not the specification of upper or lower limb identity. In humans, mutations in *HOXD13* are associated to Synpolydactyly (SPD; MIM 186000) and the Hand-foot genital syndrome (HFGS; MIM 140000).

Table 2 Inherited limb anomalies in human and their genetic basis.

Signalling molecules	Receptors/ downstream targets	Human Syndrome associated to mutations*	Phenotype
<i>Fibroblast growth factors</i>			
<i>Fgf8</i>	<i>Fgfr1*</i>	Pfeiffer syndrome (MIM 101600)	Craniosynostosis syndrome with craniofacial anomalies, short fingers, soft- tissue syndactyly
<i>Fgf4</i>	<i>Fgfr2*</i>	Apert syndrome (MIM 101200) Pfeiffer syndrome Jackson-Weiss syndrome (MIM 123150)	Severe syndactyly (soft tissue, synostoses), broad thumbs/ toes Foot abnormalities
<i>Fgf9</i>	<i>Fgfr3*</i>	Achondroplasia (ACH) Thanaphoric dysplasia (TD)	Short limbed dwarfism caused by abnormalities of long bones TDI: straight femurs, severe cloverleaf skull TDII: curved femurs, mild or lacking cloverleaf skull
<i>Fgf10</i>	<i>Fgfr4</i>		
<i>Hedgehogs (Hhs)</i>			
<i>Shh</i>	<i>Ptch*</i>	Gorlin syndrome	Brachydactyly, pre-/postaxial synpolydactyly of 2 nd / 3 rd toes
	<i>Gli3*</i>	Greig cephalosyndactyly (MIM 175700) Pallister-Hall syndrome (MIM 146510)	Postaxial polydactyly Postaxial polydactyly, syndactyly
<i>Wingless/Int</i>			
<i>Wnt7a, 3a, 5a</i>	<i>Frizzleds</i> <i>Lmx1b*</i>	Nail-patella syndrome	Dysplasia of nail, patella, elbow, renal parenchyma
<i>T-box genes</i>			
<i>Tbx3*</i>		Ulnar-mammary syndrome (MIM 181450)	Agenesis/ duplication of 5 th finger; hypoplasia of 4 th / 5 th toe
<i>Tbx4*</i>		Small patella syndrome (MIM 147891)	
<i>Tbx5*</i>		Holt-Oram syndrome (MIM 142900)	Hypoplastic, agenesis or triphalangeal thumb, hypoplasia of the radius
<i>Hox genes</i>			
<i>Hoxa9 – a13*</i>		Hand-foot genital syndrome (MIM 140000)	Anomalies of hands, feet and urogenital malformations
<i>Hoxd9 – d13*</i>		Synpolydactyly (MIM 186000)	Heterozygotes: duplication and syndactyly of the 3 rd /4 th metacarpals or 4 th / 5 th metatarsals Homozygotes: syndactyly of all fingers, pre- meso-postaxial polydactyly

3 Materials and Methods

3.1 Animals

3.1.1 Husbandry

This mutagenesis study was conducted under SPF conditions (specific pathogen free). The standard conditions for a SPF animal facility are defined by the Federation of European Laboratory Animal Science Association (FELASA): with a temperature of 22-24° C, a humidity of 55-60%, a dark/light cycle of 12h/12h (from 7am to 7pm in this case), brightness of 600lux and food/water supply *ad libitum*. For monitoring the health status, every three months, two sentinels per unit are subjected to a macro-/microscopic as well as a microbiological examination. For at least twelve weeks, these animals were abandoned to bedding weekly sampled and collected from all cages of the unit. The pathogens, which are to be analysed for a SPF animal facility are defined by the FELASA.

Moreover, the core colonies of the utilized mouse strains were held in an isolated ventilated cage system (IVC) (Biozone, England) conducted with positive air pressure and an air exchange rate of 100 changes per hour.

3.1.2 Strains

The strain used in this mutagenesis study was the inbred mouse strain C3HeB/FeJ, which was supplied by the Jackson Laboratory (Bar Harbour, Maine, USA). A core colony of 30 breeding pairs was set up in one-to-one crossings.

For chromosomal mapping another inbred mouse strain, C57BL/6J, was used. The main reason for this choice is the availability of a large number of polymorphic microsatellite and single nucleotide polymorphic (SNP) markers between the C3H and C57 mouse strains, which were needed for linkage analysis.

3.1.3 Preparation of animals

For purposes of adaptation, animals were moved into the injection room one week before ENU administration. A maximum number of four males per type II cage were not exceeded.

For ENU injection, C3H male mice between the ages of 10 to 14 weeks and between 24 and 36g bodyweight on the day of injection were selected. The animals were divided into injection groups consisting of mice with a bodyweight falling into intervals for 2.5g-steps. For each injection batch, a number of 80-200 animals were treated with ENU. The injections were performed every three to four months in order to have a constant number of fertile ENU treated males.

3.2 ENU administration

3.2.4 Preparation of ENU

Soerensen buffer

66mM KH_2PO_4 (stock A), 66mM $\text{Na}_2\text{HPO}_2 \times 2\text{H}_2\text{O}$ (stock B). For a Soerensen buffer with a pH 6.0 121ml of stock A was taken and filled up to 1000ml with stock B. pH was tested after preparation and before use at 4°C.

3.2.5 Quality control

The ENU solution should be clear and display a light yellow colour. If this is not the case, the ENU is degraded and a new flask of ENU should be used. Every single flask of ENU should be used only once for one experiment. ENU should not be stored for longer than one year. Due to its hazardous effect, each ENU lot was sent to the QC department of the manufacturer, (Serva, Heidelberg, Germany). The quality of each ENU lot was determined by its melting point (melting point \approx 90-95°C) and UV absorption analysis.

Because of continuous degradation of ENU the injection procedure was finished within 60 min after the initial ENU preparation.

3.2.6 ENU injection

The mice were injected intraperitoneally (I.P.) with 0.5ml of ice-cold ENU solution with the concentration according to the mean bodyweight of each group. I.P. injection was performed according to the procedure described in A. Nagy's „Manipulating the mouse embryo“.

3.2.7 Precautions for ENU handling and quality control

Up to the start of the project, recommendations about handling with ENU and its quality control (QC) did not officially exist; due to the known hazardous and mutagenic effect of ethyl-nitroso-urea (ENU) on germ cells there was a need to develop and implement standardised procedures for the handling with ENU and its QC. The details are described in our publication (Soewarto et al., 2003).

3.2.8 Implementation of an injection schedule

The injection schedule had to be implemented in a manner that a continuous generation of 100 F1 and 40 G3 mice per week was guaranteed for a period of several years. The following criteria were considered:

1. The appropriate ENU concentration and regime had to be determined aiming at balance of a high mutation frequency and the optimal sterility and fertility period of the injected male mice.
2. The number of produced F1 offspring per male had to be restricted to 50 in order to avoid any clustering of the same mutations coming from the population of a single spermatogonial germ cell.

For this purpose, two ENU regimes were determined to start with, which were already used in other studies with a hybrid mouse strain C3H/101 (Favor et al., 1997), including 1x160mg/kg (batches 1,2,5,6), 3x80mg/kg (batches 3,4) bodyweight ENU. These injection batches were performed in the first 15 months of the project. The males' sterility periods of each ENU batch were divided in groups of 50-79d, 80-99d, 100-150d and above 150d, and since a co-linear relation between sterility period and mutation rate was assumed a lower threshold of 80 days of sterility was determined in order to yield a higher mutation rate. Moreover, it was easier to monitor of the efficiency of each single injection batch by dividing the males in smaller sterility groups. In addition to this, the number of sterile/fertile males and the number of generated F1 animals were recorded as well. The evaluation of injection batches showed a similar result of ENU males that were treated with 1x160mg/kg and 3x80mg/kg bodyweight ENU with regard to sterility periods and the percentage of sterile ENU males that ranged between 2 to 13.8%. The sterility rate of males that were treated with 3x100mg/kg bodyweight ENU ranged between 20 to 54.8%. In addition, the numbers showed a shift to the advantage of the groups with longer sterility periods, which could be co-linear with a higher mutation frequency but also with a shorter fertility period of the male mice. With these sterility/fertility numbers the development of a reliable injection schedule was not be possible. For this reason, the two lower ENU regimes were further used for this project. For F1 production and its calculation under the given conditions, an average litter size of 5 offspring, and interval of 4 to 6 six weeks between two litters, a sterility rate of 20% within the ENU treated males and a fertility period of approximately 6 months were considered. Additional regimes were tested in the course of the project, which are summarized in Table 3.

The ENU administration for the dominant screen was changed to 3x90mg/kg bodyweight ENU in order to obtain a higher mutation frequency, which was in balance with the efficiency of F1 generation. For the recessive screen, the lower concentration of 3x80mg/kg bodyweight ENU was preferably utilized to avoid accumulation of multiple recessive mutations; the two-step-breeding strategy might resulted in a mutual interference of multiple induced mutant phenotypes.

In the course of this project, 31 ENU injections with five different regimes had been performed as presented in Table 3. In total, 2876 C3Heb/FeJ male mice in groups of 20 to 200 animals had been treated with ENU; the injections were carried out in 4 to 6-months intervals, and each group of ENU treated animals had been replaced after approximately 8 to 10 months before exceeding the number of 50 F1 offspring per male. Thus, the continuous generation of approximately 50-100 F1 or G3 animals per week at the appropriate age for each screening parameter was guaranteed.

Table 3. Overview of the ENU injections considered indicating the different regimes ^a (T12= 1x200 mg/kg; T16= 1x160 mg/kg; T31= 3x100 mg/kg; T38= 3x80mg/kg; T39= 3x90 mg/kg ENU), the batch IDs, and the last day of ENU administration. Multiple injections were applied in weekly intervals. Sterility periods of fertile ENU treated males were calculated as Δd of the last day of ENU administration and the presumed day of conception (based on the day of birth of the first F1 offspring minus 20 days of gestation).

Batch ID	Regime ^a	Last day of treatment	50-79d sterility	80-99d sterility	100-150d sterility	> 150 d sterility	Sterile ENU males	Fertile ENU males	ENU males total	Count F1	Average F1 per ENU male
1	T16	30.09.1996	14	21	8	6	1 (2%)	49	50	2248	45
2	T16	07.10.1996	17	30	16	6	11 (13.8%)	69	80	2960	37
3	T38	21.10.1996	37	21	15	1	5 (6.3%)	75	80	3399	42
4	T38	04.11.1996	17	20	3	5	5 (10%)	45	50	1752	35
5	T16	28.10.1996	8	6	4	0	2 (10%)	18	20	782	39
6	T16	20.01.1997	54	53	17	7	9 (6.4%)	131	140	2998	21
9	T31	21.05.1997	6	11	18	54	60 (40.3%)	89	149	2753	18
11	T31	17.06.1997	1	5	22	20	12 (20%)	48	60	1204	20
12	T31	29.07.1997	2	4	15	17	46 (54.8%)	37	83	651	8
14	T39	03.12.1997	0	16	56	22	56 (37.3%)	94	150	1569	10
16	T12	18.03.1998	1	22	8	11	58 (58%)	42	100	848	8
17	T12	27.05.1998	0	30	31	16	66 (46.1%)	75	141	1450	10
18	T16	01.07.1998	0	10	9	2	31 (59.6%)	21	52	446	9
19	T39	09.12.1998	0	3	11	10	33 (57.9%)	24	57	595	10
20	T39	17.02.1999	0	0	31	4	61 (63.5%)	34	95	1026	11
21	T39	14.07.1999	0	0	43	7	45 (47.4%)	7	52	922	18
22	T39	22.12.1999	3	9	9	18	24 (38.1%)	39	63	410	7
23	T39	19.04.2000	1	0	32	20	36 (40.4%)	61	97	388	4
24	T39	19.07.2000	0	6	25	4	46 (56.8%)	41	87	273	3
26	T38	25.10.2000	1	14	10	2	38 (58.5%)	27	65	125	2
30	T38	14.02.2001	5	28	46	17	53 (35.6%)	96	149	508	3
31	T38	10.05.2001	0	27	33	15	132 (63.8%)	75	207	594	3
33	T38	19.12.2001	11	17	8	5	57 (58.2%)	41	98	688	7
35	T38	19.03.2002	1	24	30	16	44 (38.3%)	71	115	759	7
39	T38	17.07.2002	3	16	40	19	90 (53.6%)	78	168	702	4
41	T38	23.10.2002	0	26	67	18	106 (48.9%)	111	217	917	4
45	T38	12.03.2003	9	26	25	7	34 (33.7%)	67	101	740	7
49	T38	09.07.2003	0	30	36	24	48 (34.8%)	102	150	1517	10

3.3 Implementation of breeding schemes

A mutagenesis project in the mouse consists of a defined series of different breeding steps: it starts initially with the first sterility testing of ENU-treated male mice followed by the breeding for the F1 generation. In case of deviant phenotypes, these are tested for inheritance, which, in case of a phenotype confirmation, finally end with the establishment of mutant lines and their backcrossing, respectively. Due to the fact that at a certain phase of the project, all breeding schemes run in parallel with a given cage capacity, the implementation and organization of standardized breeding schemes with a clear order of breeding types, allocated numbers and defined time frames were needed in order to use the capacities of the animal facility as efficient as possible.

3.3.1 Sterility testing

For sterility testing, each ENU treated male was crossed to a wild-type female between 5 to 7 weeks after the last injection in order to ensure that only those offspring, which derived from exposed spermatogonial stem cell stages, were analysed for mutant phenotypes. The maturation period from stem cell spermatogonia to mature spermatozoa in mice was determined by Oakberg in 1956 (Oakberg, 1956) with 49-51 days. The sterility period is dependent on successful repopulation of spermatogonia in the basal lamina of the seminiferous tubules. Female mice used in sterility tests that became older than six months without any conceptions were replaced in order to exclude a fertility problem from the female. Since a co-linearity of sterility period and mutation frequency in ENU treated male mice was assumed, we included only those F1 offspring for phenotyping, which derived from calculated first conceptions of more than eighty days after injection. With regard to the upper cut off, ENU treated males with a sterility period of more than 280 days were excluded as well.

3.3.2 F1 breeding for the dominant screen

The breeding scheme for the production of dominant phenotypes is shown in **Figure 2**. Fertile ENU treated males with a tested sterility period of minimum eighty days were crossed to wild-type females in a one-to-one mating producing F1 animals, which were assumed to carry heterozygous mutations. If necessary, the F1 production was adapted to the requested production of 80 to 100 F1 mice per week by using a rotation breeding system: A single male was weekly crossed to a new group of two females and after seven weeks, coming back to the first group of females beginning a new cycle. The number of offspring was limited to 50 F1 animals per ENU treated male.

3.3.3 Dominant confirmation cross and maintenance breeding

F1 animals showing a variant phenotype were mated to a wild-type animal producing G2 offspring, thus testing the inheritance of the mutant phenotype, also called dominant confirmation cross (CC). Twenty G2 offspring animals were collected and assessed for the phenotype of interest. This number

is valid for a probability of $p = 0.001$ for dominant mutations. The mutation was confirmed if at least one of the offspring displays the mutant phenotype. Establishment of new dominant mutant lines were carried out by out-crossing affected heterozygous animals to the original inbred strain. In order to save each mutant line that was not immediately further analyzed the spermatozoa of three to six affected male mice were preserved in liquid N₂, which was performed by the cryo-preservation group of the Institute of Experimental Genetics.

For a number of mutant lines that were further characterized, semi-dominant mutations were determined by crossing two affected heterozygous animals producing homozygous animals (not shown). If there was a visible or measurable difference in the severity of the phenotype between heterozygous and homozygous animals, a semi-dominant trait was concluded.

3.3.4 G3 breeding for the recessive screen

For G3 production, a strategy using F1 male mice as pedigree founders was used. The numbers shown in **Figure 2** are valid for obtaining recessive mutations with a probability of $p = 0.005$. For selecting F1 males as micro-pedigree founders, the following criteria were considered:

1. A male F1 animal was expected to carry heterozygous mutations but should not display an obvious or measurable dominant phenotype to avoid overlapping dominant and recessive phenotypes.
2. Additionally, each F1 founder should derive from a different ENU treated G0 male in order to obtain a large variety of recessive phenotypes.

For G3 production, a male F1 founder was crossed to four wild-type females producing G2 offspring. Only female G2 animals were collected here. Eight G2 females, from which 50% were presumed to be heterozygous and 50% as wild type, were crossed back to the F1 founder producing 20 G3 offspring, which were to be assessed for recessive phenotypes. Only the crossings with the heterozygous G2 female mice produced 25% of homozygous G3 offspring. According to our capacities for 50 permanent micro-pedigrees, 4 to 6 recessive families were set up and replaced every two weeks thus producing on average 100 micro-pedigrees with approximately 2000 G3 offspring per year or 40 G3 offspring per week.

3.3.5 Recessive confirmation crosses and maintenance breeding

Inheritance of a recessive mutant phenotype was tested by different breeding schemes. If the F1 male is still fertile, an assumed homozygous G3 female was crossed back to the heterozygous F1 male in order to generate G4 offspring. At least ten G4 offspring were collected for phenotyping. An assumed homozygous G3 male was crossed to a wild-type animal producing heterozygous G4 offspring. One of the G4 females was crossed back to the homozygous G3 male in order to produce G5 offspring. At least ten G5 animals were collected for phenotyping. If the G2 mother is still fertile, an assumed G3 male was crossed back to the G2 female (mother) producing G4 offspring. At least 10 G4 offspring were collected for phenotyping.

In all other standard situations, an assumed homozygous G3 animal was crossed to a wild-type animal producing heterozygous G4 offspring. Two G4xG4 intercrosses were set up in order to produce G5 offspring. At least twenty G5 animals were collected for phenotyping. This number is valid for a mutation with a full penetrance resulting in 25% of the expected phenotype. The mutation was confirmed if at least one of the offspring displayed the mutant phenotype.

A new recessive mutant line was maintained by crossing two affected homozygous animals (if possible) or by at least ten out-/inter-crossing steps in order to receive an isogenic recessive mutant line. In order to test recessive mutants with regard to their fertility, affected homozygous male and female mice were crossed to the original wild-type background in parallel. If they were homozygous, it can happen that one of the genders was not fertile. Then it was necessary to switch to a homozygote x heterozygote-breeding strategy.

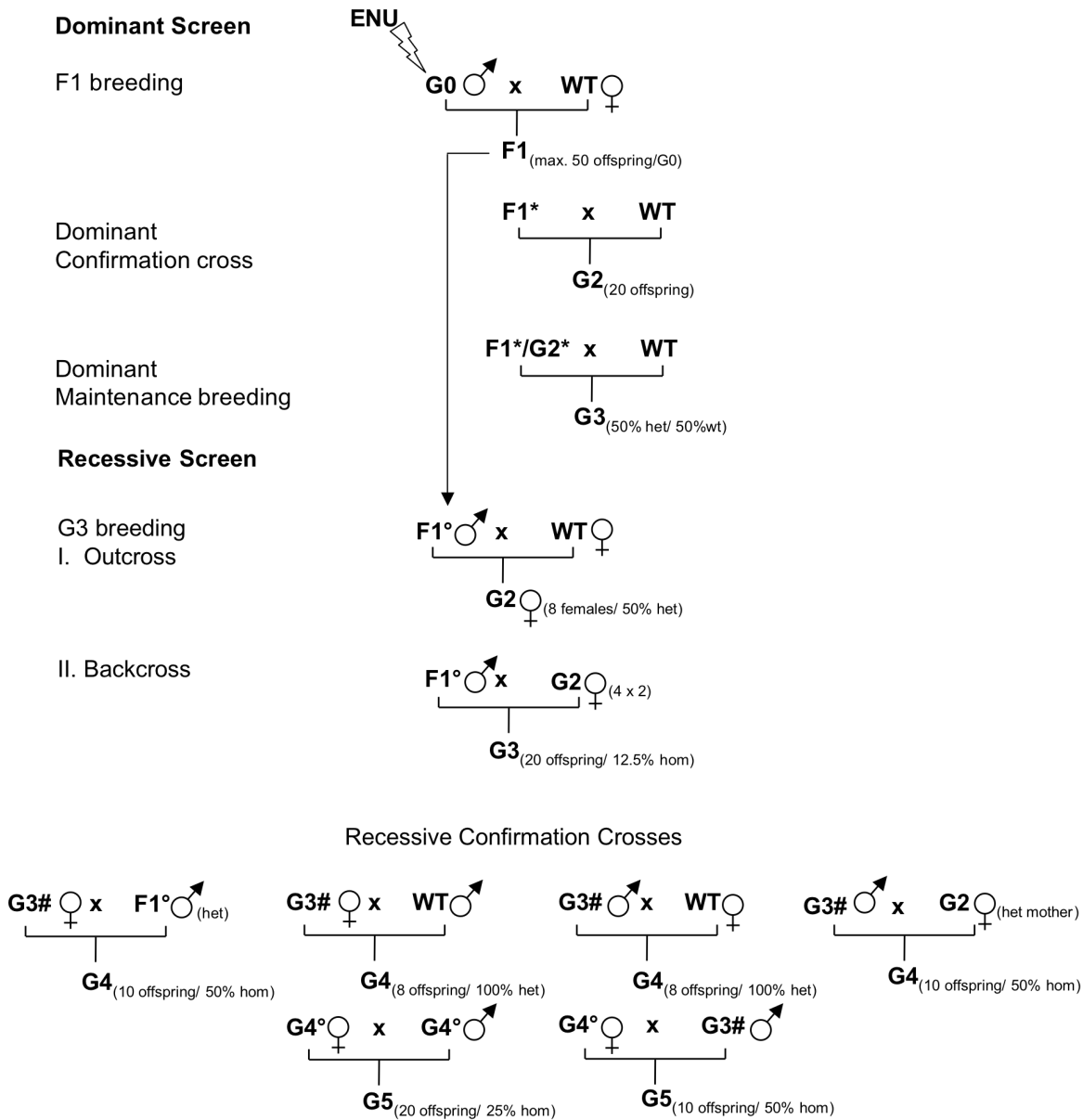


Figure 2 Breeding schemes implemented for the ENU mouse mutagenesis screen. The upper part of the figure shows the breeding scheme for the dominant screen: ENU treated male mice (G0) are crossed to wild-type females producing heterozygous F1 animals that are subjected to a panel of phenotyping procedures in order to isolate dominant mutant phenotypes. If an abnormal phenotype occurs, the inheritance of the dominant phenotype is tested in a confirmation cross by crossing an F1* animal to a wild-type mouse. If the phenotype is confirmed in at least one G2 offspring the novel mutant line is established by out-crossing affected heterozygous animals to wild-type animals in order to obtain an isogenic mutant line. The lower part of the figure shows the breeding schemes for the recessive screen using male F1 founders: male F1 founders for recessive families, which should not carry an obvious dominant phenotype (F1°), are first crossed out to a wild-type animal. Only female G2 offspring, from which 50% are heterozygous for the mutation, are collected. These are crossed back to the F1 male in order to generate 20 G3 animals that are assessed for recessive phenotypes. Only about 12.5% of the G3 offspring are homozygous. If an abnormal phenotype occurs (G3#) the inheritance of the phenotype is tested in confirmation crosses. As soon as the recessive phenotype is confirmed the mutant line is established either by crossing homozygous G5 animals or by ten repeated out-/inter-crossing steps in order to receive an isogenic recessive mutant line (*not shown*). (*: Heterozygous animal with a phenotype; ○: heterozygous animal without a phenotype; #: homozygous animal with a phenotype)

3.3.6 SLT test

The specific locus test developed by W.L. Russel in 1951 (Russell, 1951) was used to determine the optimal ENU regime for the C3Heb/FeJ strain in regard to sterility and mutation rate. For this purpose, 20 male mice treated with a certain concentration of ENU and with a minimum sterility period of 7 weeks were crossed to female mice of the Tester-stock. The homozygous Tester-stock was constructed for seven recessive, viable mutations affecting easily recognizable external traits: a (non-agouti, Chr. 2), b (brown, Chr. 4, tyrosine related protein I), c (chinchilla at albino, Chr. 7, tyrosinase), d (dilute, Chr. 9, myosine 5a), p (pink-eyed dilution, Chr. 7), s (piebald spotting, chr. 14, endothelin-B receptor) and se (short ear, chr. 9, bone morphogenetic protein 5). The mutation rate was determined by scoring the visible phenotypes in the offspring generation. Four different regimes were tested (1x160, 3x80, 4 x100, 1x200mg/kg bodyweight) for the determination of the respective mutation rate.

3.4 Workflow management

Due to the scale of this mutagenesis project a number of important biological and structural aspects had to be considered for the implementation and organisation:

- The large number of animals and different breeding types to deal with,
- The number and types of parameters to be assessed in one animal
- The number of screens involved considering their screening capacities
- Limited cage capacities for animal treatment, breeding, phenotyping, and personnel

With regard to the given conditions, an efficient workflow management was necessary in order to structure and optimize all procedures in such a large-scale project. A selection of implemented workflows that turned out to be useful and efficient are presented in the following section considering the breeding management, phenotyping procedure, the recording system and standard operation protocols (SOP) for selected working steps, such as the interaction between the core facility/screeners.

3.4.1 Breeding management

The conditions of this large-scale project with a defined number of cage capacities, a given number of F1 animals and micro-pedigrees to be generated as well as the number of participating groups made it necessary to structure and optimize as many working steps as possible. Since the core facility did not only conduct the F1/G3 production but also all necessary breeding steps for subsequent analysis, this included the maintenance of mutant lines, if the line was further analyzed, as well as the backcrossing of mutant lines for further linkage analysis/ mutation detection. The breeding management had to fulfil the following targets/ tasks:

- Maintenance of wild type stock colonies of inbred strains to provide animals for ENU treatment, for baseline animals, breeding for F1/ G3 generation, wild type mating partners for confirmation crosses, maintenance as well as backcrossing of mutant lines,
- An ENU breeding colony with a continuous production of 50-100 F1 offspring per week
- A G3 breeding colony with 60-120 micro-pedigrees per year and 20 G3 per MP,
- Confirmation crosses of dominant and recessive variants requested by the participating screeners,
- Maintenance of mutant lines for further phenotypic characterization
- Backcrossing of mutant lines for linkage analysis/ mutation detection.

Room	Project	Racks	Breeding types
26	ENU	10	ENU-breeding
25	ENU	4 IVC	Inbred strains stock colonies
24	ENU	4 IVC	Inbred strains C3H, B6, Balb/c, CAS, 129SvJ
23	ENU	1	F1 offspring (NGFN)
		3	F1 offspring (DHGP)
		2	G2 offspring
		3	Dominant Confirmation Crosses
		1	F1/ mutant males for spermfreezing
22	ENU	10	G3 production (NGFN)
21	ENU	10	G3 production (DHGP)
20	ENU	10	Recessive Confirmation Crosses (max. 64)
19	ENU	10	Recessive Confirmation Crosses (max. 64)
18	ENU	10	Backcrosses (max. 5 in parallel)
17	ENU	10	Backcrosses (max. 5 in parallel)
16	ENU	10	New mutant lines for maintenance
15	DYS	10	Dysmorphology mutant lines (max. 50 lines)
14	Sens.Screen	10	129SvJDIII isogen breeding
			ENU breeding
			F1 offspring
			Confirmation Crosses
13	Sens.Screen	10	129SvJDIII isogen breeding
			ENU breeding
			F1 offspring
			Confirmation Crosses
12	K. A.	5	ALI and CTA lines
	S. W.	3	RCO-Lines, ALI line
	D. S.	2	ALI lines
11	MouseExpress	5 (10)	Mutant Lines für MouseExpress
	ENU	5	Baseline animals

Table 4 Occupancy overview of the core facility with all breeding types used in the project. The ENU breeding room consisted of at least three injection batches of approximately 100 ENU-treated single-caged male mice each, from which one group was still in sterility testing and two mainly producing F1 animals. The inbred strain stock colonies were held in individual ventilated cages (IVC) in order to permanently maintain SPF animals in case of infections and in order to minimize loss of time. All wild type animals for F1/ G3 generation, dominant and recessive confirmation crosses, mutant line maintenance and backcrossing were recruited by the internal inbred strain stock colonies. F1 female animals were discarded latest after 21 weeks of age and male F1 were subjected to sperm freezing. Each recessive micro-pedigree was calculated with an occupancy period of 11 weeks for G2 generation and 16 weeks for G3 generation/ screening. For each confirmation cross, at least 15 G2 (for dominant variants) or 20 G4/G5 offspring (for recessive variants) were generated; if at least one offspring displayed the mutant phenotype, a mutant line was supposed to be confirmed. Maintenance of mutant lines was only considered if the lines were further characterized; if not, the spermatozoa of at least five mutant males were preserved in liquid nitrogen. For backcrossing with C57/BL6, 50-100 out-/backcross or out-/intercross offspring were generated for rough chromosomal mapping. For fine mapping and the generation on additional N2 animals the breeding was supposed to be continued by the scientist in charge.

Table 4 shows an overview of the occupancy of the animal facility for the various breeding types at a certain period of this thesis. The plan had been constantly adapted according to internal inquiries and was optimized according to the objectives of the project.

One of the most important issues and as an example for the necessity of breeding management was the workflow for confirmation crosses, since the efficiency of this part was the basis for the successful generation of novel mutant lines. The workflow presented in Figure 3 is representative for the management of the majority of breeding types used and turned out to be stringent and successful under the given conditions with regard to the turnover of deviant F1/G3 animals that were subjected to confirmation crosses.

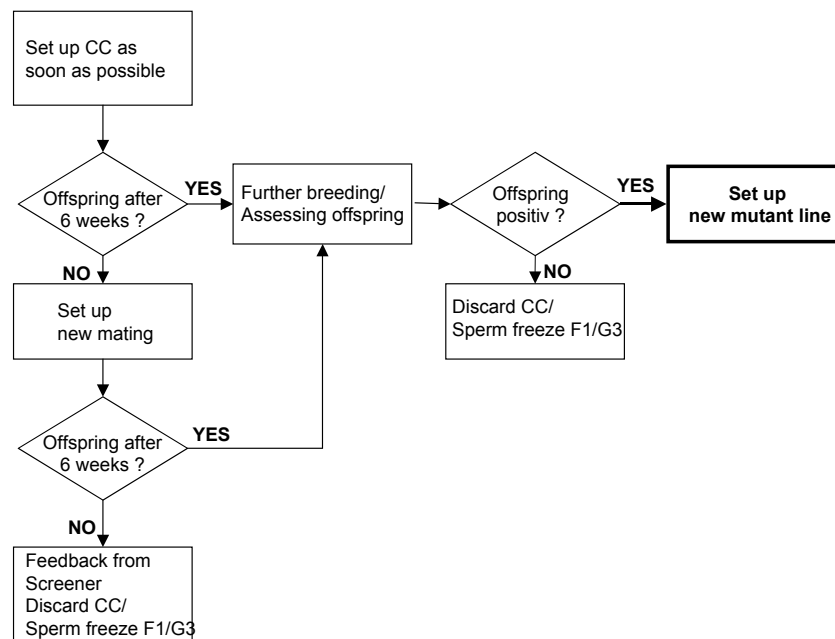


Figure 3. Breeding management of the confirmation crosses (CC). Two trials per confirmation cross were considered with a time window of six weeks in between. In case of two failed crosses, the breeding was stopped and spermatozoa of male mice were preserved in liquid nitrogen. In case that the crosses succeeded, the offspring were tested for the phenotype of interest. If at least one pup displayed the mutant phenotype it was regarded as a confirmation and the establishment of a novel mutant line.

The following points were considered in the breeding management:

- In order to avoid breeding/fertility problems the confirmation cross is set up as soon as possible after all screens having sent their feedback. In optimal cases, the animals are less than 5 months of age.
- After six weeks, it has to be checked whether offspring had been born. If not, the wild type breeding partner has to be replaced to exclude a fertility problem of the wild type animal.
- After another six weeks, it has to be checked whether offspring had been born. If not and after receiving feedback from the screener this breeding is stopped and the F1/G3 animal is discarded in case of a female or, in case of a male, the spermatozoa are cryo-preserved.

- In case that offspring had been born, they are assessed for the phenotype of interest. At least 15 offspring are generated and analysed. In case that none of them show the phenotype they are discarded, the breeding is stopped and the F1/G3 animal is discarded in case of a female or, in case of a male, the spermatozoa are cryo-preserved. In case that at least one of the descendants displays the phenotype, a new mutant line is confirmed. The positive tested animals are subjected to further breeding.

3.5 Primary Screening and Phenotyping

An appropriate workflow to obtain a comprehensive phenotyping procedure, which covers a broad range of clinical parameters, was developed and optimized according to the technical equipment and physical operations to which a single animal could be maximally subjected. All methods used in this study, either base on standard and general clinical examinations, were successfully applied to other rodents or were especially developed for this study. Common criteria appropriate for their use in a high-throughput manner were robustness of the parameters and simplicity of their performance. Moreover, all methods were non-invasive in order to minimize the stress for the animals. The order and time course of screening procedures was arranged by the core facility in a manner that each individual analysis could be regarded as independent measurement without influence or interference of other parameters due to behavioural or physiological alterations caused by previous analyses. All screens used in this study are described in the following section. In Figure 4, the workflow of the phenotyping procedure is shown in more detail. Additionally to the main screening procedures, phenotype analyses of descendants deriving from confirmation crosses and mutant line maintenance were performed under the same conditions and time points to confirm and ensure the stability of the phenotypes. In some cases, the mutant phenotype was lost in the course of the breeding due to segregation of mutant loci involved; in those cases, at least two (or more) causative mutations at different loci were considered.

3.5.1 Phenotyping workflow

At the age of 3 weeks, F1 / G3 animals were weaned, weighed and examined the first time for dysmorphological alterations. A biopsy of the tail tip was taken for further investigation in the Sex Reversal screen; the blood drops from the wound were collected on a filter, dried for at least three hours and subjected to the analysis for biochemical metabolites. In a four-week interval, body weight of the F1/ G3 mice was repeatedly determined. At the age of eight weeks the F1/ G3 mice were subjected to the modified hole board for the evaluation of the behavioural profile of the animals. In the 11th week, mice were examined a second time for obvious dysmorphologies in more detail. At the age of 12-14 weeks, a blood sample of approximately 500 µl was taken by retro-orbital puncture after ether anaesthesia, collected into heparinized sample tubes and separated into cellular components of the blood and plasma by centrifuging the samples for 10 Min. at 8000 rpm. Another 50µl blood was collected in EDTA coated tubes for basic hematology. The cell and plasma samples were

distributed for further investigation of clinical chemical, hematological, immunological, and mitochondrial parameters according to the scheme shown in fig. XX. If an additional blood sample was needed for confirmation or due to technical problems, a minimum interval of two weeks had to elapse before the next blood sample was taken. In week 16–18, the hotplate assay was performed to assess the animals for their nociceptive profile.

Animals that displayed a visible or measurable variant phenotype were subjected to inheritance testings. F1/G3 males that did not display a variant phenotype were subjected to cryopreservation of their spermatozoa; female mice were discarded.

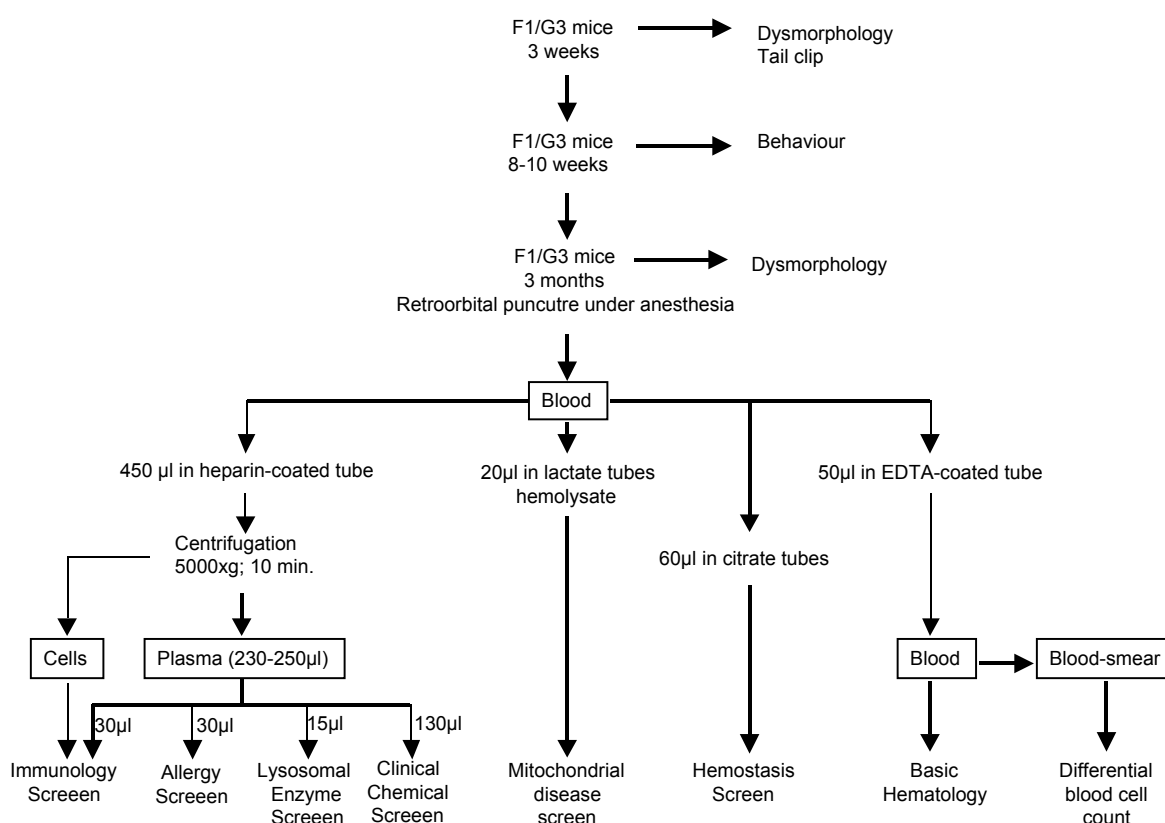


Figure 4. This scheme shows the phenotyping workflow for a single F1 or G3 mouse starting from weaning age to the age of three months. The time course comprised of three main time periods in which each animal was assessed for a broad range of parameters including dysmorphological, behavioural, and blood-based biochemical parameters.

3.5.2 Screens

3.5.2.1 Biochemical Metabolites

(The screen for biochemical metabolites was performed at the Kinderklinik und Kinderpoliklinik im Dr. von Haunerschen Kinderspital, Ludwig-Maximilians-University, Munich)

The dried blood samples 1/8” spots, equivalent to 3 µl of blood, were punched out, and after the addition of a set of 14 stable isotope-labeled internal standards, amino acids and acylcarnitines were

extracted with methanol. The dried residue was derivatized with butanolic hydrochloric acid and subjected to electrospray tandem mass spectrometry analysis.

3.5.2.2 Dymorphology

(The screen for dymorphological alterations were carried out by the members of the Core Facility of the ENU mouse mutagenesis screen (GSF Neuherberg); Dr. H. Fuchs who developed this sceening protocol was responsible for the data analysis and determination of mutant/ variant animals.)

The following procedure was performed with F1/G3 animals at the age of 11 weeks: A cage consisting of five mice was put on a table, and the group of animals was carefully observed without any disturbance. Obvious dymorphologies in coat colour, physical constitution, general behaviour or tail kinks were protocolled. Every single mouse was handled according to the following procedure: first, the animal's identity was determined by identifying its earmark, then the mouse was put on a balance, and the value was recorded. Afterwards the animal was put again on the table and examined from the dorsal side: Alterations in ears, eyes, head shape, and limbs, especially number and shape of digits were registered. In order to examine abnormalities in coat and hair development, the coat was stroked from the back to the front. The repositioning of the hairs to their initial position, hair colour, and hair distribution were observed. In order to detect external abnormalities of the vertebral column, the tail was gently examined along its entire length from the base to the tip with two fingers. Afterwards, the mouse was grasped from the backside to examine the ventral side: coat colour variations were observed; the limbs were examined more intensely; the genitals were checked for abnormalities. Malformations in the ventral and lateral sides of head and body were detected; shape, number and teeth colour were controlled. Subsequently, the mouse was hung at its tail for a few seconds while action and positioning of its legs and body were observed. Then the mouse was dropped into a separate cage from a height of approximately 25-30cm, and its landing behaviour was observed. Finally, the mice were tested for deafness using a clickbox-test by exposing the animals to a short sound of 20,000 Hz normally inducing the Preyer's reflex.

List of all dymorphological parameters:

Body: Body size, body shape, right-left-abnormality, skull shape, whiskers, tooth length, thooth shape, tooth colour, ear size, ear form, eye size, cataracts, limbs, double digits, crippled digits, syndactylism, nails, kinked tail, coiled tail

Physical appearence: General physical condition, weight, coat colour, coat structure, skin colour, skin structure, swellings, carcinoma/ tumors, strength, gait, trembling, cramping, paralysis, seizures, respiration

Behaviour: General behaviour, activity, agressiveness, exploring, head tossing, head shaking, circling, click-box-test, landing behaviour, hanging behaviour, articulation

Environment: Social structure in cage, cage, cleanness, urine, feces

3.5.2.3 Sex Reversal

At weaning age, a biopsy of the tail tip was taken. After DNA extraction a screening for the Sry gene by PCR was performed on all F1/ G3 animals.

(The screening for the Sry gene was performed by Prof. Meitinger at the Insitute of Human Genetics, GSF Neuherberg.)

3.5.2.4 Behaviour

Behavioural parameters were tested using the modified hole board (Ohl et al. 2003), which was enlarged by an additional compartment where the cage mates of the experimental animal were placed during the test period and separated from the test area by a transparent pane. The set up of the modified hole board enabled the detection of a wide range of behaviours: the number and time until the first hole visit (curiosity), number of stretched attends (caution), number of and time until the first board visit (anxiety), number and time at the partition (social behaviour), number of line crossings (locomotor activity), time to object recognition after a training phase of 48-72h (memory). Each animal was tested for 5min in the modified hole board. In order to avoid any stress and disturbances for the animals, the tests were performed only in the morning from 9am-1pm.

(The behavioural screen was performed by Dr. Steckler and Dr. Ohl from the Max Planck Institute for Psychiatry, Munich.)

3.5.2.5 Clinical Chemistry

For the investigation of blood-based parameters, blood samples were taken from 12-14 week old mice, which were fasted overnight by retro-orbital puncturing.

For hematological analysis, a volume of approximately 50µl EDTA-blood was taken and immediately applied to an autoanalyzer (Vet abc™ Animal Blood counter, ABX Diagnostics, 73037 Göppingen, Germany) to analyse basic hematological parameters. Blood smears for a differential blood count were prepared as a second line investigation on mice showing abnormalities of white and red cell counts. Air-dried blood smears were stained according to May-Grünwald-Giemsa, and microscopically analyzed for the distribution of leukocyte subpopulations, pathological cells, and changes of red blood cell morphology.

For the analysis, 17 clinical chemical parameters including various enzyme activities, as well as plasma concentrations of specific substrates and electrolytes, 130µl plasma from Li-heparin blood was diluted 1:2 with aqua dest and analysed by using a Hitachi 717 autoanalyzer and adapted reagents from Roche (Mannheim, Germany) and an Olympus AU400 autoanalyzer (Fa. Olympus, Hamburg, Germany).

All parameters analysed in the clinical chemical screen are listed below:

Basic hematology: White blood cell count (WBC), red blood cell count (RBC), hematocrit (HCT), mean corpuscular volume (MCV), mean corpuscular hemoglobin (MCH), mean corpuscular hemoglobin concentration, (MCHC), platelets (PLT)

Differential blood count: Segmented and not segmented neutrophils (SEG), lymphocytes (LYM), monocytes (MOZ), eosinophils (EOS), basophils (BAS)

Plasma enzymes activities: Alkaline phosphatase (AP), α -Amylase (AMY), Creatine kinase (CK-MB), Aspartate-aminotransferase (AST), Alanine-aminotransferase (AST), Lipase (LIP), Lactate dehydrogenase (LDH)

Plasma concentrations of specific metabolites: Glucose (GLS), Total protein (TP), Uridic acid (HS), Urea (HST), Creatinine (CREA), Transferrin (TRF), Ferritine (FER), Billirubin (BILLI), HDL, LDL, Triglyceride (TG), Cholesterol (CHO), iron (FE), unsaturated iron binding capacity (UIBC), albumin (ALB)

Plasma concentrations of electrolytes: Potassium (KAL), Sodium (NAT), Chloride (CHL), Calcium (CAL), inorganic phosphate (ANP)

(From 1997 to February 2001, analyses of the differential blood counts and clinical chemical parameters were performed by the Krankenhaus Harlaching, Dept. of Clinical Chemistry, Munich. In February 2001, the screening of clinical chemical parameters was taken over by the Clinical Chemistry screen of Prof. Wolf at the German Mouse Clinic (GMC), GSF Neuherberg.)

3.5.2.6 Hemostasis

F1 and G3 offspring of ENU-mutagenized mice were examined using a standardized protocol for clinical signs of bleeding (hematoma and petechia in the skin and in the mucosa of the mouth, hematuria). Moreover, it was searched for signs of reduced organ perfusion (e.g., neurological defects, anuria) potentially caused by hypercoagulability. In parallel, a whole blood method based on the changes in viscoelastic properties of activated blood was employed (thrombelastography, TEG). This procedure allows the separate analysis of different aspects of the hemostatic process (fibrin formation rate (coagulation), determinations of the clot growth rate (indirect estimate for platelet activation), and lysis time (fibrinolysis). In mice anesthetized with ether, 60 µl of venous blood is drawn from the retrobulbar venous plexus. By anticoagulation with citrate, the activation state of the blood sample is stabilized for 1-2 h. The procedure is started by adding 100 µl of a CaCl₂ solution plus 100 µl of a solution containing recombinant TF (and phospholipids). The duration of the assay is 60 min and 8 samples can be measured concomitantly. A variant phenotype will be assigned to those mice showing values more than three standard deviations distant from the mean value.

(The hemostasis screen started in October 2002 and was performed by Prof. Dr. Engelmann, Vaskuläre Biologie und Hämostase, Institut für Klinische Chemie, Klinikum Großhadern der Universität München.)

3.5.2.7 Immunology/ Allergy

For the screening of immunological parameters of blood cell populations and the quantification of the expression levels of selected cell surface proteins by flow cytometry as well as for basal immunoglobulin levels by ELISA, high throughput and semi-automated techniques were developed (Flaswinkel et al. 2000).

For FACS analysis, peripheral blood cells deriving from 500-600ul Li-heparin blood was resuspended; erythrocytes were removed by incubation in 10ml lysis buffer (140mM NH₄Cl/ 17mM Tris, pH 7.2) for 15 min. followed by two washing steps in FACS buffer (PBS/2%FCS/0.01%NaN₃), incubation with 10 µg/ml 4G8 rat anti mouse Fc receptor for 5 min to block Fc receptors and an additional washing step with 300 µl FACS buffer. Finally, the cells were incubated at 4°C for 20 min with 30 µl of the respective antibody combination.

The antibody panel used and the list of respective cell populations analysed during the time from 1997 to 2000 is shown below:

CD4 FITC	CD8 PE	CD19 SR	helper-, cytotoxic T-cells, B-cells
B220 FITC	IgM PE	CD5 SR	B1-, B2-, B-cells, T-cells
IgD FITC	IgM PE	CD19 SR	mature naïve B-cells
B220 FITC	CD45 RA	CD3 Cy5	B-, naïve T-cells subsets, NK-cells, Monocytes
DX5 FITC	CD28 PE	CD28 PE	NK-cells, T-cells
Ly49C FITC	$\gamma\delta$ TCR PE	CD3 ϵ SR	T-cell subpopulations
H-2Kk FITC	β 7 Intergin	CD3 ϵ SR	MHC class I expressing cells, mucosa associated T-cell subsets
λ 1/ λ 2 FITC	κ PE	CD19 SR	B-cell subpopulations
CD21 FITC	CD19 PE	Thy1.2 Cy5	activated granulocytes, DCs, T-, B-cells
I-Ak FITC	CD14 PE	F4/80 Cy5	MHC class II expressing cells, Activated monocytes, granulocytes

In July 2000, the immunology screen was taken over by the immunology screen of the German Mouse Clinic (GSF Neuherberg); due to this reorganisation, new parameters with a new antibody panel were introduced which is shown below. The detailed SOPs of the Immunology screen in the German Mouse Clinic are available on demand via the administration of the GMC.

FL-1 FITC	FL-2 PE	FL-3 Cytochrom	FL4 APC/Cy5
CD5	$\gamma\delta$ TCR	CD19	CD3
IgD	Gr-1	B220	CD11b
DX5	MHC-II	CD3	
CD103 CD25	CD8 α	CD3	
CD62L CD45RA	CD4	CD3	
Ly6C	CD8 β	CD4	CD44

Basal immunoglobulin levels were determined by using sandwich ELISAs specific for IgM, IgG1, IgG2a, IgG3, IgA and IgE. The ELISA plates were first coated with the respective rat anti mouse antibody (70 μ l, 5-10 mg/ml PBS) and incubated overnight at 4°C; uncoated positions were blocked by addition of 200 μ l PBS/1% BSA/0.01%NaN₃ for 30 min. Mouse plasma was individually diluted for each isotope and incubated for 1h at RT. All samples and standards were adjusted to 200 μ l per assay, and all values were determined in duplicates. Detection was based on AP-conjugated isotype-specific rat anti-mouse antibodies except for IgA, where goat anti-mouse serum was used.

For the detection of total IgE levels the following variation was used: the blocking reaction was performed by using 50mM Tris pH7.4/1% Tween 20/ 3% BSA and the detection was based on biotin-conjugated rat anti-mouse IgE followed by strepavidin-peroxidase and tetramethylbenzidien as substrate. Values of basal immunoglobulin levels were obtained using an ELISA reader.

(The screen for immunological parameters was performed by Prof. Pfeffer at the Institute of Microbiology and Immunology of the Technical University Munich from 1997 to June 2000. In July 2000, the screen was taken over and performed by the Immunology screen of Prof. Busch at the GMC.)

3.5.2.8 Lysosomal Enzymes

The lysosomal enzyme screen obtained 15 µl plasma for the determination of the following lysosomal enzymes: β-Hexosaminidase, α-Glucuronidase, β-Mannosidase and Sulfatases. The enzyme activities were determined based on sensitive detection assays of fluorescent substrates.

(The lysosomal enzyme screen was performed by Prof. Peters at the University of Freiburg.)

3.5.2.9 Mitochondrial screen

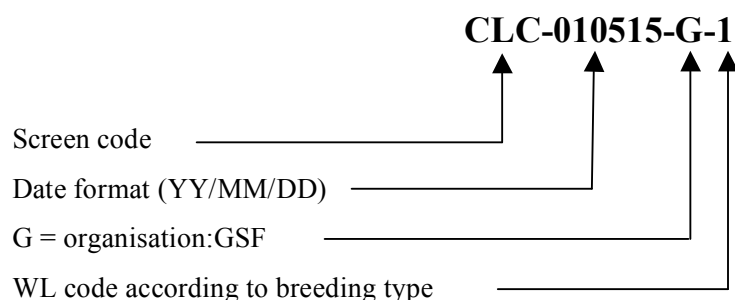
In order to obtain lactate levels, 20 µl of the Li-heparin blood sample was freshly taken by using a standardised glass capillary and immediately applied to a lactate tube (Eppendorf, Hamburg, Germany) and inverted five times until the lysate was completely diluted. The samples were analysed using an autoanalyser for lactate levels (Eppendorf, Hamburg, Germany). As a second line analysis, histology and histochemistry of muscle biopsies deriving from offsprings of a variant founder animal were performed.

(The mitochondrial screen was performed by Dr. Klopstock, Institute of Neurology, Ludwig-Maximilians-University, Munich from 1997 to 2001. In the year 2002, Dr. Klopstock joined the GMC and established the Neurology Screen.)

3.5.3 Recording system

All relevant data points of each individual mouse in this project were recorded in the animal management system (AMS) of a database called MouseNet (Pargent et al., 2000), which included a unique 8-digit identification number, earmark, strain, sex, day of birth, parents IDs, the location of a mouse including the source area, room, rack, and cage number as well as line information such as the line code, dominance of the line, line type, line owner, and mating type. With the support of MouseNet queries, it was possible to pre-select the appropriate groups of animals according to their age and breeding type that were compiled to pre-defined working lists (WL) that, in parallel, represent a record for every single sampling procedure. Due to logistical and organisational reasons, the working lists were sub-grouped into the primary screening lists for F1 and G3 animals or according to the screens involved, the different breeding types as well as the sample types, encoded by a defined combination numbers or letters (that are summarized in the table below). Each list was indicated with a working list name encoding the screen, the date, the organisation, and the breeding type.

For example:



WL code	Breeding types
1	Primary F1 screening
2	2 nd samples from dominant breeding
3	Primary G3 screening
4	2 nd samples from recessive breeding
C	Dominant confirmation cross
E	Mutant line descendant
R	Recessive confirmation cross
B1	Backcross 1 descendant
B2	Backcross 2 descendant

Every week, data of all F1/ G3 animals and other animals that had to be analysed were pre-selected and compiled in working lists for sample taking/phenotyping. The working lists included the mouse ID, ear mark, cage number, strain, sex, day of birth, day and start/end time of sample taking, initials of operator(s), sample type, amount/volume, remarks (i.e. vial type, sample condition). The operators ticked off every single sampling/ phenotyping and recorded each changing from the original list (i.e. not enough material, sample skipped/ postponed, animal died etc.) before a final version of the working list was generated.

These final working lists, including all animal information and sample records, were sent together with the samples to all participating screens.

3.5.4 Interaction Core Facility/ Screeners

In the beginning of the project, it was determined that all nine participating screening groups would have the same access to the pool of samples and animals for the isolation of mutant phenotypes. Due to the implemented phenotyping procedure the time frame of the workflow covered approximately 17 weeks before the F1/G3 animals were subjected to further breeding.

In order to minimize conflicts of interest and optimize the screening workflow, the following rules were implemented for an efficient interaction between core facility and screeners as well as among the screeners:

- Feedback from screeners is requested two weeks after the measurements latest. Animals that are phenotypically not deviant are declared as wild type.
- Only those animals that are declared as wild type from all screeners were cryopreserved (males) or discarded (females).
- If a second measurement/ blood sampling is requested a minimal period of two weeks had to elapse.
- Multiple requests from different screens for a single animal must be considered and compiled.
- As soon as a screen announced a F1/ G3 animal for a confirmation cross, this animal was defined as a (potential) founder for a line with a preliminary line ID, a line description, the parameter and

the screen as line owner in the database. In case of multiple phenotypes, the first screen giving feedback is assigned as line owner.

- A number of 15 to 20 descendants of this founder were analysed for the parameter of interest to determine the inheritance of the abnormal phenotype. F1/G3 females with a deviant phenotype and older than 6 months were not considered for a confirmation cross.
- As soon as one of the descendants displayed the same phenotype in two independent analyses the mutant phenotype was confirmed and the line obtained an internal name for the database consisting of three letters and three digits given by the screener.

3.6 Mapping of the ENU induced mutation

3.6.1 Strategies for genetic mapping of dominant and recessive mutations

In order to determine the localisation of a dominant mutation (with full penetrance) an out-backcross strategy was used by crossing affected mutant C3HeB/FeJ mice, which are assumed to be heterozygous for the mutation, to wildtype C57BL/6J mice. The N1 generation was screened for the phenotype of interest, out of which 50% should theoretically display the phenotype, and only affected animals were selected for further breeding. Affected N1 animals were again crossed back to wildtype C57BL/6J mice producing N2 animals, which were again screened for the phenotype of interest. Biopsies of the tail and spleen were taken from the N2 animals and either stored at -20°C or -80°C (for long-term storage) or for DNA preparation.

To determine the localisation of a recessive mutation an out-intercross strategy was selected by using affected mutant C3HeB/FeJ mice, which are assumed to be homozygous for the mutation, to wildtype C57BL/6J mice. According to Mendelian law, all N1 animals were heterozygous and could be intercrossed by brother-sister mating producing F2 offspring, which were screened for the phenotype of interest. Only from the affected animals, which came out with about 25%, biopsies of tail and spleen were taken and stored at -20°C for later DNA preparation.

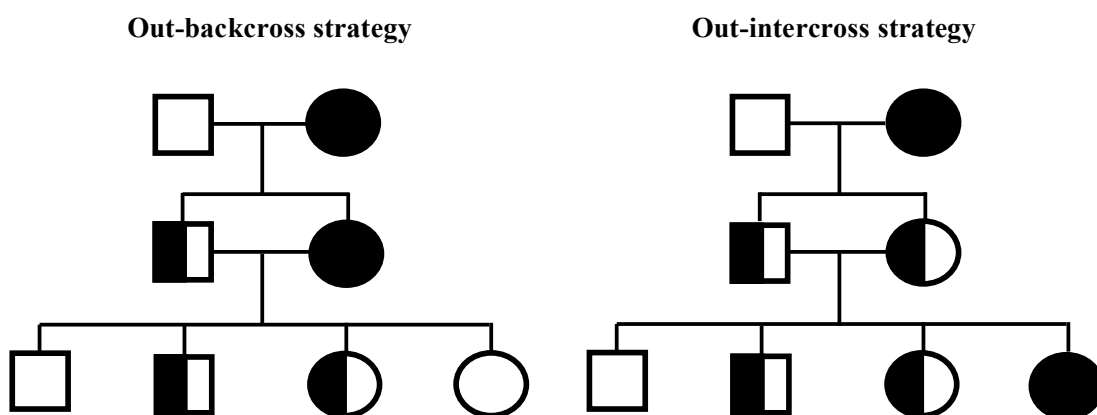


Figure 5 Genetic mapping. A backcross strategy is preferred if the mutant allele is fully dominant or if the mutant allele is recessive and homozygotes are fertile. The intercross strategy is preferred if the mutation is recessive and the homozygous animals are not fertile or if the mutation is semi-dominant and the $+/+$, $M/+$ and M/M individuals have different phenotypes, which can be easily detected.

3.6.2 DNA isolation from mouse tissue

A tail biopsy of approximately 0.5 cm or 10 mg of other tissue was taken for DNA preparation. DNA extraction was performed with Genra Puregene Kit according to the manufacturer's instructions and recommendations. DNA was dissolved in TE buffer (10mM Tris, pH7.2, 1 mM EDTA) and stored at 4°C.

DNA concentration was determined by absorption spectrophotometry on a Beckman DU® Life Science UV/Vis (Beckman, Germany). DNA solution was diluted 1:50 in H₂O dest and measured at a wavelength of $\lambda = 260\text{nm}$ (for DNA) and 280nm (for protein) against H₂O dest.

DNA concentration was calculated according to the following formula:

$$(\text{OD}_{260} \times 50 \times \text{dilution factor}) : 1000 = \text{concentration in mg/ml}$$

The yield was obtained by multiplication of concentration and volume of the DNA solution. The quotient of OD₂₆₀ and OD₂₈₀ of a purified DNA sample should be near to 2.0, whereas protein contamination increases the absorption at $\lambda = 280\text{nm}$.

3.6.3 Linkage analysis – Candidate gene approach

The rough mapping of ENU induced mutations was performed by linkage analysis with microsatellite markers which were polymorphic for the mouse strains used in this study (C3Heb/FeJ and C57BL/6J). The differences of microsatellites are indicated by length polymorphisms of repetitive and non-coding stretches of genomic mouse DNA (100-500 bp), and which are characteristic for each mouse strain. A minimal length difference of 4 base pairs was presumed, which can be technically resolved and visualized in a standard 3% agarose gel. A panel of 70 microsatellites distributed over the entire mouse genome was routinely used at our Institute resulting in a resolution of approximately 5-10 cM, which reflects a distance of 10 to 20 Mbp in the mouse genome. Primer sequences for microsatellites are available under <http://www.informatics.jax.org>. As a program for the analyses of linkage data in this study Map manager (Manly et al., 2001) was used.

Later on, the rough mapping was performed using a SNP mapping platform established and offered as a service at the Institute of Experimental Genetics. It is based on the combination of single nucleotide polymorphisms (SNP) as molecular markers of the different mouse strains and their determination by using MALDI-TOF mass spectrometry (Sequenom). The SNP markers were selected in 15Mbp intervals covering the entire genome, and resulting in a resolution appropriate for further strategies of candidate gene approach or positional cloning. Sequences of primers for mouse SNPs are available under <http://www.genome.wi.mit.edu/SNP/mouse/>. For fine mapping the region of interest, further microsatellite markers were selected in order to narrow down the region, in which the mutation is presumably localized.

At this stage of a candidate gene approach, and in parallel to the fine mapping, searches for potential candidate genes in mouse databases such as www.informatics.jox.org and www.ncbi.nlm.nih.gov describing genes and phenotypes, which might be connected to a mutant mouse line were performed.

Genes that are suitable to the mutant mouse phenotype were further subjected to sequencing in order to determine and confirm the induced molecular alterations.

Microsatellite primers for rough mapping

chr.	marker	5' primer (up)	3' primer (low)
D1	231	ACCCACAATTGCCTGTGG	GTCTTTGCAAGCCACCAAT
D1	245	TGGTTACACAAGTCCAATACCG	GGCCCAGGTCTATAAATAAGCC
D1	181	AGCCACAGCCATCTACAAC	AAACCATGTTCTGGGATTCCG
D1	26	GAGGAATCTTGAATGGGCAA	CTGACAACACCCTCTGGCTT
D1	227	TAACAAGTGAAGTCCATGGGC	AGGGGAGACAGGGACAGG
D1	362	TGTGTGACTGCTTGGAAGATG	CTGAGTCCCTAAAGTTGTCCTTG
D2	237	TTCCAAGTCACCTATTATCAAAAGG	TTGATACGGACACCAGCAAA
D2	249	GGCCTTTCCAACTCAATCAA	CTGAGAAGGGAGTCTCGGTG
D2	48	GCTCTGCAGAAGATGCTGC	GCTGAGACGCAGAGTCGC
D2	226	TTTTTGCAACTTTGTAAAGAATCC	AAAAACACCCTCCCACCCTT
D3	60	GACATCCTGGGCAACATTG	GGTGTGTTTGCTGTTGCTG
D3	101	CCTCTAGATGCATACATGTGCC	GGTCAAGTTAAGTGTATTTTTTCCC
D3	257	CCTAGCGCAGGAATAGTTAACC	ACAAACAGAACAAAACAAAAAGTCC
D3	19	CAGCCAGAGAGGAGCTGTCT	GAACATTGGGGTGTTTGCTT
D4	108	TCAGCCATCTCTATCAGGTGG	CCAATGTCAGATAATGCTTATGAG
D4	187	AGGTCTTAAGCCCTTTCTCCC	GGAGGGGAATTCAGGAACAT
D4	189	CACTACACGGGGCTGAGATT	AAGATCCAACACCCTTTTTGG
D5	148	GCTGCAAAGAAGAGAGAGGG	CCTCTGGCCAGCATGATATA
D5	135	TACACAGGAAAAGGACAGGG	AGGGAGATTTGGATTAGAGGC
D5	18	CTGTAGTGGGTGGTTTTAAAATTG	ATGCCACTGGTGCTCTCTG
D5	138	AGACAGTTACCTTCTCCCAAGG	TGTTTTCTCCCTTCTGCCATC
D6	204	TTCAAAACACAGATGGCCTG	CAGCCAGCAAGTCTGAGC
D6	146	CATCTGCTTAGGGAAATTTGC	TGGGTGTCAACACCACCTAA
D6	201	TGCTTCCTCTCTGCTGTAAGC	AACTAAGGCCAGTACTGAAAAGTACA
D7	76	CATGAGCACGTGGAGAAAGA	CGTGGAACCTGATAAACTGA
D7	230	GGGTAACTGCTTTTTAAAAGTGC	ACTTCTGCATGTTGCCCTCT
D7	238	GCATCTGCTTTTCTGCCTCT	AGGCACCTGACATTGACCTC
D8	4	CCAACTCATCCCCAAAGGTA	GTATGTTCAAGGCTGGGCAT
D8	249	AAACTCACACACAGAGACAACA	GCCCCAGTGTGACTAAGGAG
D8	215	AATACACAAGGTTGGCCTCA	ATGTGTGGATATTCATGTGCTC
D9	224	AATAAATGAATGCTTACAGGAGCA	TGGGGCTCAGAAAATGATTC
D9	104	TTAATTGAGACGCACCTTTGGG	AGGGGTATTAGAGTTGGGG
D9	130	TCAATTTATTGTTGCAGTTGGC	AACACAGCATGAGATGGATACG
D9	12	ATTCAAGGGGCAGTACACAT	TGGTCTGGTAAAATCGCT
D10	189	TGTGTAGGTATGTGTGTCATAGG	ATCAGACAGCACCTGGGAAC
D10	44	CCACCTTAGACAGTTACATGGC	CCACGCCACGCTTACTTCT
D10	42	GCATTCAGAAGCTGGAAGG	TGCCACAGCATGTTTAAAGG
D10	180	GACCTTCCTTTATACACAAGTCATAGC	GTGGTACAGAACTTAGGTGTTAATTG
D11	2	TCCCAGAGGTCTCCAAGACA	CCACAGTGTGTGATGTCTTC
D11	307	TTGAAGATTGAATGGTGGCA	TTCGAGGAGACAGGACACG
D11	349	AGTATCAGAAGATCCAGTTGGAGG	GTAGAAAAAGATACCAGTGTGAGC
D11	245	ATGAGACCATGCTCCTCCAC	TTGTCTCTGACCTTCACACC
D11	301	AATAGTCTCATCGGGTTAAACAGC	AAGTAGACTGATGTGAGGCTAAGTACC
D12	136	TTTAATTTTGAAGTGGGTTTGGC	TTGCTACATGTACTGATCTCCA
D12	68	TTGCATGATGAGATGTTTTCTATG	GACATCATGCCCCCTAGTTT
D12	101	GCTTTTCCTTATCAAGATATGCG	GCAGCAGAAAAGAGAGGGAAA
D13	3	TCAGGCTCATCCCAGATACC	TTTTGCAGAGAACACACACC
D13	126	ACTTTGACACCTTTTCTCAGTTCC	TGGGATTAAGCAGACATACAGG
D13	262	CTGCGGCTGTAGGTTAAGTATG	AGGCTGCTGCTAACAGATGG
D14	49	TTCCTGAATAAAAAGACTCCTCG	TCCTTTACTTGGTGTACGTCTGC
D14	5	CACATGAACAGAGGGGCAG	GTCATGAAGTGCCACCTTT
D14	185	TCAATTTGGGTTTCTCTTCC	GATCCAGAAGTGTGACTGG
D15	111	GTTTCAGAAGGCAATGTCTGG	GCTCAGTGTCTAATCTGACTCC
D15	209	TTGTGCTTCACTAGATGTAGACCA	TTTTATAGTTGCACATAAGCAGCA
D15	42	ACCCTGAACCTGACAAGTGG	TCCTACGGGACAGGAAAGG
D16	165	AAATCAGTTGGCTCTATTAGTTGG	AATGTAACCCTAAGTCTCTCTC
D16	12	GAACCTCAGTAAGCTCTCTATGCCC	GGAGGACTAGCAGCTAGAGC
D16	13	TTAGAACTCAGTAAGCTCTC	CTTAAACAGGCACNAATCCCATT

D16	152	AGAGACCTCTGGGGTGGG	TTCAAGATAGACTATTCTGGAAAAAGC
D17	34	TGTTGGAGCTGAATACACGC	GGTCCTTGTTTATCCCAGTACC
D17	238	TACTCCTTCCTCAACACAATACTAATT	AATGTGCTCATGCATACATGC
D17	187	TTACCTCCCAACACCTACGC	GCCATTGTTTTAAAAATCCACC
D18	70	CTGCTAGCGTTACCATATAGCC	CTGTGGTCTCCAGCCAC
D18	124	CCCAAATGGGGTGTCTTTTA	CTGCCACACATTTGTGTGTATG
D18	153	GCACTTCTGCTTACAAGGCC	CAGGAGTGCAAAGGTACATGA
D19	117	GGAACTAGCAGACTGTAGAAGAAGC	CTCCAGTCTTAGATTTGTTTTTTCC
D19	11	TCAAAGTCAAGGTGGGCAG	ACTTCCAGATGTTGGGCAC
D19	1	AATCCTTGTTCACTCTATCAAGGC	CATGAAGAGTCCAGTAGAAACCTC

Microsatellite primers for ALI3/9/12/19 fine mapping

chr.	marker	5' primer (up)	3' primer (low)
D13	76	ATGCACCTGTCTAAATGTGTGC	AGAGGGACTGTGGGACTGTG
D13	224	TTGTGTGTGTCTGTCTGTCTG	CCCCTTGATGGAGGAGAAA
D13	24	TGCATGACTGTGTAATGCTTTG	GAAGAAGTGGGAAACTGAGG
D13	26	GCCATGCATGACTGTGTAATG	CAGTCTACTGGTCTCACACGG
D13	10	AGTCCTGCCATTTGCCTCTGACC	ATGTCTTAGTCTCACATGCTGGGG
D13	248	TAAAGTAGAAGGCAGCATGAGTG	ACCCAAATGTTTTGGATCCA
D13	139	AGAATAAGTCAAGGCTATGATGTGG	TTGTTTGTGTTTGAAGTAGAACG
D13	124	CTGTTTAAATATGGGGGAGAGG	TGACAAACCAATCTTTCAGGC
D13	140	CAATTTGCAGTCTTTGTAGTAAA	AACTGCCAAAAGTAACTTGAGG
D13	64	CCTCAGCACCAAAAAGGAC	ACATCAGTGACCAGGCATCA
D13	3	TCAGGCTCATCCCAGATACC	TTTTGCAGAGAACACACACC
D13	254	TCCAAGAATCTTGAACATATTTGTG	GGGAAATTCAGTTATATAATCA
D13	13	CTGTGGTAAGTCCAGATTG	GGAAAGAGTAGGAAGATGCC
D13	231	GCACGGAGGGAGAAATGTAA	GTACTTAGGGACTCTTCAGCGTG
D13	65	AGCAACAAGTTCAGAATGATGC	CCACATACAGCCACACATCTG
D13	14	GGAACAGCAAGCTCTAAGGG	CTACCAGGCTCCCAAGATA

Microsatellite primers for ALI037 fine mapping

chr.	marker	5' primer (up)	3' primer (low)
D9	10	CCAAAGGACTGCTATTTGCG	GTAATATTGTACACTCATGCACA
D9	18	TCACTGTAGCCCAGAGCAGT	CCTGTTGTCAACACCTGATG
D9	328	CATTACTGTCTCTCTTCATTCTCTG	CTTACATCTGGTCCACAAGAAGG
D9	182	GTGAAATTGGTTATGTAAATGTCTGA	GAGATGACTAGGGTGAAGTGGG
D9	205	AATAGCCTACTCTGGATTACAGG	TACCTTCTCCTCTTTGGTTTTG
D9	227	CCAACATGACTGTTTGTGGC	TATTGTAATGATGATGATGATGATGG
D9	130	TCAATTTATTGTTGCAGTTGGC	AACACAGCATGAGATGGATACG
D9	95	TGGGAGTAAATGTGTCAAGACA	GTAAAATGGAAGGATCAGAGTGTG
D9	298	AGTTTGTGTGCAAGGCAGTG	AAAACGAAAAGAATGAGAAGTATGTG
D9	154	CTGGCTCCTGTAAACATATTGG	AGTGTAAGTTGGCATTCCCTCA
D9	256	CTTGCTCACCCTTCTCTATG	CATTTGCACAACTATCCATGC
D9	171	GTTTGTCTTTTGTGTTGTTGTTG	AGGTATGTAGACTCCTTACTCATCTGG

PCR reaction

The amplification of specific DNA fragments such as for microsatellites was performed with polymerase chain reaction (PCR) in a volume of 20ul.

Solutions:

10x PCR buffer: 166mM (NH₄)SO₄, 670mM Tris-HCl pH 8.8, 1mg/ml BSA

1x PCR reaction:

12.7 µl H₂O (Ampuwa)
2.0 µl 15m MgCl₂
2.0 µl 10x PCR buffer
1.0 µl 10pM forward primer
1.0 µl 10pM reverse primer
0.2 µl 10mM dNTP
0.1 µl Taq Polymerase (5U/µl)
1.0 µl DNA sample (10-100ng/µl)

PCR program:

2 min 94°C
(35 cycles)
20 sec 94°C
30 sec 55°C
30 sec 72°C
(final step)
5 min 72°C

PCR products were analysed on a 3% TBE agarose gel.

3.6.4 Sequencing

Sequencing was either performed by MWG Biotech AG (Ebersberg, Germany) or by the internal sequencing service of the institute (GAC) using BigDye Terminator v3.1 Cycle Sequencing Kit (AB Applied Biosystems). For this purpose, overlapping amplicons of an approximate length of 500 to 1000 base pairs were sequenced and subsequently reassembled and analyzed.

1x sequencing reaction:

1.75µl 5x Sequencing buffer
0.5µl BigDye v. 3.1
5.20µl H₂O MQ
1.0µl forward primer (10pM)
1.0µl reverse primer (10pM)
add Xµl ≈ 5-20ng DNA template

PCR conditions:

1min 95 °C
(40 cycles)

5sec	95 °C
10sec	50 °C
4min	60 °C (Final step) ∞ 4 °C

Ethanol precipitation:

10µl sample
 2.5µl 125mM EDTA, spin (EDTA has to reach bottom of tube)
 30µl EtOH

Incubated for 15 min, at RT (darkness)

Centrifuged for 30 min, 2000-3000 g, 4°C or 2500 50 min 4°C

Washed 1x with 40 µl 70 % EtOH (no centrifugation needed)

Resuspended in 30 µl H₂O (HPLC-grade from Merck - needed for sequencer)

Applied to sequencer according to the manufacturer's instructions.

3.6.5 Sequence analysis software

The sequenced fragments were reassembled and analyzed using CodonCode Aligner (CodonCode Corporation, Dedham, Maine, USA) and Sequencher 4.5 (Gene Codes Corporation, Ann Arbor, Michigan, USA).

3.7 Phenotypic characterization

3.7.1 X-ray analysis

X-ray analysis was carried out using a MX-20 Specimen Radiography System (Faxitron X-ray Cooperation, Wheeling USA) combined with EZ 40 X-ray scanner (NTB GmbH, Dickel, Germany).

3.7.2 Skeletal preparation

Skeletal preparations were performed with the alcian blue/alizarin red method, which stains cartilage in blue and calcified tissue, containing Calcium, in red.

Neonatal or adult mice were sacrificed; all internal organs and skin were removed. The samples were fixed in 100% EtOH and shaken gently for five days. For fat extraction the EtOH was replaced by acetone for another 3-4 days. After rinsing the samples with H₂O they were stained with the alcian blue/alizarin red staining solution (1 volume 0.3% alcian blue in 70%, 1 volume 0.1% alizarin red in 95% EtOH, 1 volume 100% acetic acid, 17 volumes 100% EtOH). The staining procedure was visually controlled and could take between 10-12 days for neonatal mice up to 2-4 weeks for adult mice. After rinsing the samples with H₂O the samples were incubated in 1%KOH in 20% glycerine at 37°C for 5-8 hours, afterwards at RT until all tissue was removed; the destaining solution was replaced after visual control every week. Residual tissue was cleared by storing the samples in 50%, 80% and finally in 100% glycerine (clearance could take between weeks to months).

Solutions:

Alcian blue 0,3% 1.5g Alcian blue/ 500ml 70% EtOH; shake over night
 Alizarin red 0,1% 0,5g Alizarin red/ 500ml 95% EthOH; shake over night

3.7.3 Sperm analysis

Sperm analyses were performed by the cryotechnology group of the Institute of Experimental Genetics, GSF Neuherberg, on a sperm analyser (IVOS, Parallabs, Worcester, MA, USA), which measured the concentration, motility and progressivity of spermatozoa from wildtype and mutant mice. For this purpose male mice were sacrificed, and the cauda epididymis was prepared to isolate the spermatozoa.

(Protokoll)

3.7.4 Histology

Histological analyses were in part (embedding and sections) performed in cooperation with the Institute of Pathology, GSF, Neuherberg. Collected organs were fixed in 4% formalin, embedded in paraffin and 7µm-thick sections were subsequently prepared by standard hematoxylin and eosin (HE) staining. Stained sections were analyzed by light microscopy with indicated magnifications.

3.7.5 Immunohistochemistry

Immunostaining of paraffin sections with CyclinD1, p27 and PCNA were carried out using the Vectastain Kit (Vector Laboratories, Burlingame, CA, USA). The tissue sections were first deparaffinized by 2x 5min xylol and rehydrated by treating the sections 2 x 5min in 100% EtOH, 1 x 5min in 95% EtOH, 1 x 5min in 75% EtOH and 1 x 5min ddH₂O and subsequently rinsed under tap water. Afterwards, they were first incubated for 45min in 0.3% H₂O₂ and then placed for 4min in boiling 10mM citrate buffer in order to reveal the epitopes. To block unspecific binding of the antibody the sections were incubated for 20 min in diluted normal blocking serum (150µl of normal blocking serum (yellow label) to 10ml of TBS buffer). After blotting excess serum from the sections they were incubated for 1h with 400µl of the primary antibody diluted in TBS buffer (CyclinD1 1:50, p27 1:50, PCNA 1:50). Afterwards they were washed for 5 min in TBS buffer before another incubation step for 1h with 400µl diluted biotinylated secondary antibody solution (1:2000 in diluted blocking serum) followed by another washing step for 5 min in TBS buffer. The sections were then incubated in 400 µl Vectastain Elite ABC Reagent for 30 min (the reagent was prepared before according to the manufacturer's instructions) and again washed for 5 min in TBS buffer before being stained with 400 µl DAB staining solution until a specific staining was visible. The sections were rinsed under tap water and then counterstained for 30sec with Hematoxylin solution.

Stained sections were analysed by light microscopy with indicated magnifications.

Solutions:

Citrate buffer

TBS buffer

DAB staining solution: dissolve one tablet of UREA in 5ml H₂O, then dissolve one tablet of DAB reagent (Sigma #D-4293) in the same solution.

3.8 Expression analysis

3.8.1 Genotyping ALI037

The determination of the ALI037 specific genotype was carried out by a combined amplification of a genomic region including exon 7 resulting in a 1512 bp-PCR product. A following BbsI-digestion (#) of this fragment resulted in three DNA fragments of 848bp, 409bp and 255bp indicating the wild-type allele. Due to the missing second BbsI site the mutant allele displayed two DNA fragments of 848bp and 664bp, respectively.

Primers used for ALI037 genotyping:

Forward primer ATATCCCAGAGTCCCAGGGTTC

Reverse primer CCCTGTGTGAATGAGCAAAC

1x PCR reaction carried out in 20µl volumes:

12.7 µl	H ₂ O (Ampuwa)
2.0 µl	15m MgCl ₂
2.0 µl	10x PCR buffer
1.0 µl	10pM forward primer
1.0 µl	10pM reverse primer
0.2 µl	10mM dNTP
0.1 µl	Taq Polymerase (5U/µl)
1.0 µl	DNA sample (10-100ng/µl)

PCR program:

2 min	94°C
(35 cycles)	
30 sec	94°C
30 sec	59°C
1min 45 sec	72°C
(final step)	
5 min	72°C
1x BbsI-digestion:	
3 µl	10x enzyme-specific buffer (buffer G, Fermentas)
6.7 µl	H ₂ O (Ampuwa)
0.3 µl	BbsI = Bpil (Fermentas)

The enzyme reaction was performed for 2 h at 37°C in a moisture chamber. The DNA fragments were analysed in a 1.25% TBE agarose gel.

3.8.1.1 Generation of mouse embryos

For RNA in situ hybridisation, mouse embryos at a stage of 10.5 dpc to 12.5 dpc, which derived from timed matings, were mainly used. For this purpose, crosses were set up between 4 pm and 5 pm in the afternoon. In the morning, between 9 am and 11 am, the female mice were checked for a vaginal plug presuming an embryonic stage of 0.5 dpc of the developing embryos. On the defined day, the pregnant female mice were sacrificed by cervical dislocation, and the uterus horns containing the embryos were placed in ice-cold PBS/DEPC (150mM NaCl, 15mM sodium phosphate buffer pH 7.3 in 0.01% DEPC/ H₂O) buffer for at least one hour. Afterwards, embryo preparation was performed in PBS/ DEPC under RNase-free conditions. Since the phenotype was not obvious at this developmental stage, the yolk-sacs of all embryos were collected for further genotyping analysis.

For further RNA in situ hybridization, the embryos were fixed over night at 4°C in 4% PFA and then dehydrated in 25%, 50% 75% and 100% MetOH in PBS/DEPC for each 10min. The embryos were then bleached for 1h at 4°C in a 1:6 dilution of a 30% hydrogen-peroxide solution (H₂O₂), washed 2x5 min in 100% MetOH in PBS/DEPC and stored at -20°C for further use.

Solutions:

PBS/DEPC buffer: 150mM NaCl, 15mM sodium phosphate buffer pH 7.3 in 0.01% DEPC/ H₂O

3.8.1.2 DNA extraction from mouse embryonic yolk-sacs

Due to the small amount of material from mouse embryonic yolk sacs, DNA extraction was performed with QIAMP®DNA Mini Kit (QIAGEN, Hilden, Germany) according to the manufacturer's instructions. All DNA samples were stored in TE buffer (10mM Tris, pH 7.2, 1mM EDTA).

3.8.1.3 RNA extraction

The isolation of total RNA from mouse tissue was performed using the RNeasy Midi Kit (QIAGEN, Hilden, Germany) according to the manufacturer's instructions. The concentration of the yielded RNA was determined according to the determination of DNA concentration see under 2.6.2. RNA concentration was calculated according to the formula: (OD₂₆₀ x 40 x dilution factor) : 1000 = concentration in mg/ml.

3.8.1.4 cDNA synthesis

To obtain cDNA from total RNA SuperScript II RT (Invitrogen) was utilized. The reactions were performed in 20 µl volumes with 1-5 ng of total RNA according to the manufacturer's instructions.

3.8.2 Working with bacteria

3.8.2.1 Media for bacterial culture

All media for bacterial culture were autoclaved for 20 min at 121°C. To generate media for agarose plates, 1.5% (w/v) agarose was added before autoclaving.

LB-medium (modified after Bertani, 1951): 10 g caseinhydrolysate, 5 g yeast extract, 4 g NaCl ad to 1l with H₂O bidest, pH7.4

SOC-medium (Sambrook et al., 1989): 2 g tryptone, 0.5 g yeast extract, 0.2 g MgCl₂ x 6 H₂O, 0.25 g MgSO₄ x 7 H₂O, 0.36g glucose ad to 0.1l with H₂O bidest

Supplements, which were heat-sensitive, such as ampicillin (100µg/ml) and kanamycin (30µg/ml), were sterile filtered and added after equilibration to 45°C (for LB-agarose plates) or before inoculation of liquid media.

3.8.2.2 Bacterial stocks and their maintenance

Bacterial stocks used in his study were the Escherichia coli K12 substrains XL1-blue, XL10 and DH5α.

The bacterial stocks were maintained on agarose plates at 4°C (for up to 3 months). For this purpose, LB-amp-agarose plates (1.5% agarose, 100µg/ml ampicillin in LB medium) were inoculated by single colonies and incubated overnight at 37°C. The plates were sealed with parafilm (America National Can, Chicago, USA) and stored at 4°C. The other method was the maintenance in glycerol stocks at -80°C for long-term storage. For this purpose, 5ml of LB medium (containing 100µg/ml ampicillin or 30µg/ml kanamycin) was inoculated with single colonies and incubated overnight at 37°C. 500µl of the bacterial culture were added to 500ml of 80% sterile glycerol in Nunc Cryo Tube™ Vials (Merck, Bruchsal), gently mixed by inverting and stored at -80°C.

3.8.2.3 Generation of chemically competent E.coli cells

The generation of chemically competent E. coli cells was carried out according to the protocol of Nishimura et al. 1990.

100ml of medium A was inoculated either with a single colony or 0.5ml culture. The bacteria were cultured at 37°C in a shaking incubator to a mid log growth phase, which was photometrically determined at OD600 with a value between 0.4 and 0.8. The culture medium was subsequently kept on ice for 10 min and then centrifuged for 10min with 1500x g at 4°C. The cell pellet was re-suspended in 1ml of pre-cooled medium A on ice; then, 5ml of medium B (36% glycerol, 12% PEG (MW7500), 12mM MgSO₄·7H₂O added to LB and sterilized through filtration) was added. The suspension was divided into 100µl aliquots, shock frozen and stored at -80°C.

Solutions:

LB-medium (modified after Bertani, 1951): 10g caseinhydrolysate, 5g yeast extract, 4g NaCl add to 1l with H₂O bidest, pH7.4

Medium A: LB supplemented with 10mM MgSO₄·7H₂O and 0.2% Glucose

Medium B: 36% glycerol, 12% PEG (MW7500), 12mM MgSO₄·7H₂O added to LB and sterilized through filtration

3.8.2.4 Transformation of competent E. coli cells

The multiplication of plasmid DNA was carried out by transformation and culturing in E. coli cells. The majority of plasmid DNA samples were stored in TE buffer (10mM Tris, pH7.2, 1mM EDTA). cDNA clones from other laboratories were sometimes shipped as filter-spots and were then diluted and re-suspended in 100-200µl TE buffer (10mM Tris, pH7.2, 1mM EDTA).

10µl of plasmid solution were added to 50 µl of competent E. coli cells, mixed gently by inverting and then incubated for 30 min on ice. The cells were then exposed to a heat-shock for exactly 30 sec at 42°C and then immediately transferred on ice for 2 min. 250µl of SOC medium (2g tryptone, 0.5 g yeast extract, 0.2 g MgCl₂ x 6 H₂O, 0.25 g MgSO₄ x 7 H₂O, 0.36g glucose ad to 0.1l with H₂O bidest), pre-warmed to room temperature, was added to the cells and incubated for one hour at 37°C by shaking at 200 rpm. 10-50µl of the cell suspension was spread on pre-warmed LB-amp-agarose plates (1.5% agarose, 100µg/ml ampicillin in LB medium) which were subsequently incubated overnight at 37°C. The next day 10-12 colonies were picked and further cultured for clone analysis.

Solutions:

LB-amp-agarose: 1.5% agarose, 100µg/ml ampicillin in LB medium

TE buffer: 10mM Tris, pH 7.2, 1mM EDTA

SOC-medium (Sambrook et al., 1989): 2g tryptone, 0.5 g yeast extract, 0.2 g MgCl₂ x 6 H₂O, 0.25 g MgSO₄ x 7 H₂O, 0.36g glucose ad to 0.11 with H₂O bidest

3.8.2.5 Cloning of PCR products

In order to introduce Taq polymerase-amplified PCR products into a vector the TOPO TA Cloning Kit containing the plasmid vector pCRII-TOPO and chemically competent TOP10 cells (#K4600-01, Invitrogen) was used. Between 0.5 and 4 µl fresh PCR product was applied for each cloning reaction, which was performed according to the manufacturer's instruction. After the cloning reaction and transformation in TOP10 cells, 10-50 µl from each transformation was spread on a selective agarose plate.

3.8.2.6 Plasmid maxi preparation

To obtain a sufficient amount of plasmid DNA a maxi preparation from the bacterial stock of interest was carried out using GenElute HP Plasmid MaxiprepKit (#NA0310, Sigma-Aldrich, USA).

For this purpose a pre-culture was set up by inoculating 5ml of LB-medium (100µg/ml ampicillin in LB medium) with 10 µl of glycerol stock and pre-incubation for 5h at 37°C and 200 rpm. Afterwards, 500µl of this bacterial suspension was added to 150 ml LB-medium (100µg/ml ampicillin in LB medium) and incubated overnight at 37°C and 200 rpm. The next day, DNA was prepared using GenElute HP Plasmid Maxiprep Kit (#NA0310, Sigma-Aldrich, USA) according to the manufacturer's instructions. The yielded DNA concentration was determined by absorption spectrophotometry. The DNA was diluted 1:50 in H₂O dest and measured at a wavelength of $\lambda = 260$ nm (for DNA) and 280 nm (for protein) against H₂O dest.

Solutions:

LB-medium (modified after Bertani, 1951): 10 g caseinhydrolysate, 5 g yeast extract, 4 g NaCl ad to 1l with H₂O bidest, pH7.4

3.8.3 Whole mount in situ hybridisation

The whole mount in situ hybridisation in mouse embryos was based on the detection of mRNA expression with a digoxigenin-labelled cDNA probe. The successful hybridisation was visualized by applying an alkaline phosphatase-conjugated anti-digoxigenin antibody and a following enzymatic reaction of alkaline phosphatase, in which its substrate resulted in a dark violet staining.

3.8.3.1 Labelling the riboprobe

For the generation of riboprobes, 10µg of template DNA was linearized with the respective restriction enzyme. In order to remove all residuals of the enzymatic reaction, the DNA was purified using a QIAquick spin column (#28304, QIAGEN) in an end volume of 30 µl, yielding approximately 330ng/µl DNA. For the labeling reaction following components were mixed and subsequently incubated for 2 h at 37°C:

10 µl DNA
 3 µl dd H₂O (AmPuWa)
 2 µl TS-buffer (#, Company)
 2 µl rNTPs DigMix (#, Company)
 1 µl RNase inhibitor (#, Company)
 2 µl RNA-polymerase (depends on template-DNA: T7, Sp6, T3) (Roche)

The labelling product was optionally checked on a 1% agarose gel for 5 min at 300V. Remaining double-stranded DNA was removed by an incubation step with 2µl DNase for 15 min at 37°C. The riboprobe was then purified with a QIAGEN RNeasy Mini Kit (#74106, QIAGEN), finally resolved in 50 µl Ampuwa and immediately stabilized with 1µl RNase-inhibitor (Roche). The riboprobes could be stored at -20°C for several months. The labeling product was checked on a 1% agarose gel for 5min at 300V under visual control.

3.8.3.2 Hybridization

The fixed embryos stored in 100% MetOH were re-hydrated through a series of 75%, 50% and 25% MetOH/PBS steps of 10min each. (If not indicated, all described steps were carried out on ice.) The samples were then washed in freshly prepared in PBT for 2x 10min and 1 x 5min followed by a washing step for 10min in RIPA buffer without shaking and 2 x 5 min in a large volume of PBT without shaking. The samples were subsequently fixed for 20min with 4% PFA/0,2% glutaraldehyde in PBT and then washed 2 x 5min with PBT.

A 1:1 mixture of hybe-buffer/PBT was set up, and the samples were incubated for 10 min at RT and for another 10min in hybe-buffer alone. The embryos were sorted out according to the applied probes and pre-hybridized with tRNA/hybe-buffer (100µg/ml) for 3h at 68°C. Shortly before the hybridization step, the probes were denatured for 3 min at 90°C, diluted 1:100 in the pre-hybridization-buffer (tRNA/hybe-buffer (100µg/ml)) and then applied to the samples overnight at 68°C.

3.8.3.3 Removal of unbound probe and antibody

The next day, the probes were carefully removed, and the embryos were washed 2 x 30min with 65°C preheated hybe-buffer at 65°C and let cool down to RT. Afterwards, the samples were applied to washing steps with hybe-buffer/RNase solution (1:1 mixture) for 5min and another 5min with RNase solution followed by an 1h incubation at 37°C with RNase solution containing 100µg/ml RNase A. Then, the embryos were washed in a 1:1 mixture of RNase solution/(SSC/FA/Tween20) for 5min at RT and then transferred to SSC/FA/Tween20 alone and heated up to 65°C. The washing steps in SSC/FA/Tween20 at 65°C were repeatedly carried out for 2 x 5min, 3 x 10min and 5 x 30min. Afterwards, the samples were equilibrated to RT and washed for 1 x 5min in a 1:10 mixture of (SSC/FA/Tween20)/1x TBST, for 2x 10min at RT in 1x TBST, for 2 x 10min in MABT and finally incubated for 1h at RT in 10% blocking solution/MABT. Before the actual antibody reaction, the DIG-antibodies (1:5000 -dilution) were pre-absorbed for 1h at 4°C in 1% blocking solution and

then applied to the samples overnight at 4°C. In order to remove the antibody, the samples were repeatedly washed with TBST for 3 x 5min and 8 x 1h at RT (can be optionally varied and extended).

3.8.3.4 Staining

For the staining reaction, the samples were washed for 4h in TBST and 2 x 5min in freshly made alkaline phosphatase buffer at RT and then stained in staining solution overnight at 4°C in the dark. The staining was visually controlled under the microscope and optionally continued until a clear dark blue/ violet staining was visible. The staining procedure was stopped by fixing the embryos overnight in 4% PFA in PBS at 4°C in which they could be stored for several months.

3.8.3.5 Solutions

All solutions used before and for hybridization had to be absolutely RNase-free: all RNase-free solutions were prepared using DEPC and autoclaved; Tris buffer could not be prepared with DEPC and was therefore autoclaved twice.

DEPC-H2O	0.01% DEPC (50 µl in 500ml H2O), mix strongly incubated overnight at RT under fume hood and autoclaved 3 x 20min
PBS	30 ml 5 M NaCl 15 ml 1 M Na-phosphate buffer pH 7.3 Filled up to 1 l with DEPC-H2O
4% PFA/PBS	4 g PFA 100 ml 1x PBS-DEPC add few drops of 10N NaOH and heated up to 55°C until PFA was dissolved; subsequently cooled on ice, adjusted to pH7 with HCl
PBT	PBS with 0,1% Tween20
tRNA	10 µg/µl in DEPC-H2O Phenolized 2x and stored as aliquots at -20°C
Proteinase K buffer	10 ml Tris-HCl (pH 7) 1 ml 0,5 M EDTA Filled up to 500 ml with H2O
PBT/glycine (make fresh)	2 mg/ml glycine in PBT
RIPA	DEPC-H2O, NaCl, and EDTA; 2,5 ml 10% SDS 15 ml 5 M NaCl 5 ml NP40 25 ml 10% Deoxycholate 1 ml 0,5 M EDTA 25 ml 1 M Tris-HCl pH 8.0 Filled up to 500 ml DEPC-H2O
4% PFA/0,2% glutaraldehyde in PBT	4% PFA/PBT Added 400 µl 25% glutaraldehyde, added to 50 ml PBT
Deionized formamide	10 g BioRad Ag501-X8 in 100 ml formamide Stirred for 1 hr, filtrated and stored at -80°C
20x SSC	17,53 g NaCl 8,82 g NaCitrate Dissolved in 80 ml DEPC-H2O pH was adjusted with a few drops of conc. HCl to pH 7

	Added to 100 ml DEPC-H ₂ O and autoclaved
Heparin	100 mg/ml Heparin (Sigma H3149) in DEPC
Citric acid	1M in DEPC-H ₂ O
Hybe buffer	5 ml deionized formamide 2,5 ml 20x SSC 5 µl heparin solution 10 µl Tween 20 2,05 ml DEPC-H ₂ O Adjusted to pH 6 with 1 M Citric acid (ca. 450 µl/10ml)
SSC/FA/Tween20	5 ml 20x SSC 25 ml formamide 50 µl Tween20 Added to 50 ml with H ₂ O
10x TBST	8 g NaCl 0,2 g KCl 25 ml 1M Tris-HCl pH 7.5 10 ml Tween20 Added to 100 ml with H ₂ O
RNase solution	1 ml 5 M NaCl 100 µl 1 M Tris-HCl pH 7.5 10 µl Tween20 8,89 ml H ₂ O
RNase A	RNase A (Sigma R4875) dissolved at 10 µg/µl in 0,01M NaAc (pH 5.2) Heated to 100°C for 15 min, equilibrated to RT Adjust to pH 7.4 by adding 0,1 vol. of 1 M Tris-HCl pH Aliquots stored at -20°C
MAB	11,6 g maleic acid (f.c. 0,1 mol/l) 8,8 g NaCl (f.c. 0,15 mol/l) 800 ml H ₂ O Adjusted to pH 7.5 with solid NaOH, filled up to 1l with H ₂ O
MABT	MAB + 0,1% Tween20
Blocking stock solution	Blocking reagent (Roche Diagnostics - Boehringer) dissolved in MAB to a f.c. of 10% (w/v) autoclaved (add 0,1 % Tween20 afterwards) and stored as aliquots at -20°C
DigAb coupled to AP	Boehringer
TBST/Levamisole	2 mM Levamisole in TBST
Alkaline phosphatase buffer (make fresh)	1 ml 5 M NaCl 2,5 ml 1 M MgCl ₂ 50 µl Tween20 5 ml 1 M Tris-HCl pH 9.5 2 mM Levamisole, filled up to 50 ml with H ₂ O
Staining solution	Boehringer BM purple Ap substrate (#1442074) 2 mM Levamisole 0,1% Tween20 Centrifuged, only the supernatant was used

3.9 Databases

3.9.1 MouseNet

The MouseNet database was used for the organisation and management of the mouse colony in area B of the GSF animal facility. It consisted of an animal management system based on a Sybase system

representing a relational database. MouseNet was especially developed for this mutagenesis project due to the necessity to handle large numbers of animals and phenotyping data. Due to the structure of the mutagenesis experiments, it was necessary to introduce unique ID numbers for each individual animal as an eight-digit number. For each individual mouse a set of additional data were stored such as earmark, date of birth, strain, generation, treatments, weights, locations (room, cage) during its lifespan, the history of matings, IDs of ancestors and offspring, and line information. After the implementation of a number of query functions, it was possible

- To determine sterility periods of ENU treated males
- To trace back the founders of a mutant phenotype in a pedigree,
- To follow the breeding schemes used for a specific mutant line, or
- To get an overview about the mutant phenotypes generated so far.

3.9.2 Map viewer

Map viewer developed by NCBI (<http://www.ncbi.nlm.nih.gov/projects/mapview/>) is a database for genomes of different species with annotated genes/gene products and the links to respective other databases for genes, transcripts, proteins other phenotypes and alleles or literature. Map viewer was the starting point for all candidate gene strategies performed in this study.

3.9.3 ClustalW for homology studies. Domain studies

ClustalW2 is a general purpose multiple sequence alignment program for DNA or proteins (<http://www.ebi.ac.uk/Tools/clustalw2/index.html>). In this work ClustalW was utilized for homology studies by multiple sequence alignments and calculating the best match for the selected sequences.

3.9.4 PhosphoSite

PhosphoSite provides an accurate and comprehensive source of information about mammalian protein phosphorylation sites (<http://www.phosphosite.org/homeAction.do>). This database helps to identify and organize information about all in vivo phosphorylation sites in human and mouse proteomes and to provide information and resources facilitating phosphorylation research.

3.10 Chemicals and Reagents

All chemical and reagents used in the experimental procedures of this work were purchased from the following companies:

Reagents	Supplier
1-Nitroso-1-ethylurea	Serva, Heidelberg, Germany
Acetic acid	Merck, Darmstadt, Germany
Aceton	Merck, Darmstadt, Germany
Agarose (ultra Pure)	Gibco-BRL Life Technologies/ Invitrogen
Alcian blue	Sigma, Taufkirchen, Germany
Alizarin red	Sigma, Taufkirchen, Germany
AMPUWA-Water	Fresenius
BbsI	Fermentas

BigDye Terminator v3.1 cycle sequencing kit	AB Applied Biosystems
BSA / Albumine, Bovine Fraction V	Sigma, Taufkirchen, Germany
Citric acid	Sigma, Taufkirchen, Germany
cyclin D1 rabbit polyclonal	Santa Cruz Biotechnology
Deoxycholate	Sigma, Taufkirchen, Germany
di-amino-benzidine (DAB)	Sigma, Taufkirchen, Germany
Diethyl Pyrocarbonate (DEPC)	Sigma, Taufkirchen, Germany
Di-Potassiumhydrogenphosphate dihydrate	Merck, Darmstadt, Germany
Di-Sodiumhydrogenphosphate dihydrate GR	Merck, Darmstadt, Germany
DNA preparation kit	Genra
Easy-A PCR Clonig Enzyme	Stratagene
EDTA	Sigma, Taufkirchen, Germany
Eosin Y	Sigma, Taufkirchen, Germany
Ethanol (EtOH)	Merck, Darmstadt, Germany
Formamide	Sigma, Taufkirchen, Germany
Glutaraldehyde	Sigma, Taufkirchen, Germany
Glycerine	Merck, Darmstadt, Germany
Glycine	Sigma, Taufkirchen, Germany
Hematoxilin sol. Harris	Sigma, Taufkirchen, Germany
Heparin	Sigma, Taufkirchen, Germany
Herculase	Stratagene
KH ₂ PO ₄	Merck, Darmstadt, Germany
Magnesium chloride (MgCl ₂)	Merck, Darmstadt, Germany
Maleic acid	Merck, Darmstadt, Germany
Methanol	Merck, Darmstadt, Germany
Na ₂ HPO ₂ x 2 H ₂ O	Merck, Darmstadt, Germany
NP40	Sigma, Taufkirchen, Germany
Nucleotide Removal Kit	Qiagen, Hilden, Germany
Nucleotides (dATP, dTTP, dGTP, dCTP)	Fermentas
Oligo(d)T	Gibco-BRL Life Technologies/ Invitrogen
p27 rabbit polyclonal	Santa Cruz Biotechnology
Paraformaldehyde	Sigma, Taufkirchen, Germany
PCNA rabbit polyclonal	Santa Cruz Biotechnology
PCR 10x buffer	Fermentas
PCR 10x buffer Q	Qiagen, Hilden, Germany
PfuTurbo DNA Polymerase	Stratagene
pH strips	Merck, Darmstadt, Germany
Potassium chloride	Sigma, Taufkirchen, Germany
Potassium hydroxide (KOH)	Sigma, Taufkirchen, Germany
Proteinase K	Sigma, Taufkirchen, Germany
QIAquick Gel Extraction Kit	Qiagen, Hilden, Germany
Random primers	Roche
RNA-polymerase Sp6	Roche
RNA-polymerase T7	Roche
Rnase A	Roche
Rnase inhibitor	Roche
RNeasy Mini/Midi Kit	Qiagen, Hilden, Germany
rNTPs DigMix	Roche
Sodium chloride	Sigma, Taufkirchen, Germany
Sodium dodecyl sulfate (SDS)	Sigma, Taufkirchen, Germany
Sodium hydroxide (NaOH)	Sigma, Taufkirchen, Germany
sodiumcitrate dihydrate	Sigma, Taufkirchen, Germany
β-Mercaptopethanol (β-MEtOH)	Sigma, Taufkirchen, Germany
SuperScript II RT	Gibco-BRL Life Technologies/ Invitrogen
Taq-Polymerase	Gibco-BRL Life Technologies/ Invitrogen
Taq-Polymerase	Fermentas

TOPO TA Cloning Kit
Tris-HCl
Tween20
X-gal
XL1-blue (electr. Competent cells)
xylo

Gibco-BRL Life Technologies/ Invitrogen
Sigma, Taufkirchen, Germany
Sigma, Taufkirchen, Germany
Roth
Stratagene
Merck, Darmstadt, Germany

4 Results – Part I

Development, implementation and optimization of a large-scale ENU mutagenesis screen

Aim of the Munich ENU mouse mutagenesis project was a systematic generation of mutant mouse models for human inherited diseases in a large scale by using two different strategies, a dominant and a recessive screen. The generated mouse models were determined to serve as tools to reveal phenotype-genotype correlations and to elucidate gene function within its pathogenesis. The project started in May 1997 in the framework of the German Human Genome Project (DHGP), had been later continued in the National Genome Network (NGFN) and finished its work in October 2004. The consortium consisted of nine participating research groups from the Technical University Munich, the Ludwig-Maximilian-University Munich, from the Max-Planck-Institute for Psychiatry, the University of Freiburg and the GSF Research Centre Neuherberg.

Aim of the first part of this thesis was the implementation and optimization of all processes in the core facility of the ENU mouse mutagenesis screen. The core facility at the GSF was appointed to set up and maintain the stock colonies, to set up and optimize the ENU injections, for the generation of F1 and G3 animals as well as the organization of all breeding steps, which is described in section 0 in detail. Additionally, the core facility was responsible for the implementation and organization of all phenotyping procedures i.e. sample taking of tissue/ blood, sample distribution and the performance of a number of screening parameters including the dysmorphological parameters, the basic hematology and hemostasis. Moreover, the data and workflow management, which was supported by a database, and the archiving of all mutant mouse phenotypes, was managed by the core facility, which was covered by the bioinformatics groups and the cryo-preservation group, respectively, and therefore not part of this thesis. For this purpose, the core facility received a capacity of 16 rooms with 350 type II-cages each (for max. 20.000 mice) within the GSF animal facility including the personnel and infrastructure. The original goal was to produce and to screen up to 5000 F1 animals per year for the dominant screen, which means an average of 100 F1 animals per week including all resulting crosses for confirmation, backcrossing and maintenance of mutant lines; for the recessive screen, up to 100 micro-pedigrees per year were planned, which means 4 to 6 micro-pedigrees every 2 weeks.

4.1 Screening outcome

4.1.1 Data sets used

All results used in this thesis are based on data that had been generated at the GSF core facility of the ENU mouse mutagenesis screen. Data of the core facility Moorversuchsgut Badersfeld of the LMU were not included here. The data sets for the ENU injections derived from jSQL queries within the animal management system of the MouseNet database. Only those ENU induced mutant lines and batches of ENU injections were included,

a) which were dedicated to the ENU mouse mutagenesis projects in the framework of the German Human Genome Project (DHGP) and the National Genome Network (NGFN),

b) where the groups of ENU treated male mice had been completed (F1 production was finalized); batches of still producing ENU matings and the subsequent F1 production were not included, and
c) where the groups of ENU treated male mice were used for both, dominant and recessive, breeding strategies. Otherwise, it was indicated respectively. Therefore, this analysis represents only the results of a strongly restricted and clearly defined part of the entire project.

4.1.2 Screening numbers and mutant recovery rates (MRR)

In total, 33224 F1 animals were generated and subjected to a systematic assessment of dominant mutant phenotypes with dysmorphological abnormalities, out of which approximately 19500 F1 animals were assessed for blood-based, behavioural and nociception parameters as well. For the implementation of the baselines, 50 animals per sex, strain and cross were generated and assessed for all parameters; and as soon as the breeding conditions changed due to infrastructural changing, the baselines have been repeated under the new condition. It has to be considered that much more F1 and G3 animals were deviant to the standard phenotype that were not recorded and entered into the database; due to structural limitations, the screeners selected mutant phenotypes according to their own priority. Altogether, 1233 F1 animals displayed a deviant phenotype compared to the remaining F1 population or the wild type baseline controls. Those animals that showed the deviance in two independent analyses within a two-weeks-interval were set up for conformation crosses in order to test the inheritability of the abnormal phenotype. Altogether, 307 crosses confirmed the phenotype and were established as dominant mutant lines, whereas in 926 crosses the phenotypes were not confirmed or failed due to breeding problems.

For the recessive screen, 482 male F1 animals were selected to found recessive micro-pedigrees out of which 342 have been producing G2 animals for further G3 generation. This represents a breeding success rate of 71% of all F1 founders. In total, 10389 G3 animals from 342 micro-pedigrees were analyzed for abnormal phenotypes. Altogether, 610 G3 animals displayed a deviant phenotype among the entire G3 population and/or the wild type controls and were subjected to inheritability testing. In 141 crosses the mutant phenotypes were inherited to the next generation and established as recessive mutant lines, whereas 469 crosses did not succeed due to non-inheritability or fertility problems. All confirmed mutant lines were given an internal name consisting of three letters (presenting an abbreviation for the phenotype) and a three-digit number according to the chronological appearance of a certain phenotype class (i.e. ABE001 for **A**bnormal **BE**haviour no. 1 or WBS005 for **W**hite **B**elly **S**pot no. 5).

The mutant recovery rate for dominant phenotypes was defined as the percentage of genetically confirmed mutant lines among all F1 animals that were assessed, which resulted in an overall mutation recovery rate of 0.92% for all dominant phenotypes. The screen-specific mutant recovery rates of all participating screens for both strategies are summarized in Table 5. It was considered for the mutant recovery rates in the dominant screen that the individual screens had not assessed equal numbers of F1 animals due to different starting dates or restricted analysis capacities. The mutant

recovery rate for recessive phenotypes was defined as the percentage of genetically confirmed mutant lines among the number of micro-pedigree founders and calculated with a recovery rate of 41.23% or one mutant per 2.4 micro-pedigrees for all recessive phenotypes assessed.

4.2 Comparison: Dominant versus Recessive screen

The outcome of the comparison of dominant versus recessive screen analysis can give useful indications for the design of other genetic screens in the mouse in consideration of the scale of a project, prevalence and preference of certain phenotype categories, and thus, resulting in the choice of the appropriate strategy and in maximizing the number of mutant phenotypes in a given experiment. Moreover, this project had been so far the only genome-wide genetic screen in the mouse, which had been run both strategies in parallel. In order to investigate the differences between the two strategies the mutant recovery data of the project were evaluated with respect to different aspects. The mutant recovery data derived from a period in which both strategies had been performed in parallel and were analyzed a) with regard to efficiencies of each participating screen, b) with regard to prevalence of phenotype categories, and c) with regard to the efficiency of different ENU regimes used in.

Figure 6 This figure displays the distribution of confirmed dominant and recessive mutant phenotypes for each screen in percent. Statistical analysis revealed significant preference in the recovery of either dominant or recessive mutant phenotypes for the clinical chemical, dysmorphology, and immunology screen.

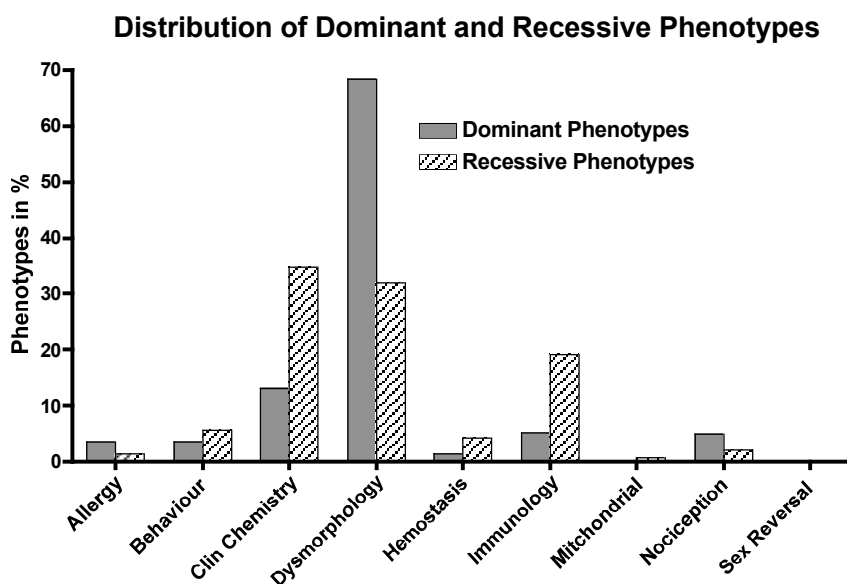


Table 5 Overview of confirmation crosses and mutant line numbers for each screen deriving from the dominant and recessive strategy.

Screen	Dominant Screen					Recessive Screen					Comparison dominant versus recessive strategy	
	CC ^a	CCs failed	Mutant lines	CR ^b in %	Total MRR in %	CC	CCs failed	Mutant lines	CR in %	Total MRR ^f in %	Screen-specific CR P-value ^g	Screen-specific mutant recovery P-value ^g
Allergy	102	91	11	10.78	0.06 ^c	34	32	2	5.88	0.58	0.517	0.3623
Behaviour	23	12	11	47.83	0.06 ^c	15	7	8	53.33	2.14	1	0.3194
Clin. Chemistry	153	113	40	26.14	0.21 ^c	117	68	49	41.88	14.33	0.008**	<0.0001***
Dysmorphology	711	501	210	24.53	0.63 ^d	188	143	45	21.94	11.16	0.1456	<0.0001***
Hemostasis	25	21	4	16	0.09 ^e	44	38	6	13.64	1.75	1	0.0788
Immunology	50	44	16	32	0.08 ^c	103	76	27	26.21	7.89	1	<0.0001***
Mitochondrial	111	111	0	0	0.00 ^c	80	79	1	1.25	0.29	0.4188	0.3147
Nociception	53	37	15	28	0.08 ^c	29	26	3	10.34	0.88	0.0924	0.203
Sex Reversal	1	1	0	0	0.00 ^c	0	0	0	0	0	n.a.	n.a.
Total	1233	926	307			610	469	141				

^a Confirmation cross = CC

^b Confirmation rate = CR; the CR refers to the total number of test crosses set up for each screen

^c The MRR in the dominant screen of clinical chemistry, immunology, allergy, behaviour and nociception refer to a number of approx.19500 assessed F1 animals.

^d The MRR in the dominant screen of dysmorphological parameters refers to a number of 33224 assessed F1 animals.

^e The MRR in the dominant screen of the hemostasis screen refers to a number of 4500 assessed F1 animals since the screen started its work later in the course of the project.

^f The MRR of the recessive screen refers to a number of 342 producing micro-pedigree founders.

^gP-value from Fisher's exact test: *** $P < 0.001$, ** $P < 0.01$, * $P < 0.05$

4.2.3 Evaluation of the individual screens

The evaluation of each participating screen was performed by analyzing and comparing i) the project-specific distribution of mutant phenotypes in both strategies, and ii) the screen-specific confirmation rates (CR) in both strategies. Figure 6 presents the distribution of dominant and recessive phenotypes in percent indicating the overall efficiency and contribution of a screen as well as a preference of a certain screen to recover preferentially dominant or recessive phenotypes in the context of the entire project. Statistical analysis of absolute mutant numbers per screen referring to all dominant or recessive mutant phenotypes revealed significant results in groups as presented in Table 5; the clinical chemistry (13.03% vs. 34.75%) and the immunology screen (5.21% vs. 19.15%) had isolated more recessive than dominant phenotypes with high significance ($P < 0.001$), whereas the dysmorphology screen (68.4% vs. 31.91%) had recovered significantly more dominant than recessive phenotypes ($P < 0.001$). The screen-specific CRs in % as presented in Table 5 represent the proportion of confirmed mutant phenotypes that derived from all variant phenotypes that had been subjected to confirmation crosses. When comparing both strategies, only the CRs of the clinical chemical parameters were significantly different (26.14% vs. 41.88%) displaying a higher efficiency to recover recessive phenotypes. For the screens analyzing IgE (10.78% vs. 5.88%), and the function of nociceptive receptors (28% vs. 10.34%) statistical analysis were not significant; however, both screens showed a higher tendency to recover dominant phenotypes. All other screens such as dysmorphology (24.53% vs. 21.94%), hemostasis (16% vs. 13.64%), immunology (32% vs. 26.21%) and the behaviour screen (47.83% vs. 53.33%) displayed almost equal confirmation rates in both strategies that were statistically not significant as well.

4.2.4 Evaluation of individual phenotype categories

For the evaluation of occurring phenotypes in the dominant and recessive screen, all parameters of each participating screen were summarized and divided into functional phenotype categories representing, either organ systems, physiological pathways or certain behavioural patterns. This first step was necessary in order to increase the numbers in each single group being able to conduct the statistical analysis appropriately. The list of phenotype categories is shown in Table 6 in which the screen-specific distribution of each phenotype category (DPC) was included as a percent value in both strategies.

In view of the entire project, more recessive mutant phenotypes were revealed for the majority of blood-based parameters as shown in Table 6; a significant preference for recessive phenotypes was recovered in the categories of electrolytes (0.32% vs. 4.26%), kidney function (0.32% vs. 6.38%), pancreas function (0.65% vs. 5.67%), high clotting time (0.65% vs. 3.55%), as well as for immunological parameters such as basal immunoglobulin levels (2.93% vs. 10.64%) and B- and T-cell markers (1.95% vs. 8.51%). In the case of glucose levels, lactate level, muscle function, trembling and eye function comparisons were not possible due to lack of mutant phenotypes isolated in one of

the groups. In contrast, a significant preference for dominant traits was shown in the categories of bone parameters (14.66% vs. 4.96%), and deafness (4.56% vs. 0.71%). All other dysmorphological parameters such as abnormal behaviour (10.42% vs. 4.96%), coat colour (10.42% vs. 5.67%), and limb phenotypes (9.77% vs. 4.26%) demonstrated at least a tendency for dominant traits except for body size abnormalities (with a majority of smaller animals), which were observed more often as a recessive trait (3.25% vs. 5.67%). The most stable groups of phenotypes were detected for the behavioural and nociceptive parameters with almost equal phenotype distributions for both inheriting traits.

On the level of individual screens, the analysis of DPC (distribution of phenotype categories) referring to the absolute screen-specific outcome can reveal a preference for certain parameters or phenotype categories independent from the synopsis of a project. Only two screens demonstrated significant differences in three phenotype categories as presented in Table 6; the clinical chemical screen showed a significant preference for dominant blood cell count alterations (50% vs. 21.15%) and for recessive kidney dysfunctions (2.5% vs. 17.31%). In addition, the dysmorphology screen demonstrated a significant preference for recessive body size abnormalities (4.76% vs. 17.78%). Eye dysfunctions had to be excluded from this comparison due to lack of mutant phenotypes in the recessive screen.

Table 6 Overview of phenotype categories across the participating screens in both of the strategies as well as their screen-specific and project-specific distribution.

Phenotype categories	Dominant Screen		Recessive Screen		Comparison dominant versus recessive strategy	
	Phenotypes <i>n</i> = 307	Screen-spec proportion in %	Phenotypes <i>n</i> = 141	Screen-spec proportion in %	Screen-specific DPC ^b <i>P</i> -value ^a	Project-specific DPC <i>P</i> -value ^a
Allergy	<i>n</i> = 11		<i>n</i> = 2			
IgE high	4	36.36	1	50	1	1
IgE low	7	63.64	1	50	1	0.4448
Behaviour	<i>n</i> = 11		<i>n</i> = 8			
Anxiety	7	63.64	4	50	0.6577	0.7472
Cognition	2	18.18	1	12.5	1	1
Exploration	1	9.09	2	25	0.5459	0.2349
Hyperactivity	1	9.09	1	12.5	1	0.5309
Clinical Chemistry	<i>n</i> = 40		<i>n</i> = 52			
Alk. Phosph.	5	12.5	2	3.85	0.2327	1
Blood cell count	20	50	11	21.15	0.0071**	0.689
Cholesterin	6	15	8	15.38	1	0.0763
Electrolytes	1	2.5	6	11.54	0.1331	0.0047**
Iron metabolism	1	2.5	3	5.77	0.6298	0.0943
Glucose	1	2.5	0	0	0.4348	1
Kidney function	1	2.5	9	17.31	0.0388*	0.0002***
Liver function	3	7.5	1	1.92	0.3135	1
Muscle function	0	0	4	7.69	0.1296	0.0095**
Pancreas function	2	5	8	15.38	0.1774	0.002**
Dysmorphology	<i>n</i> = 210		<i>n</i> = 45			
Abnormal behaviour	32	15.24	7	15.56	1	0.0703
Body size	10	4.76	8	17.78	0.0056**	0.2988
Bone	45	21.43	7	15.56	0.4228	0.0024**
Coat Colour	32	15.24	7	15.56	1	0.0703
Deaf	14	6.67	1	2.22	0.482	0.0447*
Eye	20	9.52	0	0	0.0295*	0.0008***
Limb	30	14.29	6	13.33	1	0.0598
Skin/ Hair	24	11.43	7	15.56	0.453	0.3204
Teeth	3	1.43	1	2.22	0.5424	1
Trembling	0	0	1	2.22	0.1765	0.3147
Immunology	<i>n</i> = 16		<i>n</i> = 27			
Basal Immunglobulins	9	56.25	15	55.56	1	0.0014**
B-/T-cell markers	6	37.50	12	44.44	0.7548	0.0028**
TGGE	1	6.25	0	0	0.3721	1
Nociception	<i>n</i> = 15		<i>n</i> = 3			
Fast	6	40	1	33.33	1	0.4413
Slow	8	53.33	2	66.67	1	0.7316
Jump	1	6.67	0	0	1	1
Mitochondrial	<i>n</i> = 0		<i>n</i> = 1			
Lactate	0	0	1	100	n.a.	0.3147
Hemostasis	<i>n</i> = 5		<i>n</i> = 7			
High clotting time	2	40	5	71.43	0.5581	0.0343*
Low clotting time	3	60	2	28.57	0.5581	0.652

^a *P*-value from Fisher's exact test: ****P*<0.001, ***P*<0.01, **P*<0.05

^b DPC = distribution of phenotype categories

4.2.5 Evaluation of ENU regimes

For the evaluation of ENU regimes, the dominant and recessive mutation recovery rates (MRR) of each ENU injection batch were recorded, and the mean MRR of each ENU regime were calculated for both strategies. Especially in the recessive screen, only those injection batches had been included, from which micro-pedigree founders were recruited as presented in Table 7. With regard to the mean dominant MR rate, the T39 regime (3x90mg ENU/kg bw) was most efficient with 0.96%, followed by T31 (3x100mg ENU/kg b.w.) with 0.86%, followed by T12 (1x200mg ENU/kg b.w.) with 0.75%, followed by T38 (3x80mg ENU/kg b.w.) with 0.59%, and finally T16 (1x160mg ENU/kg) with 0.44%. With regard to the mean recessive MRR, at first sight, the T12 and T16 regimes seemed to be most effective with 1.29 and 1.25 mutants per MP, followed by T39 with 0.44 and T38 with 0.22 mutants per MP. Nevertheless T12 and T16 were not further considered for a comparison since both regimes were only included one time for the recruitment of MP founders, and from the T31 ENU batches no single MP founder was recruited for the recessive screen.

Table 7 Mutation recovery rates across the ENU regimes and ENU injection batches.

Regime	Batch Id	Dominant MRR ^a	Mean dom. MRR ± S.D.	Recessive MRR ^b	Mean rec. MRR ± S.D.
T12	16	0.47	0.75±0.39	1.29	1.29 ^c
	17	1.03		n.a.	
T16	1	0.49	0.44±0.10	n.a.	1.25 ^c
	2	0.47		n.a.	
	5	0.26		n.a.	
	6	0.53		n.a.	
	18	0.45		1.25	
T31	9	0.33	0.86±0.50	n.a.	n.a.
	11	1.33		n.a.	
	12	0.92		n.a.	
T38	3	0.50	0.59±0.31	n.a.	0.22 ^d ±0.15
	4	0.46		n.a.	
	26	0		0.40	
	30	0.98		0.42	
	31	1.01		0.25	
	33	0.44		0.16	
	35	0.40		0.34	
	39	1.00		0.23	
	41	0.65		0.22	
	45	0.54		0	
	49	0.53		0	
T39	14	1.47	0.96±0.86	n.a.	0.44 ^d ±0.58
	19	0.34		n.a.	
	20	0.10		0	
	21	0.98		1.40	
	22	0.24		0.60	
	23	1.03		0.15	
	24	2.56		0.07	

^a MRR = mutant recovery rate

^b mean values are calculated only for those batches from which MP founders had been recruited

^c ENU batches no. 16,18 cannot be considered due to a different selection procedure of MP founders

^d MP founders underwent a pre-selection: descendants of different ENU treated males, no obvious dominant phenotype

For this reason, only T38 and T39 were included for further statistical analysis by testing the MRR of both regimes in the dominant or recessive strategy using an unpaired t-test with Welch's correction, which resulted in fact with a significantly higher MRR for T39 in both dominant and recessive strategies, as shown in the first row of graphs of Figure 7. Two other parameters that are essential for breeding management of F1 generation had been analyzed by focusing on the sterility periods and lifespan of ENU-treated male mice as shown in the second row of graphs in Figure 7. For the comparison of sterility periods, the medians of all T38 and T39 injection batches were determined and tested; the mean values of medians of each injection batch were determined as $m = 107.4 \pm 3.857$ for T38 and $m = 116.2 \pm 4.383$ for T39 and tested by using an unpaired t-test with Welch's correction but were not significantly different. The same analysis was performed by testing the mean values of medians of lifespan in days as $m = 293.3 \pm 6.996$ for T38 and $m = 328.3 \pm 7.614$ for T39 that turned out to be significantly different with $P = 0.0041$.

Comparison of ENU regimes T38 and T39

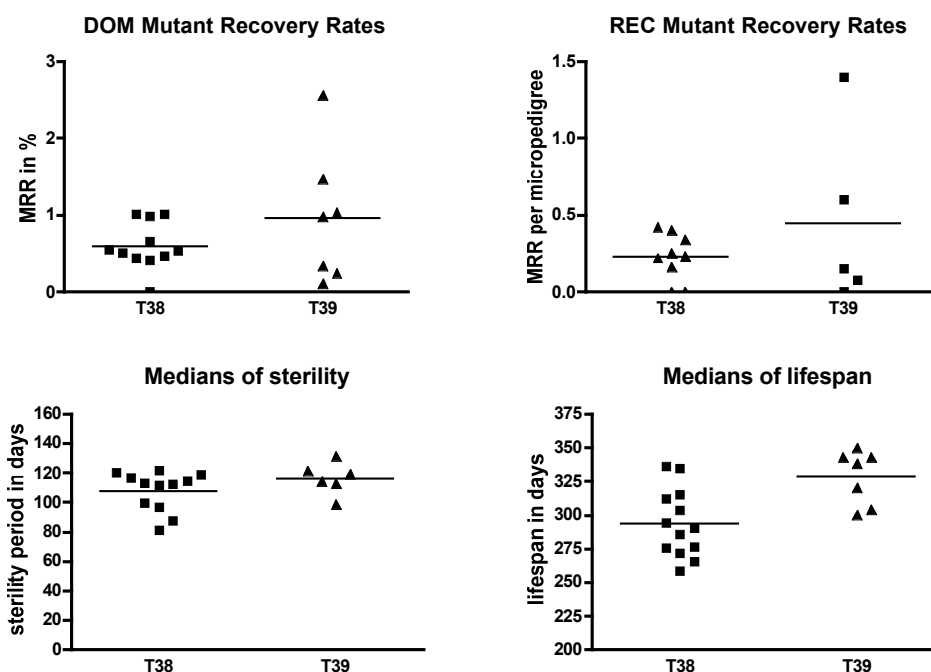


Figure 7 Comparison of mutant recovery rates, sterility periods and lifespan of male mice treated with T38 and T39 ENU regimes. For statistical analyses, the mutant recovery rates of T38 and T39 in both strategies, represented as individual data points in the scatter dot plots in the upper row, were tested using an unpaired t-test with Welch's correction, which resulted in a significantly higher MRR for T39. The sterility and lifespan medians of each injection batch of T38 and T39 had been determined and tested by using an unpaired t-test with Welch's correction. Each data point in the scatter dot plots represents the median sterility periods or life spans of individual injection batches including the mean value of each group.

5 Results - Part II

Characterization of ALI mutants (ALI3, ALI9, ALI12, ALI19 and ALI037)

The second part of this thesis comprise the molecular and phenotypical characterization of ENU induced mutant mouse lines with dysmorphological abnormalities to underline the role of mouse models as tools for the analysis of gene function and their role in the elucidation of pathomechanisms in human inherited diseases. Five mutant lines showing abnormal limb phenotypes (= Abnormal LImb) were selected for further molecular and phenotype analysis.

5.1 Characterization of ALI3/9/12/19

5.1.1 Phenotype description of ALI3/9/12/19

ALI3, ALI9, ALI12 and ALI19 were all isolated as dominant phenotypes in the dysmorphology screen that displayed a preaxial polydactyly at the hindlimbs with full penetrance and that were completely viable, as shown in **Figure 8**.

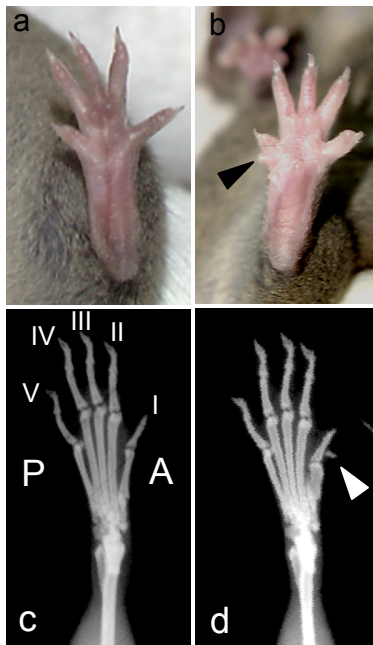


Figure 8 External examination of ALI3/9/12/19 revealed a similar abnormal phenotype at the hindlimbs. Here, an example of ALI3 is shown: a), c) External view and x-radiography of a wild type hindlimb. b) Example of a pre-axial polydactyly (extra toe). d) Example of an X-radiography of showing an extra toe at the hindlimb of a mutant animal

Secondary effects could not be detected, and all other blood-based parameters did not display any other alterations so far. The breeding performance of heterozygous animals that were crossed to wild-type animals was normal compared to wild type breeding pairs with litter sizes between 4-8 pups and 6 to 10 litters per breeding pair (data not shown); thus, embryonic lethal offspring could be excluded due to the mutant phenotype. The phenotype was detected externally and in skeletal preparations starting from embryonic stage 14.5 dpc in heterozygous animals of ALI3/9/12/19 embryos, as shown in **Figure 9b**. External examination of 12.5 dpc embryos demonstrated already a broadening at the preaxial side of the forelimb paddles, which became more pronounced in the newborn offspring of ALI3/9/12/19 mutants. The preaxial polydactyly varied from a small appendix attached to the first digit (**Figure 9c**) to a clearly pronounced additional digit with phalagial bones and claws (**Figure 9d**)

To generate homozygous animals two heterozygous ALI mutants were crossed presuming the Mendelian 1:2:1-ratio of wild type, heterozygous, and homozygous animals. All four mutant lines displayed very similar malformations leading to the assumption that the mutated genes belong to the same signalling pathway or even represent alleles of the same gene. Approximately 20-30% of the embryos died, the majority in utero at stage E18.5, some were born but died around birth, and displayed a number of malformations such as a reduced body size, in some cases an open brain (exencephalus, spina bifida) as shown in **Figure 9e, f**, or an impaired eye development that resulted in a complete aphthemia (**Figure 9h**). In addition, some these offspring displayed malformations at the limbs of different severity such as severe forms of polydactyly at fore- and hindlimbs with an impaired patterning of digit identity and strongly affected tarsal and carpal bones (**Figure 9I, k**) or in rare cases shortened hind limbs due to extremely shortened tibia and/or fibula (**Figure 9j**); those animals were considered as homozygous for the mutation.

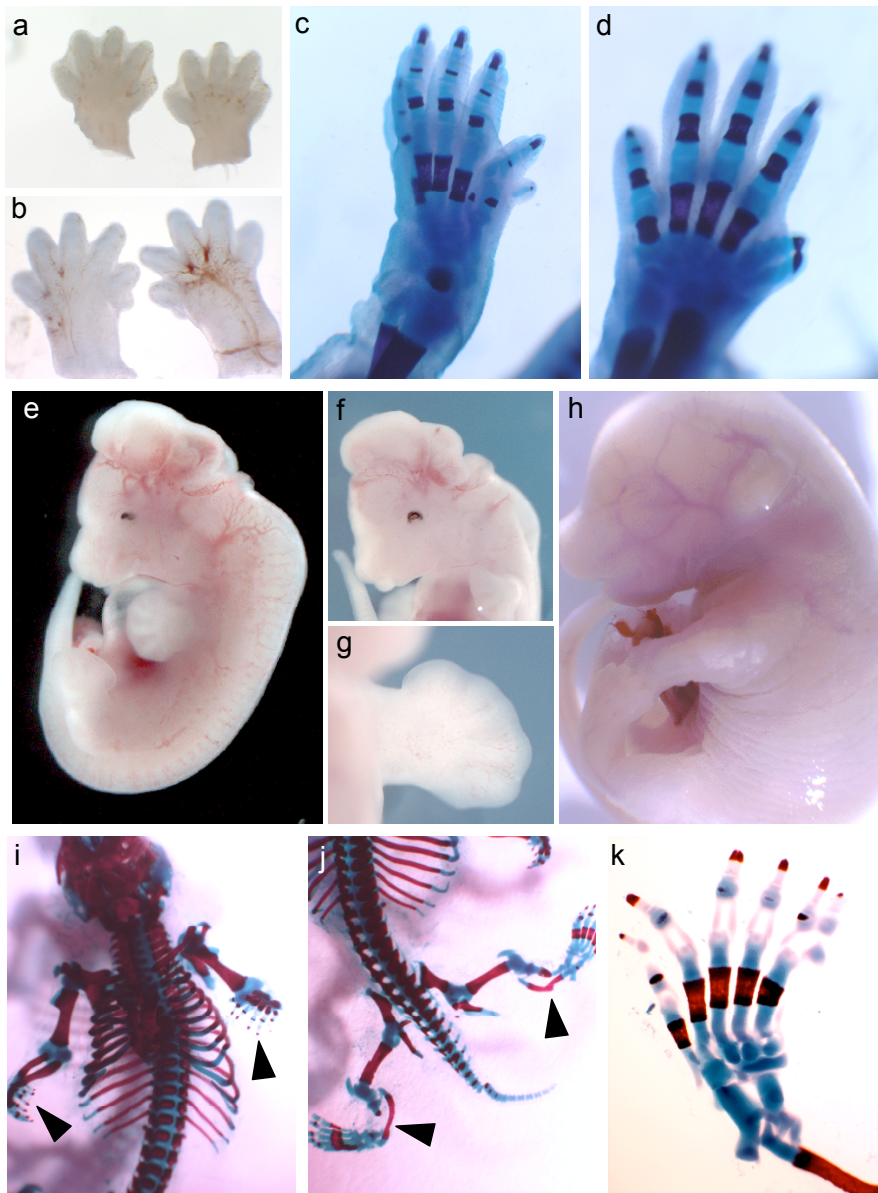


Figure 9 A selection of ALI3/9/12/19 phenotypes. a) Hindlimbs of a wt C3HeB/FeJ embryo at stage E14.5 b) The hindlimbs of a heterozygous ALI3 mutant at embryonic stage E14.5 with a preaxial polydactyly. The extra toe become more pronounced during development until birth .c) and d) show a skeletal preparation of affected heterozygous ALI9 and ALI12 newborn animals. The preaxial polydactyly can range from a mild form with a small extra toe that seems to be just slightly attached to the first digit or a clearly pronounced extra digit with an own phalangeal bone and a claw. e) to k) Selection of presumed homozygous ALI3/9/12/19 offspring at different embryonic stages: e, f, g) A presumed ALI9 homozygous offspring at stage E12.5 with a reduced body size, an open brain (exencephalus), and broad paddles at both hind- and forelimbs. h) A presumed homozygous ALI19 offspring where the eye development is impaired resulting in an aphthemia. i) Skeletal preparation of a presumed homozygous ALI3 newborn animal displayed malformations at the forelimbs with a severe polydactyly and j) malformations at the hindlimbs with a very pronounced shortening of tibia and fibula. k) The forelimbs of a presumed homozygous ALI12 newborn animal with a polydactyly and an impaired patterning of digit identity.

In order to clarify the question whether the mutated genes were members of the same molecular pathway or even allelic variations of a single gene a complementation test was carried out by crossing two heterozygous animals of each ALI3/9/12/19 mutant line with the other and analysing the morphology of the generated embryos. The crossing table and the results are shown in **Table 8**. The embryos were isolated between E 12.5 and E16.5 for morphological analysis. In approximately 25% of the offspring, the embryos displayed the same malformations as each single homozygous ALI3/9/12/19 mutants such as reduced body size, severe malformations at fore- and hindlimbs, excencephalus and/ or aphthemia. These animals were considered as double heterozygous for the respective crossings.

Table 8 Crosses of the complementation test and the resulting phenotypes in presumed homozygous or double heterozygous mutant embryos.

	ALI3 het	ALI9 het	ALI12 het	ALI19 het
ALI3 het	Excencephalus/ Polydactyly	Excencephalus/ Polydactyly	-	Excencephalus/ Polydactyly
ALI9 het	-	Excencephalus/ Polydactyly	Polydactyly	-
ALI12 het	-	-	Polydactyly	Excencephalus/ Polydactyly
ALI19 het	-	-	-	Excencephalus/ Polydactyly/Aphthemia

5.1.2 Molecular characterization of the ALI3/9/12/19 mutation

Due to the dominant phenotypes of ALI3/9/12/19 an out-backcross strategy was selected for backcrossing the four mutant lines. Altogether, 48 heterozygous ALI3 N2 offspring, 71 heterozygous ALI9 N2 animals, 100 heterozygous ALI12 N2 animals and 75 heterozygous N2 animals of ALI19 animals were generated out of which 24 of each line were subjected to rough chromosomal mapping with a panel of 140 micro-satellites that were polymorphic for the strains C3HeB/FeJ and C57BL/6J and that cover the entire genome. All PCR results were analysed with the help of MapManager (Manly et al., 2001). The data of the rough chromosomal mapping revealed a linkage to mouse chromosome 13 for all four lines. In the second step, additional ALI3/9/12/19 N2 animals were analysed with additional microsatellite markers that are specific for mouse chromosome 13 in order to narrow down the chromosomal region of the mutated genes. The evaluation of the mapping data resulted in a linkage to a region flanked by the micro-satellite markers *D13Mit3* and *D13Mit14*. In parallel, the mouse databases were screened for appropriate candidate genes with descriptions of mutant alleles, located on chromosome 13, which might be connected the ALI3/9/12/19 phenotypes. The most convincing candidate was the transcription factor Gli3 due to the high similarity of its described Gli3^{Xt/J} allele/ phenotype. All 16 exons of the Gli3 gene were sequenced in the ALI3/9/12/19 mutant lines. A number of three individuals per mutant line and wild type C3HeB/FeJ as well as C57BL/6J animals were used for the sequencing reactions, which were performed by MWG Biotech (Ebersberg, Germany). In all four cases, the induced mutations were successfully characterised as shown in **Figure 10**: The molecular characterization of ALI3 revealed a base pair

exchange from T to A in exon 11 of Gli3, at nucleotide 1779 (on cDNA level), which represents an amino acid exchange from histidine to arginine. In ALI9, the mutation was revealed in exon 9 of Gli3 as a transversion from T to C at nucleotide 1668+2, which represents an alteration in the 5' splice site of intron 9. In ALI12, the mutation was identified in exon 8 of Gli3 as a transversion from C to T at nucleotide 1522 (on cDNA level), which leads to an amino acid exchange from glutamine to a premature stop codon. Finally, the mutation of ALI19 was identified as a transition from A to T in exon 8 of Gli3 at nucleotide 1483 (on cDNA level), which leads to an amino acid exchange from lysine to a premature stop codon. Further sequence analysis with regard to known functional domains of the transcription factor revealed that all four mutations are located in the zinc finger region of Gli3, which represents a common DNA-binding domain for transcription factors.

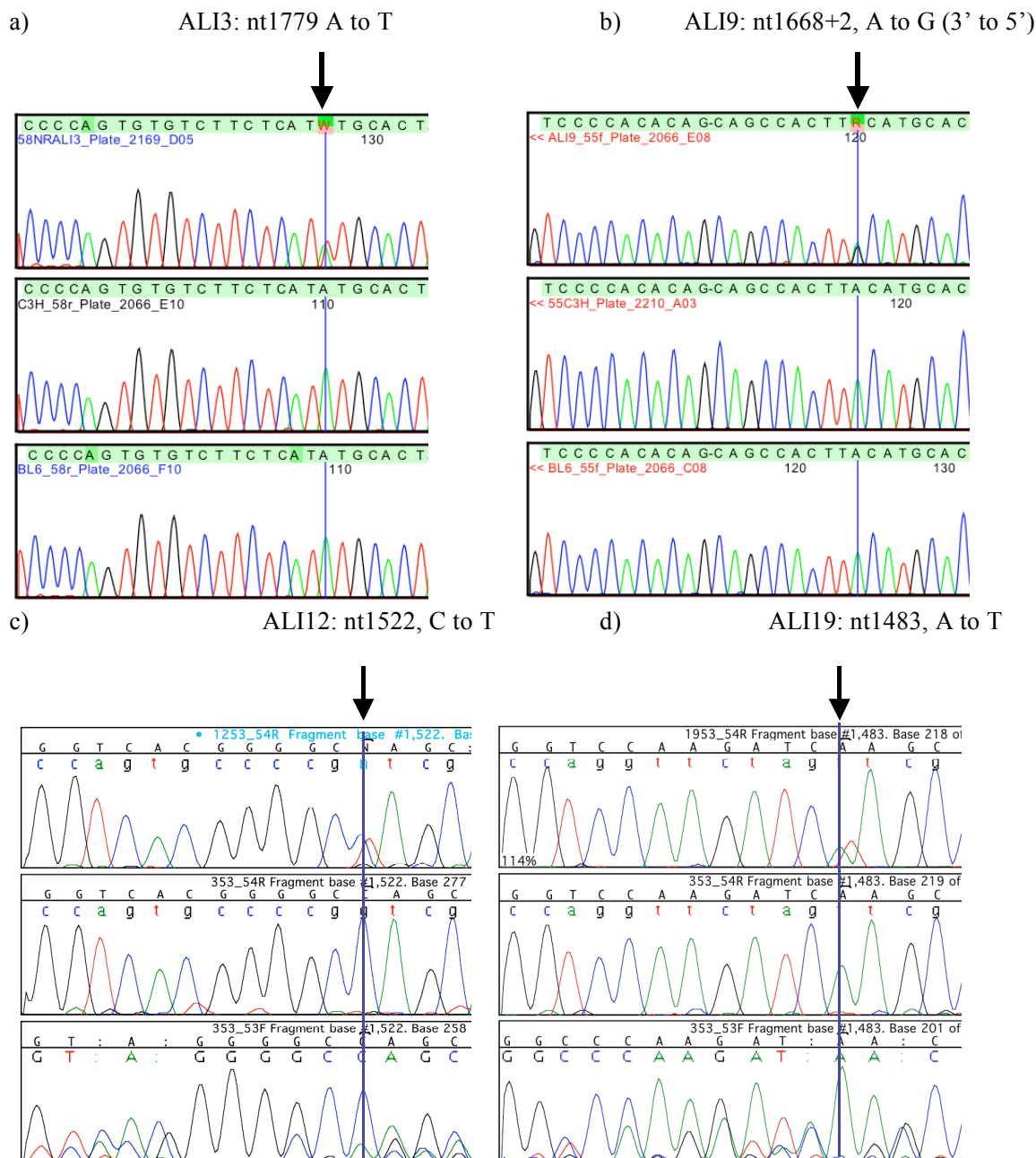


Figure 10 Sequencing of Gli3 in ALI3/9/12/19 revealed the molecular alterations induced by ENU treatment: a) In the first row, the ALI3 sequence revealed an A to T transition at nt 1779 of Gli3 leading to an aminoacid exchange from histidine to arginine. The second and third rows represent the wild-type C3HeB/FeJ and C57BL/6J sequences. b) The first chromatogram showed the mutation in ALI9 as an A to G transversion at nt 1668+2 located in the splice/acceptorsite of intron 9 of Gli3. The second and third rows represent the wild-type C3HeB/FeJ and C57BL/6J sequences. c) The mutation in ALI12 was revealed as a C to T transversion at nt1522 resulting in an aminoacid exchange from glutamine to a premature stop codon. The third and second rows represent the forward and reverse sequences of a wild-type C3Heb/FeJ mouse. d) In ALI19, a basepair exchange represent from A to T at nt1483 was recovered also leading to an aminoacid exchange from lysine to a premature stop codon. The third and second rows represent the forward and reverse base sequences of a wild-type C3Heb/FeJ mouse.

5.2 Characterization of ALI037

5.2.1 Phenotype description of ALI037

5.2.1.1 Limb and other skeletal phenotypes of ALI037

ALI037 was isolated as a dysmorphological abnormal phenotype, which is inherited in an autosomal recessive manner. The ALI037 phenotype was already visible at birth and characterised by malformations in the pelvic girdle and hind limbs. Another phenotype observed in the ALI037 mutants was a slightly reduced body length, out of which one could assume additional malformations in the vertebral column. In order to analyze the skeletal malformations in more detail and which were not detectable in x-radiography due to the low resolution, preparation of skeletons stained with alizarin red/alcian blue for the differentiation of bone and cartilage were performed. In the ALI037/ALI037 mutants, the position of the pelvis was obviously more flattened, and the positioning of the femur to the hip joint was abnormal compared to those of the wild type littermates (Figure 11), which resulted in an abnormal gait. External morphological analysis displayed polydactyly at both hind limbs, which could vary in severity. In most cases, the polydactyly was connected to an equal shortening of femur and tibia, which could be clearly observed in x-radiography, see also Figure 12a, b. Additionally, the morphology of the fibula was altered; the mutant fibula could be observed in parallel over the entire length of the tibia ending at the tarsal bones, whereas in the wild type situation, the length of the fibula was normally only two third of the tibia's length and, at its distal end, fused to the tibia. When comparing the morphology of the mutant fibula to the forelimbs of a wild type mouse, where ulna and radius are completely separated over their entire length, one could describe this phenomenon as an anteriorization of the hind limbs. The most severe tibia phenotype in a male ALI037 mutant observed was an unequal shortening of tibia and fibula resulting in an extremely bending of the fibula and a 90°-distorsion of the right hind limb, shown in **Figure 13a**. More distal along the hind limb, the tarsal region showed a thickening and broadening of the heels, and a malposition of the hind paws. A detailed analysis of the tarsal region revealed a second *os calcis*, which was smaller compared to the main *os calcis*, a ventral fusion of the intermediate and lateral cuneiform (see asterisk in **Figure 13i**), and a duplication of the intermediate cuneiform. This second *os cuneiforme intermedium* was the basis of the metatarsal of digit I, which was morphologically transformed into a second digit II including two phalangeal bones. Moreover the analysis could reveal, that the brachydactyly in the ALI037 mutants was a result of shortened metatarsal and phalange bones. Careful morphological examination of the vertebral column demonstrated 14 thoracic vertebrae in ALI037 mutants and an additional pair of ribs, as demonstrated in **Figure 13c**, whereas the wild type littermates displayed the normal pattern of 13 thoracic vertebrae and pairs of ribs. More posterior of the vertebral column, mutant animals showed fusions of the *processi transversi* of the sacral vertebrae S1 to S4, as indicated with an asterisk in **Figure 13d,g**; in wild type animals, only fusions of the *processi transversi* of S1 to S3 could be observed. In addition,

the size of all vertebrae was slightly reduced in the mutants compared to the wild type situation, which could be observed in x-ray analysis explaining the reduced body length of ALI037 mutants.

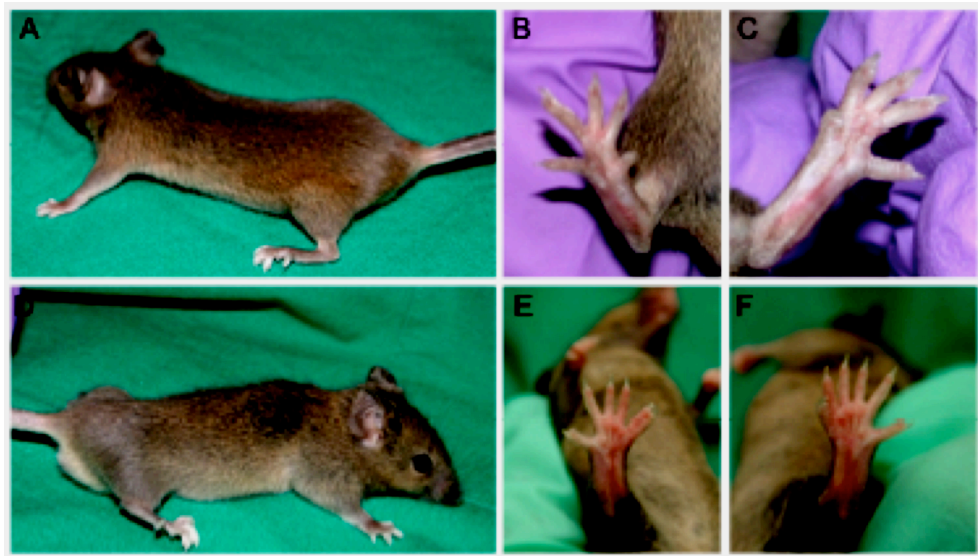


Figure 11 External examination of ALI037 animals revealed A) malformation of the pelvic girdle and shortened hind limbs in the ALI037 mutant and B), C) polydactyly at both hind limbs compared to wild type C3HeB/FeJ D, E, F).

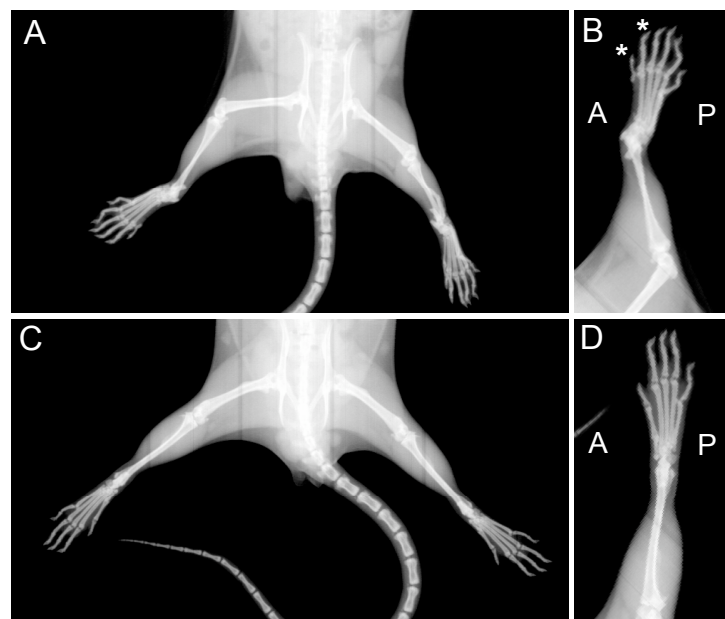


Figure 12 X-ray analyses of ALI037 and wild type C3HeB/FeJ mice revealed a shortening of femur and tibia/fibula in the ALI037 mice A), a polydactyly and brachydactyly at both hind limbs B) compared to wild type animals C, D).



Figure 13 Skeletal preparation showing skeletal malformations at the hind limbs and the vertebral column of ALI037: A) lateral view of a right hind limb of a ALI037 mutant with shortened femur, extremely shortening of tibia and a bending of the fibula resulting in a 90°-distorsion of the hind limb, b) dorsal view of the hind paw with brachydactyly and polydactyly at the hind limbs, and a transformation of digit I to digit II, d) dorsal view on the sacral vertebrae with fusions of the processi transversi of S1 to S4, c) dorsal view on the thoracic vertebrae with 14 vertebrae and an additional pair of ribs, compared to the wild type situation. E) Lateral view of a wild type hind limb with tibia/ fibula, F) dorsal view of a wild-type hind limb, G) dorsal view of the sacral vertebrae of a wild-type animal. H) Dorsal view on the tarsus showing a polydactyly with a duplication of the *os cuneiforme intermedium* and a transformation of digit I to digit II, I) ventral view on the tarsus revealing a second *os calcis* and a ventral fusion of the *os cuneiforme intermedium* and *laterale*. Tarsal region of a wild type J) dorsal view, K) ventral view

5.2.1.2 Fertility phenotype of male ALI037 mutants

A completely different aspect connected to the ALI037 phenotype was a reduced fertility, which was mainly observed in homozygous ALI037 male mice. The comparison of breeding performances of homozygous male and female ALI037 mutants, held in permanent one-to-one crosses with the respective wild-type partners, did not reveal any significant difference with regard to the number of pups as shown in Table 9. Moreover, the litter sizes of the homozygous ALI037 females were slightly reduced compared to the litter sizes of wild type C3HeB/FeJ females with 5.7 offspring on average as known from literature (<http://www.jax.org>). With regard to the fertility period, the number of sterile -/- ALI037 males strongly increased only a few weeks after the males gained their sexual maturity. As shown in Table 9, on average, the -/- ALI037 males only gave birth to 1.25 to 1.64 litters reflecting a severe fertility problem. The majority of the -/- ALI037 males lost their fertility after 12 weeks of age; 80% became sterile after two litters, and the remaining 20% became sterile after having given birth to a third litter, at an age of 16 weeks. Due to these fertility problems, additional analysis of the testis and the spermatozoa were performed in cooperation with the cryo-preservation group at the Institute of Experimental Genetics. Altogether, thirteen ALI037 males between 62 to 269 days of age and thirty wild type males between 73 to 160 days of age were available and subjected to sperm analysis. During the preparation of spermatozoa, the macroscopic examination already revealed a size difference of the testes and *caput epididymis* of the ALI037 males, which were much smaller than those of the age-matched control animals (not shown). The analysis of spermatozoa comprising motility, progressivity and concentration that reflect the viability and quality of the germ cells showed a clear age-dependent decrease of all values in the ALI037 mutants beginning with an age of 8 weeks as shown in Figure 14. The concentration of the ALI037 spermatozoa were already clearly lower than the mean of all wild-type values with $m = 99,46 \pm 44,9$ (S.D.) $\times 10^6/\text{ml}$; in samples of mutants, which were older than three months, no viable spermatozoa could be detected anymore (with one exception).

Histological analysis of the testes of two, three and nine month old ALI037 male mutants and the respective wild-type controls confirmed these findings as shown in Figure 15. A number of agametic seminiferous tubules were already registered in sections of eight weeks old ALI037 testes, and the depletion of spermatogonia continued progressively with age in three months old animals, as shown in Figure 15B, C. In cross-sections of testes of nine months old mutants, only agametic tubules with *Sertoli* cells at the basal lamina could be detected. The histological analysis was underlined by determining the percentage of functional versus agametic tubules in testes from ALI037 males and wild-type animals at different ages, as shown in Figure 16. For this purpose, cross-sections of testes from three animals of each genotype and age group, ALI037 and wild-type animals at the age of two, three, and nine months, were scored.

Table 9. The breeding performance of homozygous ALI037 animals characterised by the mean litter size and the number of litters per breeding pair reflecting the fertility period.

Crosses	Mean litter size \pm S.D.	Mean No. of litters \pm S.D.	n
-/- male X +/+ female	4.75 \pm 2.75	1.25 \pm 0.5	4
+/+ male X -/- female	4.37 \pm 2.26	4.33 \pm 0.58	3
-/- male X -/- female	3.93 \pm 1.72	1.64 \pm 0.92	11

Analysis of wildtype and ALI037 spermatozoa

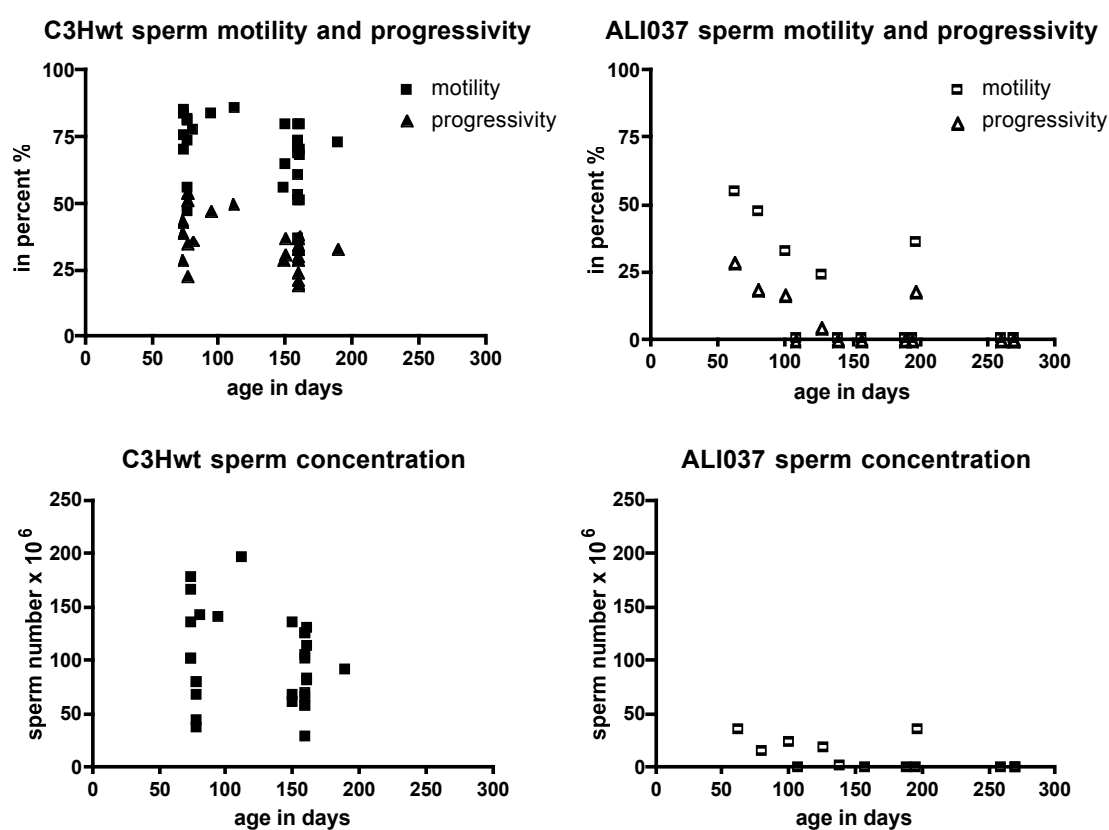


Figure 14 Sperm analysis of ALI037 male mutants and wild-type animals. The quality of spermatozoa was determined by measuring a) the motility and progressivity of 13 ALI037 mutant and 30 wild type sperm samples in percent, and b) the concentration in $\times 10^6$ /ml revealing a strong and progressive decrease of all parameters in ALI037 males already starting at an age of 8 weeks. Mutant animals that are older than 3 months did not show any viable spermatozoa.

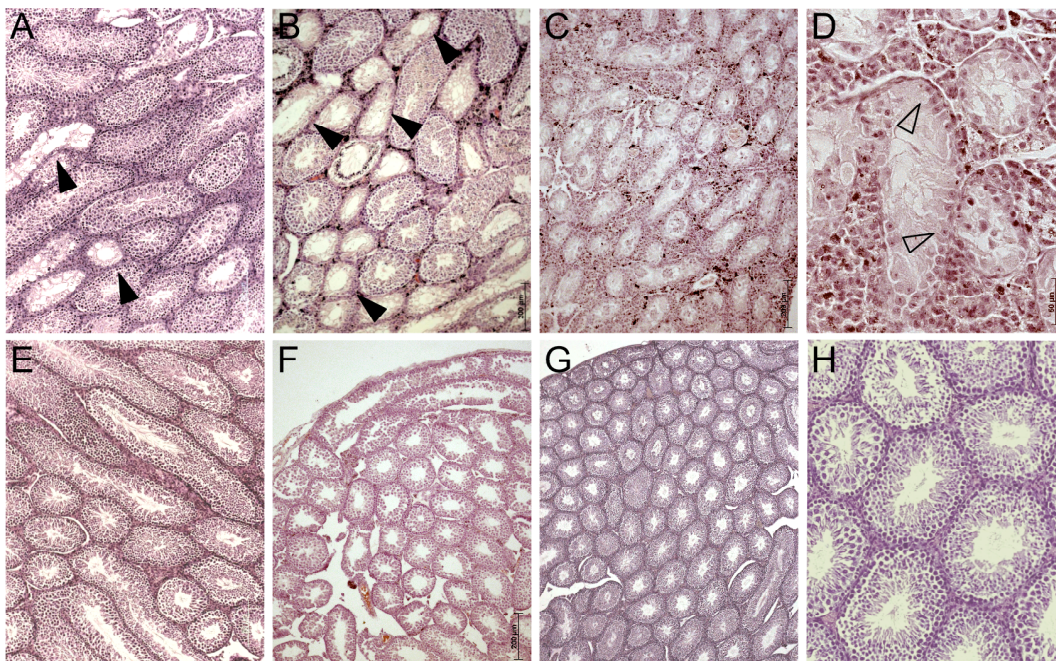


Figure 15 Histological sections of ALI037 mutant and wild-type testes stained with haematoxylin/eosin. A) At the age of two months, the sections of ALI037 testes already displayed a number of empty seminiferous tubules (arrowheads) that missed all stages of male germ cells. B) At the age of three months, the depletion of spermatogonia continued progressively in the ALI037 mutants. C, D) At the age of nine months, almost all seminiferous tubules were empty, only the *Sertoli* cells remained at the basal membrane of the tubules. In comparison, sections of testes from wild type males of two months E), three months F), and nine months of age G, H) displayed completely functional seminiferous tubules with all stages of spermatogenesis.

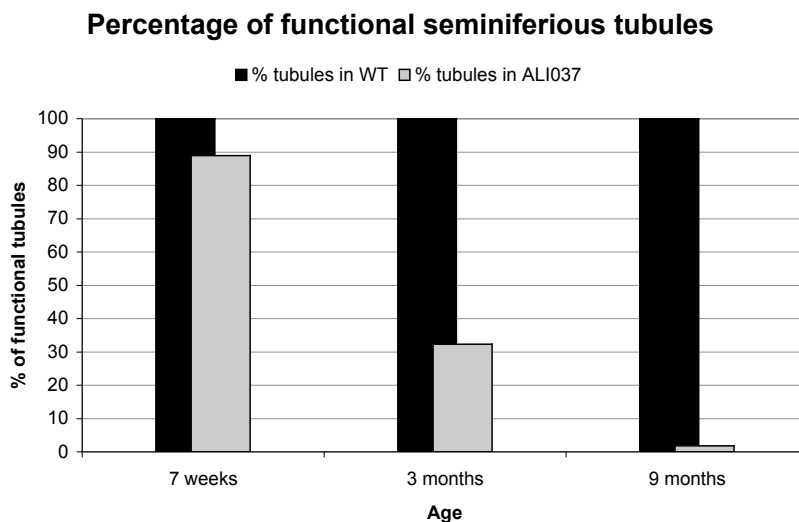


Figure 16 Percentage of progressive germ cell loss in testes of ALI037 males compared to wild-type animals at the age of two, three, and nine months.

5.2.2 Molecular characterization of the ALI037 mutation

For backcrossing the ALI037 mutation an out-/intercross strategy was selected. Altogether, 138 homozygous N2 animals were generated out of which 48 were subjected to the very first run of the SNP mapping panel consisting of 151 SNPs distributed over the entire mouse genome. On the first trial, 95 SNPs delivered a result with an overall success rate of 63.4%; 13 SNPs did not work at all, 37 SNPs worked with a success rate of less than 80%, and 45 SNPs with a success rate between 80% to 100%. The evaluation of the SNP mapping revealed the highest χ^2 -value of 88 with a probability of $p < 0.0001$ for marker *rsWI_WGS_9_65027538* that is located at 66.83 Mbp of mouse chromosome 9. In order to narrow down the region of the mutated gene, three groups of additional micro-satellite markers between *rsWI_WGS_9_65027538* (66.83 Mbp) and *rsWI_WGS_9_32840501* (33.4 Mbp) were selected and used for linkage analysis.

In parallel to the fine mapping, the mouse databases were screened for appropriate candidate genes with description of mutant alleles, located on chromosome 9, which might be connected to the ALI037 phenotype. Four genes were considered as candidates for the ALI037 mutation, as shown in the table of **Figure 17**. *Zbtb16* was the most promising candidate gene due to the high similarity of its knockout phenotype to ALI037; therefore, all exons covering the coding region of this gene were sequenced first. The mutation was detected as a C to T base pair exchange in exon 7 at position 2292 on transcript level of the gene *Zbtb16*, or *Zfp145* encoding *Plzf*, as shown in **Figure 17**. This result was confirmed in five individual mutant animals. Five individual samples of the inbred strains C3HeB/FeJ, C57BL/6J, 129X1, BALB/cByJ and CAST/Ei were analysed as well in order to exclude a single nucleotide polymorphism in the C3HeB/FeJ background at this position.

Further sequence analysis of the mouse *Zfp145* sequence revealed a restriction fragment length polymorphism (RFLP) for BbsI due to the induced mutation in ALI037 mutants. Therefore, determination of the ALI037 specific genotype was carried out by a combined amplification of a genomic region including exon 7 resulting in a 1512 bp-PCR product. A following BbsI-digestion (Fermentas) of this fragment resulted in three DNA fragments of 848bp, 409bp and 255bp indicating the wild-type allele. Due to the missing second BbsI site the mutant allele displayed two DNA fragments of 848bp and 664bp, respectively.

Gene	Allele	Mb position	Phenotype
<i>Catb</i>	<i>Catnbtm2Kem</i>	120.93	Limb dysmorphism: forelimb abnormalities; limb truncation at humerus and ulna hind limb abnormalities: absence of hind limb
<i>Ryk</i>	<i>Ryktm1Stac</i>	102.75	Short limbs, reduced length of long bones; hind limb abnormalities; microphthalmia
<i>Scamp5</i>	<i>Sc5dtm1Fdp</i>	57.6	Extremity defects: abnormal phalanges; short limbs, kinked tail
<i>Zbtb16 or Zfp145</i>	<i>Zbtb16tm1Ppp</i>	48.86	Abnormal hind limb morphology: digit I homeotically transformed into digit II, polydactyly; abnormal tarsus morphology: complete fusion of metatarsal region; 36 % with short limbs

Sequence analysis of *Zfp145*

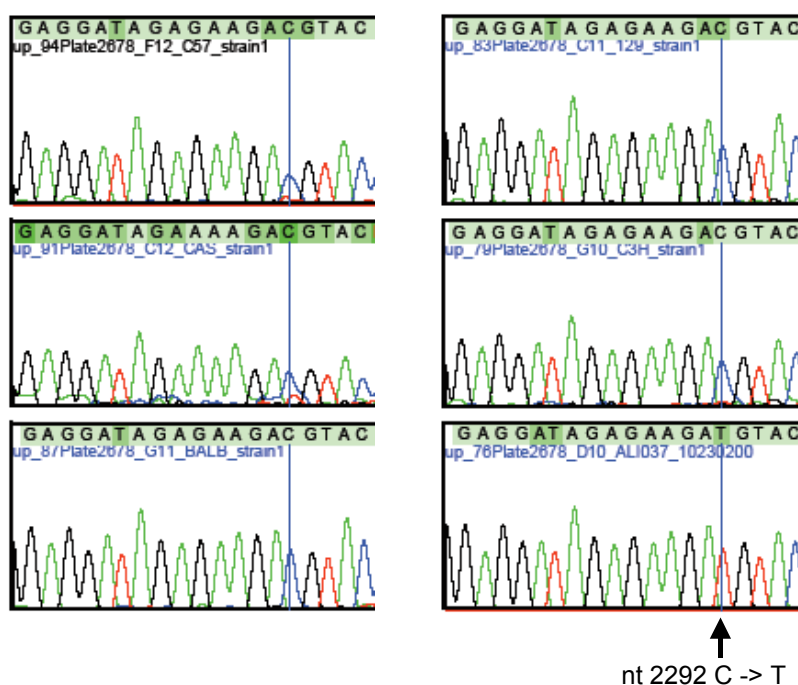


Figure 17 Candidate genes for the ALI037 mutation and sequence analysis of *Zfp145*. The most promising candidate for the ALI037 mutation was *Zfp145* due to the high similarity of the knockout phenotype to ALI037. Sequence analysis of *Zfp145f* revealed a C to T base pair exchange in exon 7 at nucleotide position 2292 on transcript level in ALI037 mutants, which was confirmed in five individuals. Five other inbred strains including C3HeB/FeJ, C57BL/6J, CAST/Ei, BALB/cByJ and 129X1 were analyzed as well in order to exclude a polymorphism of this base pair exchange in C3HeB/FeJ

On protein level, the Zfp145ALI037 mutation resulted in an amino acid exchange at position 609 from threonine to methionine, which was located in the carboxy terminal region of the zinc finger domain, as shown in **Figure 18**. In order to elucidate the potential function of the domain in the carboxy terminal region complete and partial protein sequences of *Plzf* (encoded by *Zfp145*) and *Plzf*ALI37 were aligned against the *Plzf* sequences of other vertebrates including *Gallus gallus*, *Canis familiaris*, *Rattus norvegicus*, *Pan troglodytes*, and *Homo sapiens* by utilizing the sequence analysis tool ClustalW from EBI <http://www.ebi.ac.uk/clustalw/index.html>, as shown in Figure 18. The result of the protein sequence alignment showed a high degree of conservation in the carboxy terminal region of *Plzf* across the species analysed, except for *Rattus norvegicus*. Since a functional domain for the carboxy terminus of *Plzf* had not been yet described in literature, another bioinformatical tool ProSite from ExPasy, which is a prediction tool for functional domains of proteins, was used. Beside the known BTB/POZ and zinc-finger domains a potential phosphorylation site for Thr609 in *Plzf* was predicted. In the *Plzf*ALI037 protein sequence the phosphorylation site at position 609 was missing due to the amino acid exchange from threonine to methionine. Unfortunately, ProSite did not deliver a probability value for the phosphorylation site predictions, and under this circumstances, it was not possible to estimate the quality of its prediction. Therefore, an additional tool, NetPhos 2.0 (<http://www.cbs.dtu.dk/services/NetPhos/>) that was especially developed for the prediction of phosphorylation sites in proteins, was used. Here, the threshold for potential phosphorylation sites was defined as a value > 0,5. NetPhos predicted 26 serine, 3 tyrosine, and 8 threonine phosphorylation sites for *Plzf*; for Thr609 the phosphorylation scoring displayed a value of 0.510.

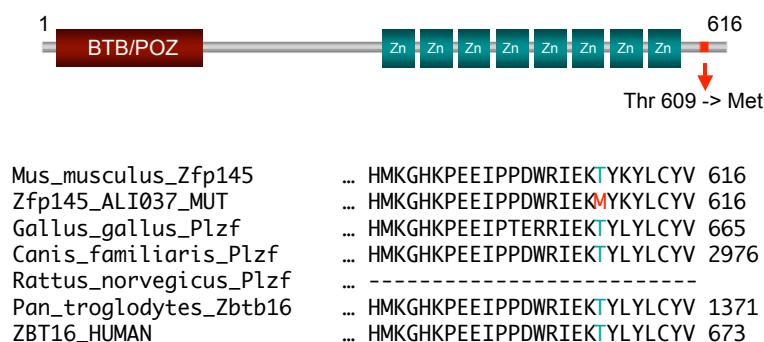


Figure 18. Sequence analysis of the ALI037 mutation revealed a restriction fragment length polymorphism (RFLP) using the restriction enzyme BbsI. Location and result of the ALI037 mutation on protein level, and sequence homology alignment of the referring carboxy terminal region with other vertebrate sequences. *Plzf* is described as a phosphoprotein with two main functional domains, a BTB/POZ (for “bric a brac/tramtrack/broad complex, poxvirus and zinc-finger”) domain at the amino terminus, a typical protein-binding motif, and a zinc-finger domain with nine Krüppel-type zinc-finger motifs at the carboxy terminus. The protein sequence in the carboxy terminal region of the zinc-finger is highly conserved across the species analysed except for *Rattus norvegicus*.

5.2.3 Functional analysis of the *Zfp145*^{ALI037/ALI037} mutation

5.2.3.1 *Zfp145* expression in E 11.5 mouse embryos

In order to understand the role of *Zfp145* in early mouse development, the expression pattern of *Zfp145* was studied with whole mount in situ hybridisation (WISH) analysis in wild type (and homozygous ALI037) E11.5 mouse embryos where the development of the majority of inner organs is almost terminated whereas major remodelling processes at the vertebral column and the appendicular skeleton (fore/hind limb) can be observed. Specific *Zfp145* expression was observed in several tissues along the entire body axis and the extremities, which is presented in

Figure 19.

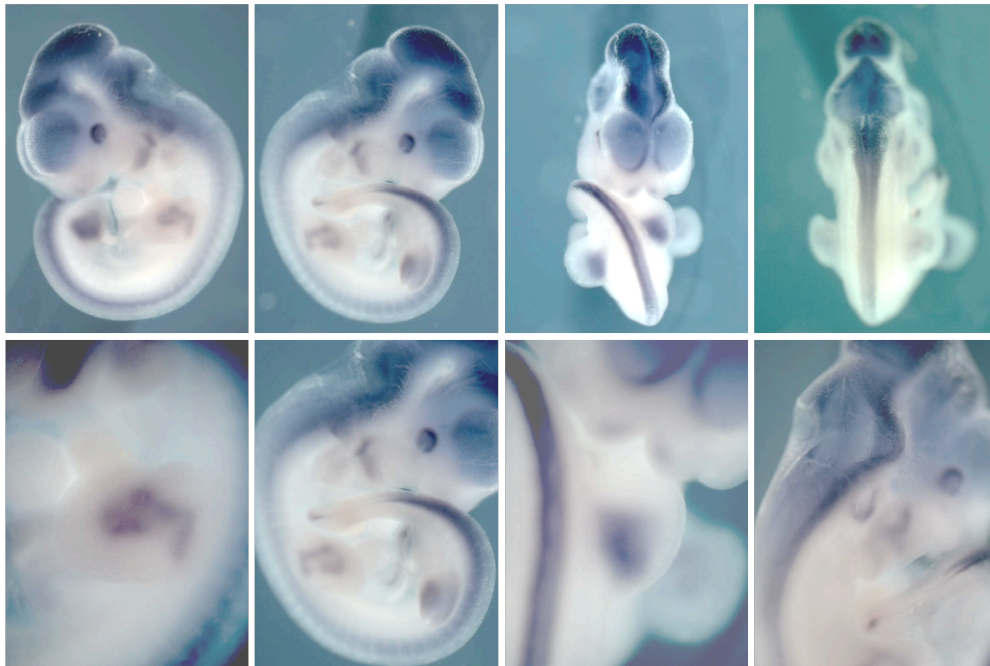


Figure 19 *Zfp145* expression in E 11.5 wild type embryos. Main expression was detected in the brain, vertebral column, fore- and hind limbs, as well as the otic vesicle and the first/ second branchial arches.

The caudal region of the hindbrain in E11.5 wild type embryos strongly expresses *Zfp145*, whereas weaker *Zfp145* expression domains were observed on the lateral areas of the midbrain/ forebrain boundary

Figure 19. When comparing to the anti-sense *Zfp145* probe (not shown), a clear specific positive staining was displayed in the eye. In addition, a small, faint and more ectopic expression pattern was observed at the edge of the optic vesicles as well as a positive staining in the first and second branchial arches that later form the mandibles (Gilbert, 2000). *Zfp145* expression was additionally observed along the entire vertebral column beginning in the rostral region at the basis of the hindbrain and the first cervical somites that become weaker in the cervical and thoracic somites, and getting again more intense towards the caudal region in the sacral and lumbar somites. The most caudal somites of the tail lack *Zfp145* expression. Furthermore, the forelimbs showed a specific

expression of Zfp145, which seemed to be restricted to the mesenchymal tissue and condensing cartilage, whereas a strong, triangle shaped area of Zfp145 expression was observed in the proximal area of the outgrowing hind limb. When comparing Zfp145 expression pattern of a wild type embryo to a homozygous ALI037 embryo no obvious differences were detected.

5.2.3.2 Influence of ALI037 mutation on the expression pattern in E 11.5 mouse embryos and limbs

A number of molecular pathways and genes have been identified that are essential for the development of the outgrowing appendicular skeleton (Manouvrier-Hanu et al. 1999). As for all outgrowing structures, limb development and the connected molecular pathways being responsible for the first patterning are divided into three axes, the proximal-distal (PD), dorsal-ventral (DV) and anterior-posterior (AP) axis. Being responsible for AP patterning, two major players in Sonic hedgehog (Shh) signalling, Shh itself and Gli3 as downstream element, were analyzed on messenger RNA level by whole mount *in situ* hybridisation to elucidate the influence of Zfp145 on Shh signalling. In addition to AP patterning, the aspect of DV patterning and the differentiation of the cartilaginous skeletal elements of the limb was thereby analysed using Bmp4 as a representative for the bone morphogenetic protein family.

Signalling pathways for the determination of positional information along the body axis were first identified in *Drosophila* with a group of homeobox (Hox) genes that were later sub-grouped into the Hoxa to Hoxd cluster. Especially the 5' genes in Hoxa and Hoxd clusters play essential roles in limb development, with Hoxa13 and d13 being responsible for digital development, Hoxa11 and Hoxd11, radius and ulna/fibula and tibia (Niswander, 2003). Barna and colleagues could show alterations in Hoxd expression upon Zfp145 depletion and implied that Zfp145 protein act as upstream regulator of Hoxd expression (Barna et al., 2000); they demonstrated in a later publication that Zfp145 is regulating Hoxd11 expression by direct physical interaction through Polycomb proteins with DNA resulting in chromatin remodelling (Barna et al., 2002). For this reason, influences of Zfp145 on Hoxd9 to d13 expression were analysed in wild type and homozygous ALI037 E11.5 mouse embryos with emphasis on limb patterning by whole mount *in situ* hybridisation

In E11.5 wild type embryos, Bmp4 expression was observed in the craniofacial region, in the neural ganglions as well as in the developing limb, as shown in Figure 20. In the limbs, Bmp4 expression was restricted to the posterior and a little weaker to the anterior margins of the limbs buds. Gli3 was expressed in the craniofacial region, the ventricles, fore-, mid- and hindbrain as well as in the limb buds according to literature. In the wild type embryos, Gli3 was expressed in the anterior mesenchyme of the limb bud. Shh was exclusively expressed to the posterior and apical margin of the limb buds, the zone of polarizing activity (ZPA), as described in literature (Gilbert, 2000). In homozygous ALI037 E 11.5 embryos, there was no obvious difference in the expression pattern of the investigated genes Bmp4, Shh, and Gli3 compared to the wild type situation (Figure 20).

Also the expression patterns of all Hoxd genes were not altered between the wild type and the homozygous ALI037 embryos except for Hoxd11 as presented in Figure 21. Careful examination of homozygous ALI037 embryos revealed an anteriorly extended area of Hoxd11 expression at the apical ridge of the hind limbs (arrows in Figure 21) compared to the wild type hind limb. In addition, there seemed to be a second sickle-shaped Hoxd11 expression domain more proximal in the mesenchyme of the homozygous ALI037 hind limb, which could not be seen in the wild type hind limb.

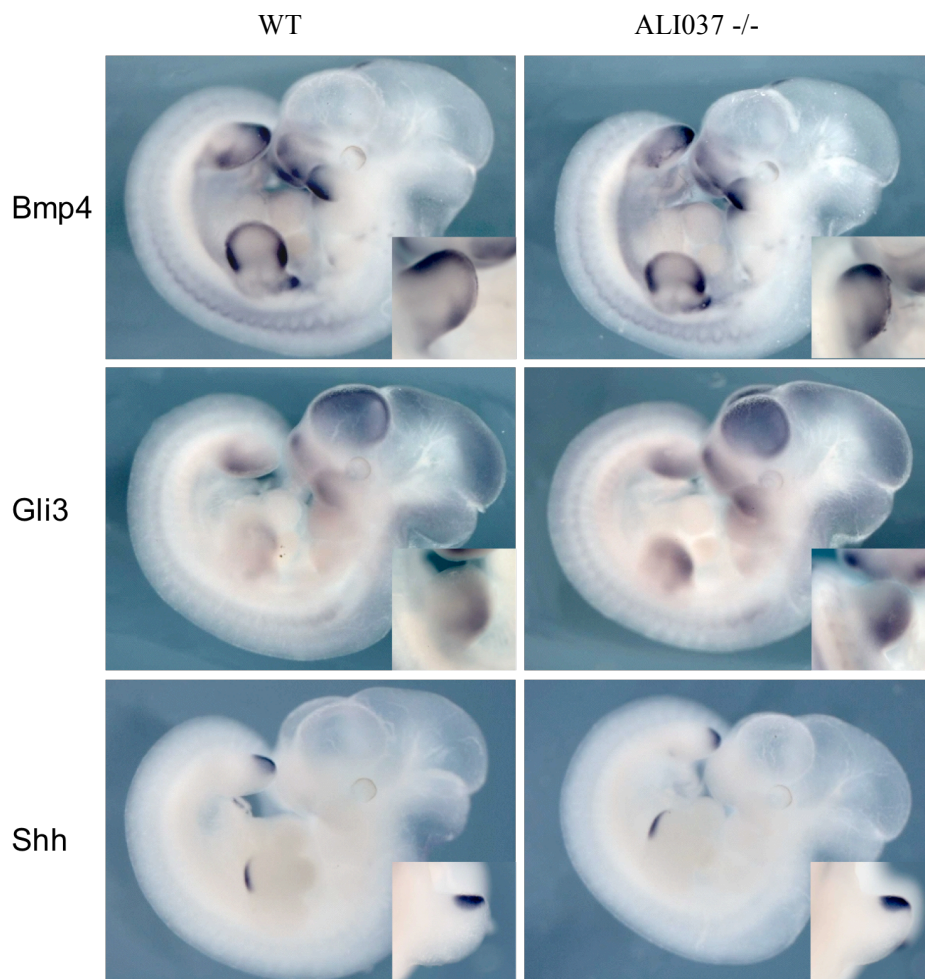


Figure 20. Expression analysis of mRNA levels by whole mount in situ hybridisation in wild type and homozygous ALI037 E11.5 embryos with emphasis on hind limb. In E11.5 wild type embryos, Bmp4 is expressed in the craniofacial region, the neural ganglions and at the posterior and anterior margins of the limb buds. Gli3 is expressed in the craniofacial region the brain and the anterior domain of the limb buds. Shh expression was observed exclusively at the posterior apical ridge of the limb buds. The same expression patterns for Bmp4, Gli3 and Shh were observed in homozygous ALI037 embryos.

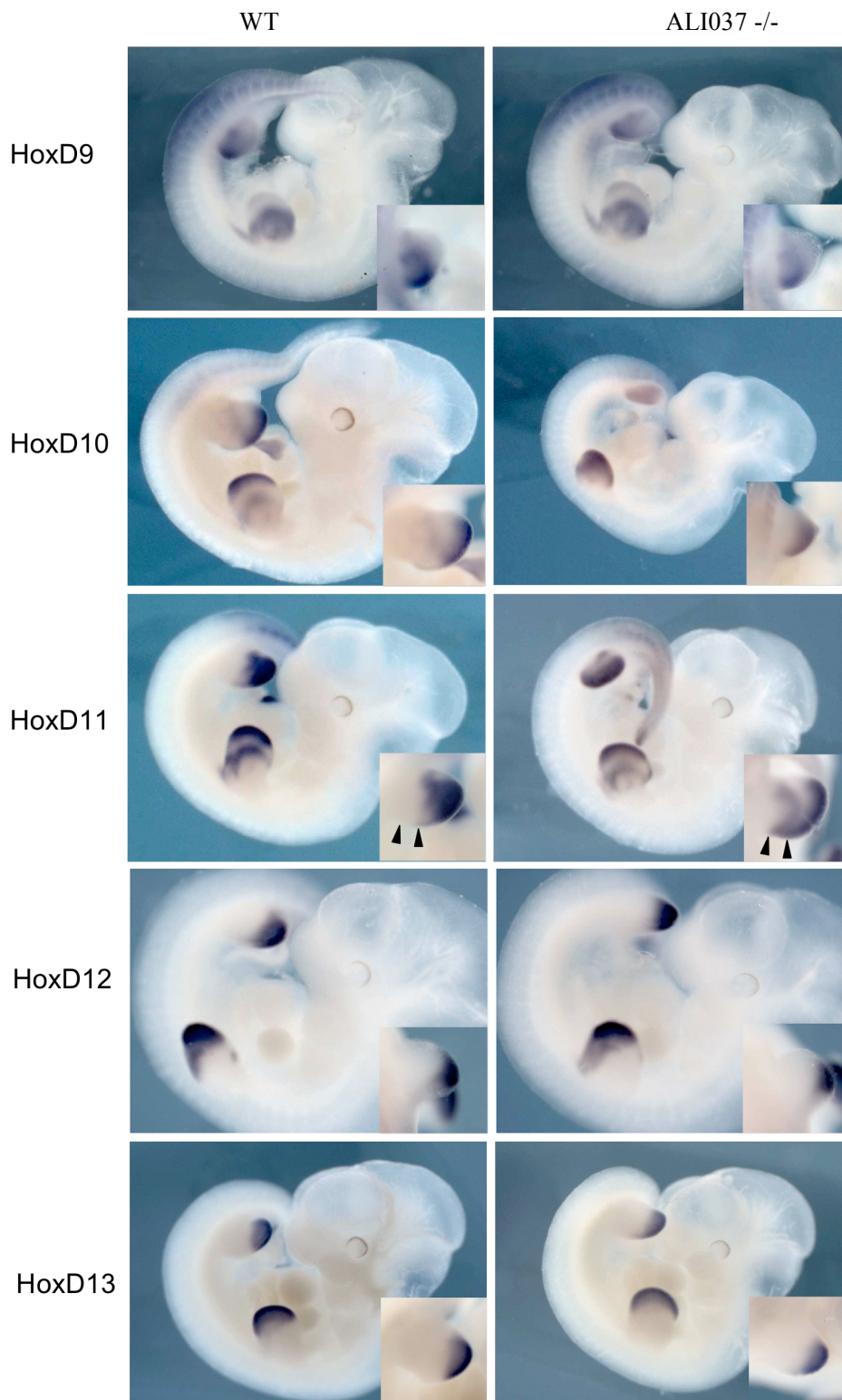


Figure 21. Whole mount in situ hybridisation of wild type and homozygous ALI037 E11.5 embryos with 5' genes of the Hoxd cluster, Hoxd9-d13 that play major roles in the development of ulna/ radius, tibia/ fibula and digits. There was no difference in the expression patterns of Hoxd9 to d13 in wild type and homozygous ALI037 embryos except for Hoxd11 in the hind limbs. In the wild type hind limb, the Hoxd11 expression is on the posterior side of the limb whereas in homozygous ALI037 embryos, the expression domain is anteriorized and an additional more proximally Hoxd11 expression domain was detected (see arrows).

5.2.3.3 Immunohistochemistry of testes

In order to understand the processes that lead to a progressive loss of spermatogonia in male ALI037/ALI037 mice, proliferating cell nuclear antigen (PCNA) and CyclinD1 as distinct markers for proliferative spermatogonia (Beumer et al., 2000; Wrobel et al., 1996), and p27 for Sertoli cells (Beumer et al., 1999) were used in immunohistochemistry. With these markers, it can be elucidated whether the progressive loss of spermatogonia is based on an intrinsic factor or on a reduction and abolishing function of the surrounding Sertoli cells and Leydig cells. Cross sections of testes from ALI037/ALI037 and wild-type males of about 12 weeks and older than 24 weeks old animals were first stained with the antibodies and subsequently counterstained with haematoxylin.

In 12 weeks old ALI037 male mice, most of the tubules were already agametic and only a few tubules showed populations of PCNA-positive spermatogonial cells as shown in **Figure 22(B)**. The tubules of 12 weeks old wild type animals were in contrast completely populated with all stages of male germ cells, especially with PCNA-positive spermatogonial stem cells that are mainly localized at the basement membrane. In both genotypes, only few Leydig cells were observed in the interstitial areas surrounding the tubules.

All tubules of old (> 24 weeks old) ALI037 male mice were *PCNA*- and *CyclinD1*-negative (see **Figure 22 D, H**) but they retained p27-positive Sertoli cells along the basement membrane (**Figure 22, F**). In addition, ALI037 male mice showed an increased proliferation of Leydig cells surrounding the agametic tubules compared to the situation in the wild-type animals. In the > 24 weeks old wild type males, the morphology of all spermatogonial stages, the tubule content, and the Leydig cells did not change with increasing age compared to the 12 weeks old wild type animals.

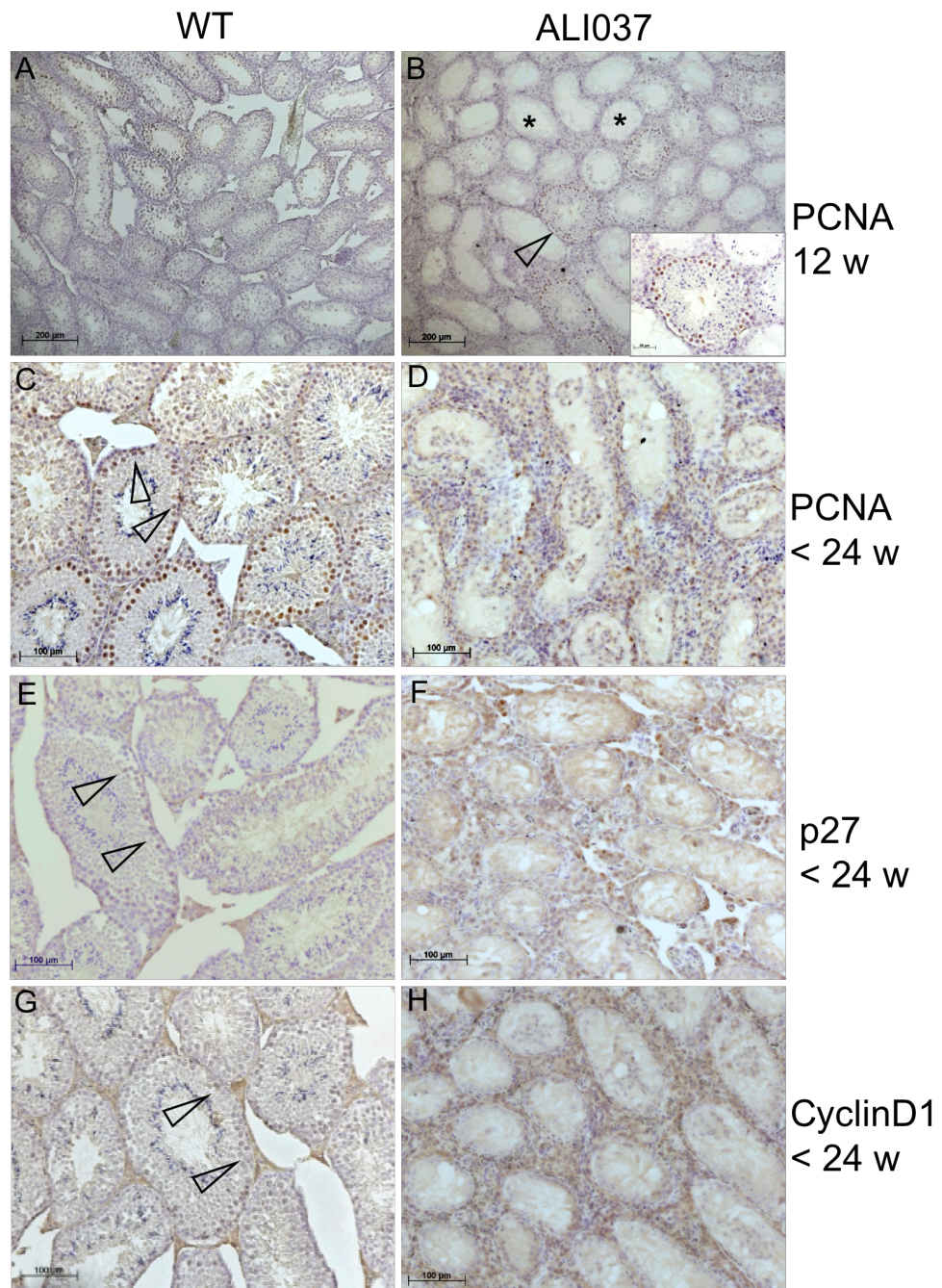


Figure 22 Immunohistochemistry of testes ALI037^{+/+} and ALI037^{-/-} mice. Staining of testes with PCNA showed a clear reduction of PCNA-positive spermatogonial cells in 12 weeks old ALI037^{-/-} mice (B) and the majority of tubules are agametic compared to the age-matched wild-type controls (A). This situation became more pronounced in > 24 weeks old animals: no tubules with PCNA-positive and Cyclin D1-positive spermatogonial cells can be observed in the ALI037^{-/-} mice anymore (D, H) compared to the wild-type animals (D, G) Whereas, the p27 staining as markers for the Sertoli cells displayed no difference in both groups. Moreover, the >24 weeks old ALI037^{-/-} testes showed an increased proliferation of the Leydig cells surrounding the agametic tubules.

6 Discussion

The emphasis of the first part of this PhD work was the implementation of the core facility in a framework of a genome-wide and large-scale ENU mouse mutagenesis project aiming at the systematic production of mouse models for monogenic inherited diseases in humans (Brown and Peters, 1996; Hrabe de Angelis and Balling, 1998). Due to the scale of the project, the first challenge was the implementation and optimization of all workflows within the core facility in order to guarantee standardized procedures for ENU handling, ENU injection, all relevant breeding procedures and phenotyping procedures at a large scale. Its success was the basis to efficiently support all participating scientific groups in isolating and analyzing large numbers of mouse models that cover a broad spectrum of mutant phenotypes being relevant for human diseases.

Subsequent in depth analysis of isolated mouse models and their clarification of phenotype-genotype correlation are supposed to contribute to a better understanding of the interlinking networks of genetic signals that underlies the pathogenesis of diseases in humans. Therefore, the second part of this PhD work was dedicated to the phenotypic and molecular characterization of five mutant mouse lines with dysmorphological abnormalities at the limbs in order to demonstrate proof-of-principle, to show the spectrum of the different ENU induced mutations and to underline the impact of this strategy towards the dissection of genotype-phenotype correlation especially with regard to the pathogenesis of human genetic disease.

6.1 Implementation of a large-scale genome-wide genetic screen in the mouse

6.1.1 Improvement of ENU treatment QC

In the course of this project, the quality control of ENU administration could be improved regarding the failure rate of ENU treatments thus consistently supporting the efficiency of the project. Considering that each injection batch of ENU-treated males is the basis of a long-term experiment generating F1 offspring over a period of one year or more, the failure rate of ENU administration had to be minimized. When starting the project, quality control of ENU solution consisted mainly of visual control of the solution that had to be clear and light yellow; once in an injection procedure, we obtained a whitish ENU solution from an older production batch indicating degradation of the substance and resulting in a reduced mutagenicity. ENU is known to be hygroscopic and instable with increasing pH (Shibuya and Morimoto, 1993), but a manufacturer's recommendation about storage duration did not exist. In order to minimize the risk of treatment failure, the manufacturer was requested to analyze each single ENU flask used for its UV spectrum and specific melting point temperature (TMP) indicating the presence of its alkylating side group and its purity grade, respectively. The outcome of this analysis was that variations in the purity grade occurred in each batch of ENU production (data not shown). For this reason, we decided to use each ENU batch for only one year, to use one single ENU batch for each multiple injection group and to send each ENU

bottle for UV spectral analysis and TMP; not until receiving a positive result from the analysis an injection group was approved for F1 generation. After implementation of the internal ENU treatment quality control, not a single failing attempt of ENU administration was recorded.

6.1.2 Optimization of breeding schemes

Within this work dominant and recessive breeding schemes were successfully implemented and optimized for an efficient generation of dominant and recessive ENU induced phenotypes in the frame of a large-scale mutagenesis screen considering the number as well as the variety and quality of phenotypes (Soewarto et al., 2003).

The implementation of a dominant breeding scheme is simple since it includes only one breeding step. The generation of F1 animals can be easily accelerated since ENU administration was subjected to male mice that are not restricted with regard to number of germ cells, a fertility period of a more than 12 months, and by using a rotating breeding system where one male is mated to a group of two females generating 12 offspring in a weekly interval a single male mouse could, in theory, produce 624 offspring in 52 weeks. Nevertheless, the number of F1 offspring was restricted to 50 F1 per ENU treated male due to the risk of generating identical mutations also known as clusters. ENU administration is mainly affecting spermatogonial stem cells that still undergo mitotic divisions before their transition into meiosis (Justice et al., 1999). Due to its cytotoxic effect, ENU depletes the majority of germ stem cells and post-meiotic phases of spermatogenesis. The smaller the remaining population of pre-meiotic germ cells carrying mutations that further proliferate the higher the risk of clustered mutations. The problem of clustered mutations was never observed in the dominant screen presumably due to the restriction of 50 F1 per ENU-treated male. But we could show that we produced clustered mutations in the beginning of the recessive screen. Initially, an out/backcross strategy with male F1 founders was used without any restrictions neither with regard to the F1 founder numbers or origin from certain ENU males nor pre-existing dominant phenotypes. Each pedigree generated 40 G3 offspring and all variants (independently from which micro-pedigree) were subjected to confirmation cross without any restriction. On one side, this resulted in a high mutation frequency of 1.25-1.4 mutant lines per pedigree, on the other side in the occurrence of identical phenotypes in several lines deriving from a single founder and presumably from the same affected spermatogonial stem cell as demonstrated in Figure 23. In addition, this strategy allowed an overlay of dominant and recessive phenotypes within a micro-pedigree thus complicating the confirmation of phenotypes and, later on, the molecular characterization of the mutations. In order to overcome this problem, a new strategy was chosen that turned out to enhance the efficiency and simplify the isolation of recessive phenotype and its subsequent molecular characterization. From a logistical and scientific point of view, the screen improved with regard to time, cage capacity and variety of phenotypes. First, every single F1 male that was selected as micro-pedigree founder had to derive from a different ENU treated male, and second, all F1 founders had to be subjected to the primary screen first and were not allowed to carry any obvious dominant phenotype.

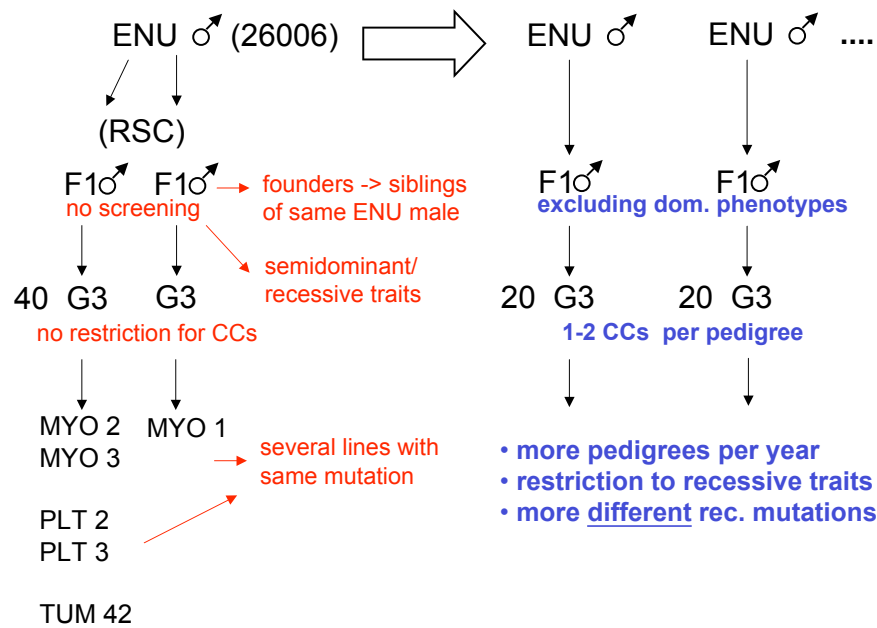


Figure 23 Example of the initial recessive breeding scheme without restrictions and its consequences. F1 founders were randomly selected without considering the number and origin of a certain ENU-treated neither male nor existing dominant phenotypes. Moreover, all existing variants were set up for test cross, and in case of confirmation were established as independent mutant lines. Analysis of a number of micro-pedigrees resulted for example in five mutant lines (MYO2, MYO3, PLT2, PLT3, TUM042) with three phenotypes that derived from a single ENU treated male (ID 10026006). Moreover, a non-complementation test revealed that MYO2 and MYO3 presumably derived from the same population of affected spermatogonial stem cell. Although an allelism test was not conducted it was very likely that this was the same case for PLT2 and PLT3 as well. After introducing restrictions with regard to the selection of F1 founders and variants the efficiency in recessive screen with regarding the number of pedigrees and the variety of phenotypes could be clearly enhanced.

Moreover, only 20 G3 offspring per pedigree were generated and systematically checked for multiple phenotypes before a confirmation cross was set up. As a result, the screen was selectively focused on pure monogenetic recessive traits and, with a given cage capacity (of 660 cages), the number of pedigrees per year was doubled from a maximum number of 60 pedigrees per year, with an occupancy period of 37 weeks per pedigree, to 120 pedigrees with an occupancy period of 27 weeks per pedigree. In addition, due to the pre-selection of F1 founders from different ENU treated males a broader range of independent recessive phenotypes was isolated.

6.1.3 Workflow management

The success of a large-scale genome-wide mutagenesis screen set up as a multi-partner project with a core facility and externally operating screening groups is strongly dependent on efficient workflow management at different levels including the phenotyping procedures, data management, interaction procedures between core facility and screening groups as well as standard operating procedures for the core facility.

Breeding management

The implementation of standard operation protocols for animal breeding had become necessary in order to guarantee an optimal turn over and efficient workflow in all crossings of the mutagenesis project aiming at a high efficiency of mutant isolation. As illustrated with the example of conformation crosses, the breeding management in this project was based on a concentration on fertile mutant phenotypes by regular monitoring of breeding performance and by excluding infertility of the respective wild type partner. And although clinically relevant infertile variants are excluded with this strategy they are maintained as cryo-preserved spermatozoa and could be recovered and analyzed at a later stage (Marschall et al., 1999).

Standardization of Phenotyping

For a comprehensive phenotyping procedure a large number of parameters covering a broad range of clinical relevant parameters are needed. In order to enhance the probability to isolate mutant mice a large number of animals has to be screened, and this requires easy, robust, and fast detection assays with a high sensitivity, specificity and reproducibility (Soewarto et al., 2003). For the successful identification of mutant phenotypes environmental, technical and endogenous factors that might influence the result have to be minimized. Therefore, standardization with regard to phenotyping procedures at the core facility included housing conditions, animal handling, group definition of animals at which age and under which condition a parameter is most appropriately to be measured, as well as standardized sample processing had to be determined. The number of 448 mutant lines isolated in the defined period demonstrated the success of this approach. Only in one case, a mutant phenotype of a line (TUM48) was lost after two outcross generations presumably due to segregation of multiple mutated loci that were responsible for the phenotype. All other mutant phenotypes were successfully maintained across the generations using the implemented phenotyping procedures under the conditions of the core facility. It still has to be considered that the phenotyping procedures sometimes need to be adapted in other facilities with different environmental conditions, in special for complex phenotypic traits such as weight or IgE levels indicating allergy predisposition. The overview of mutant phenotype categories clearly illustrated that a broad variety of clinical relevant phenotypes could be revealed, such as eye dysfunctions (Graw et al., 1999; Graw et al., 2001a; Graw et al., 2005; Graw et al., 2001b; Graw et al., 2001c; Graw et al., 2001d; Graw et al., 2002a), kidney dysfunctions (Aigner et al., 2007a; Rathkolb et al., 2005) or hypercholesterolemia (Aigner et al., 2007b; Mohr et al., 2004). The design of the screen accepted the loss of developmental phenotypes being embryonic lethal (Anderson, 2000; Kasarskis et al., 1998) or age related as well as late onset phenotypes. The focus on developmental or late onset phenotypes would need other specific phenotyping protocols with different infrastructural conditions and time courses as recently established in other labs such as Baylor College, Huston, Texas or RIKEN, Japan.

Data management

In the framework of a large-scale ENU mutagenesis project different types of data are created and need to be managed such as animal data, phenotyping data as well as sample data. Large numbers of

data points per animal are generated, and genetic traits had to be followed across a number of generations. Even though not part of this thesis, storage and management of all data generated in this project were essential for the organization of the core facility. For this reason a database was developed according to the special needs of this projects called MouseNet (Pargent et al., 2000) consisting of three main functional units including an animal management system (AMS), a result documentation system (RDS), and a sample tracking system (STS). The development of the database during the implementation of the project needed a strong interaction between the core facility and the bioinformatics team in order to precisely define the specifications of each procedure within the functional units. With the help of database queries additional valuable information had been available about treatment, sterility and offspring information as well as mutant line information such as pedigree information, breeding performance, backcrossing status to support the management of the core facility and to present the mutant lines to the scientific community in the WWW. Also other large-scale ENU mutagenesis projects such as the ENU mutagenesis program at the MRC, Harwell developed their own database called *Mutabase* (Strivens et al., 2000) or the MUSBD developed by RIKEN (Masuya et al., 2004).

6.1.4 The mutation recovery rate is actually higher

One of the main issues in such a phenotype-driven mutagenesis screen is a high mutant recovery rate (MRR), which is supported by optimized mutagen administration for the mouse strain used (Justice et al., 2000; Weber et al., 2000) and subsequent efficient phenotyping protocols. In this project, the MR rates were calculated in the dominant screen as the percentage of established mutant lines referring to the number of F1 animals screened (0.92%). The MR rate for recessive phenotypes was defined as the percentage of genetically confirmed mutant lines among the number of micro-pedigree founders (41.23%) and not among the numbers of G3 animals screened in order to allow a correct comparison of efficiencies between the breeding schemes. If the mutant recovery rate is calculated as the percentage of recessive mutants among the total G3 animals screened some important genetic implications are not considered: First, the micropedigrees and the number of founders are not considered with this calculation method because it does not differentiate between the recovery rate of a recessive breeding scheme that, for example, generate 100 G3 animals deriving from a single F1 founder from a breeding scheme that produced the same number of 100 G3 animals deriving from five different F1 founders with each 20 G3 offspring. Thus and secondly, the variety and “genetic” independency of mutant phenotypes are also not considered. A phenomenon, called clustering, can occur in mutagenesis experiments where a number of mutant lines derive from a single mutagen-treated spermatogonial germ cell. Due to the cytotoxic effect of ENU on stem cells in general, the number of remaining intact spermatogonial germ cells can extremely vary. The lower the numbers of remaining intact germ stem cells, which are still in a proliferating state prior to meiosis, the higher the rate of point mutations per germ cell and the probability of clusters in the descendants’ generations. Within a breeding scheme in which 100 G3 offspring derive from a single F1 founder it is therefore

more likely that mutant lines with similar phenotypes derive from the same germ stem cell with the same point mutation. With each additional F1 founder from a different litter of the same or even from a completely different ENU treated male the probability of revealing independent recessive mutant phenotypes and mutations is therefore increased and multiplied. We therefore decided for the calculation of the recessive mutant recovery rate to refer the number of genetically confirmed mutant lines to the number of micro-pedigrees, which considers the selection of F1 micro-pedigree founders from different ENU treated males and reflect the independent nature of recessive phenotypes and their underlying mutations.

However, it has to be kept in mind that not all deviant F1/ G3 phenotypes could be subjected to further inheritance testing due to structural limitations assuming that the mutation recovery rate is actually higher. For the dysmorphology screen, as an example, the complete data set of all deviant F1 animals was available (personal communication H. Fuchs). Among the 33224 F1 animals assessed in the dominant screen, 2576 F1 animals were deviant to the other F1 animals but only 711 F1 variant were subjected to inheritance testing. The selection of variants for inheritance testing remained under the responsibility of each screener/ scientist according to their own prioritization in terms of focus of the own lab, the condition and assumed fertility of the variant phenotype. In case that the remaining 1865 deviant F1 animals would have been included, even considering a reduced fertility rate, additional dominant mutant phenotypes could have been expected, thus, resulting in an additional increase of the screen-specific MRR. Although this correction factor would have to be considered, the same conditions had been valid for all participating screens. Similar mutant recovery rates for dominant phenotypes had been reported by other genome-wide large-scale ENU screens (Masuya et al., 2005; Nolan et al., 2000a). Therefore, a correction of all mutant recovery rates would presumably not change the following evaluations and conclusions.

6.2 Dominant versus recessive screen

To date, a comparison of genome-wide screens for dominant and recessive mutant phenotypes with the same comprehensive panel of phenotyping procedures had never been carried out since the majority of former mutagenesis projects had mainly focused on recessive region-specific screens or on a smaller and specified phenotype panel (Justice and Bode, 1988a; Rinchik et al., 2002; Rinchik et al., 1990; Shedlovsky et al., 1986; Shedlovsky et al., 1993). A comparison of dominant versus recessive screen with regard to mutant recovery rates and phenotype categories in this project may give considerable indications for the choice of an appropriate strategy for other genetic screens the with regard to scale of the project, specific phenotyping panels as well as ENU administration which can optimize the number of mutant phenotypes in a given experiment.

6.2.1 Considerations about mutant recovery rates and external limiting factors

At first sight, the comparison of mutation recovery rates (MRR) of 0.92% for the dominant and 41.23% for the recessive screen clearly illustrates the advantage of the recessive screen in the given setting of this project. The difference in the MRR is not surprising since the effect of a recessive

mutation is in most cases a loss of function thus reducing or completely abolishing a gene product. On one hand it can be only hypothesized that dominant mutant phenotypes may have less detrimental effects on animals such as coat colour, limb abnormalities or skeletal defects due to compensatory or secondary effects, and therefore have a higher threshold for inducing apoptotic activity in the cells (Weber et al., 2000). On the other hand in a dominant mutation, the mutant organism still carries another wild type allele, thus producing at least 50% of the gene product, which is in most cases sufficient for normal function. For some few gene products, however, 50% of the normal function is not normal, and haploinsufficiency produces an abnormal phenotype, which is inherited in a dominant manner. Therefore, the majority of isolated dominant phenotypes are very likely to be semi-dominant.

However, for the comparison of efficiencies of both strategies the aspects of infrastructural conditions and time have to be considered as well, as shown in the following calculation: For a given setting of 350 cages (type II, 5 mice per cage), up to 1750 F1 animals can be maximally housed in the dominant screen. Due to the phenotyping turnover of 17 weeks the animals can be exchanged three times in a 52 weeks-period resulting in 5250 F1 animals that could be assessed. With the given MR rate of 0.92%, approximately 48 dominant mutant phenotypes could be expected. For the same setting and conditions in the recessive screen, 35 micropedigrees (MP) (10 cages per MP for G2/G3 generation, 20 G3 /MP) and a period of 34 weeks for G3 generation and phenotyping have to be calculated. Due to the phenotyping turnover of 17 weeks the MPs can be exchanged 1.5 times per year resulting in 51 micropedigrees with 1020 G3 animals. With the given MR rate of 41.23%, approximately 21 recessive mutant phenotypes could be expected. Regarding the breeding scheme, time scale, and absolute numbers of mutant phenotypes, now, the dominant screen became advantageous due to the short breeding time of one generation, the higher assessment turnover across the year and the higher number of mutant phenotypes, whereas in the recessive screen, a two breeding step strategy with a longer turnover period had to be applied. A genome-wide screen with a comprehensive phenotyping protocol covering as many organ systems as possible to identify dominant and/or recessive mutant phenotypes make sense if there are no limitations of infrastructure, personnel, and time. If one of the factors is restricted, it is possible and preferable to scale down the project focussing on certain phenotypes (developmental, behaviour), specific pathways, chromosomes (locus-specific, balancer) or parameters that can be assessed at an early time point that allow a much faster turn-over of assessment and replacement of animals.

6.2.2 Dominant and recessive strategy across the screens

It has to be considered which appropriate phenotyping protocols are available for the model organism of interest, and whether the parameters are simple, robust and easy to measure and analyze. For the set up of the project workflow, it is essential to estimate how many measurements can be performed in which time period under the same conditions; the limitation for the scale is always given by the phenotyping panel or screening protocol with the lowest capacity. But the first real indication for the efficiency of a screen is the mutant outcome within the project. With regard to the absolute recovery

of dominant phenotypes, the dysmorphology screen was most successful (68% of all dominant mutants) followed by the clinical chemistry (13%) and the immunology screen (5.21%). Here, it has to be kept in mind that the number of F1 animals being assessed for dominant phenotypes had been strongly variable across the screens. Compared to the recessive strategy, the clinical chemistry screen was most successful (34.75% of all recessive mutants), followed by dysmorphology (31.91%) and the immunology screen (19.15%). The leading roles of these screens is not surprising considering that 112 out of 132 parameters had been analysed by three screens only. Interestingly, the same three groups revealed a clear significant preference for either one of the strategies: Whereas the blood-based screens showed a statistical significant preference to recover more recessive mutant phenotypes, the dysmorphology screen was more prone to isolate more dominant mutant phenotypes. These facts reflect the situation in genetic diseases where the majority of inherited physiological dysfunctions known so far are based on loss of function mutations that tend to be recessive (Read, 2003) pp. 463.

Another indication for the quality of screens is the mutant recovery rate in relation to the number of confirmation crosses being set up. The screen-specific confirmation rate (CR) reflects, in general, the robustness of measured parameters and the reliability of their analyses. The majority of screens in this project had displayed relatively constant CRs in both strategies with their given phenotyping set up, which is an indication of high robustness of the selected parameters. The only exception was the clinical chemistry screen with a significantly higher CR for recessive (41.88%) than for dominant phenotypes (24.16%), which had had a number of technical and structural reasons: At the beginning of the project, a threshold of a two-fold standard deviation had been defined and was changed at a later stage to three standard deviations. Therefore, at the very beginning of the project, the clinical chemistry screen had presumably determined a higher rate of false positive variants that later were not confirmed. In addition to this, there was a change of the diagnostic lab in the course of the project, beginning of 2001, which was not beneficial for the stability of the measurements. Nevertheless, in general, the parameter panels selected for this project had demonstrated to be efficient, robust and therefore appropriate for a large-scale genetic screen in the mouse.

6.2.3 Some phenotype categories show a higher prevalence in dominant or recessive strategy

Analysis of phenotype categories is an additional point for strategic considerations giving indications about preferences of phenotype categories that can be expected in either one of the strategies. For this evaluation, all screening parameters had been assigned to functional phenotype categories that represent either organ systems, physiological pathways or certain behaviour patterns as previously described.

The distribution of phenotype categories in relation to all isolated mutants is a very project-specific value and would completely change if, for example, a large group of parameters (i.e. dysmorphology) would not be assessed but normally isolated a considerable number of mutants. Therefore, this value is less informative for the estimation of phenotype categories to be expected in a potential future

project. For this reason, the main emphasis for further analysis was put on the screen-specific distribution of phenotype categories presented as a percent value in Table 6 .

Only three phenotype categories in two screens showed significant preference for either one of the strategies: The clinical chemistry showed a significant preference for dominant blood cell count alterations (50% vs. 21.15%) and for recessive kidney dysfunctions (2.5% vs. 17.31%)(Aigner et al., 2007a; Rathkolb et al., 2005). In contrast, the dysmorphology screen demonstrated a significant preference for recessive body size abnormalities (4.76% vs. 17.78%). Body size abnormalities can be based on developmental defects of the vertebral column or on metabolic defects effecting skeletal growth such as *Campomelic dysplasia* (MIM114290), involutional osteoporosis (MIM166710), *osteogenesis imperfecta* (MIM166200) or *Marfan* syndrome (MIM154700). All other phenotype categories had demonstrated a similar distribution in both strategies.

However, beside the prevalence of phenotypes, this evaluation can give a rough but valuable estimation about the scale and prerequisites of a prospective genetic screen in the mouse by multiplying the total screen-specific mutant recovery rate and the proportion of a specific phenotype category/ parameter as shown in table xxx. (These screens could be carried out, for example, on different genetic wild-type backgrounds in order to isolate modifier genes, or on sensitized genetic backgrounds, i.e. a knock-out line, in order to obtain new interaction partners of a given signalling pathway.) By taking two examples of the clinical chemical parameters ‘kidney dysfunctions’ and ‘blood cell count’, the use of these numbers can be demonstrated: The project-specific mutant recovery rate for the clinical chemistry (CLC) screen in the dominant strategy is 0.21%, which means that one in 476 F1 animal has a clinical chemical phenotype. The MRR for the CLC screen in the recessive screen is 14.33%, which means that one of 6.5 micro-pedigrees (with each 20 G3) or one of 130 G3 would show a clinical chemical phenotype.

Phenotype categories	DOM Phenotypes	Screen-spec proportion in%	dom MRR in %	screened F1 per mutant recovery	REC Phenotypes	Screen-spec proportion in%	rec MRR in %	screened G3 for mutant recovery	screened MP for mutant recovery
Total	<i>n</i> = 307				<i>n</i> = 141				
Allergy	<i>n</i> = 11				<i>n</i> = 2				
IgE high	4	36,36	0,06	4584	1	50	0,58	6897	345
IgE low	7	63,64	0,06	2619	1	50	0,58	6897	345
Behaviour	<i>n</i> = 11				<i>n</i> = 8				
Anxiety	7	63,64	0,06	2619	4	50	2,14	1869	93
Cognition	2	18,18	0,06	9168	1	12,5	2,14	7477	374
Exploration	1	9,09	0,06	18335	2	25	2,14	3738	187
Hyperactivity	1	9,09	0,06	18335	1	12,5	2,14	7477	374
Clinical Chemistry	<i>n</i> = 40				<i>n</i> = 52				
Alk. Phosph.	5	12,5	0,21	3810	2	3,85	14,33	3625	181
Blood cell count	20	50	0,21	952	11	21,15	14,33	660	33
Cholesterin	6	15	0,21	3175	8	15,38	14,33	907	45
Electrolytes	1	2,5	0,21	19048	6	11,54	14,33	1209	60
Iron metabolism	1	2,5	0,21	19048	3	5,77	14,33	2419	121
Glucose	1	2,5	0,21	19048	0	0	14,33	n.a.	n.a.
Kidney function	1	2,5	0,21	19048	9	17,31	14,33	806	40
Liver function	3	7,5	0,21	6349	1	1,92	14,33	7269	363
Muscle function	0	0	0,21	#DIV/0!	4	7,69	14,33	1815	91
Pancreas function	2	5	0,21	9524	8	15,38	14,33	907	45
Dysmorphology	<i>n</i> = 210				<i>n</i> = 45				
Abnormal behaviour	32	15,24	0,63	1042	7	15,56	11,16	1152	58
Body size	10	4,76	0,63	3335	8	17,78	11,16	1008	50
Bone	45	21,43	0,63	741	7	15,56	11,16	1152	58
Coat Colour	32	15,24	0,63	1042	7	15,56	11,16	1152	58
Deaf	14	6,67	0,63	2380	1	2,22	11,16	8073	404
Eye	20	9,52	0,63	1667	0	0	11,16	n.a.	n.a.
Limb	30	14,29	0,63	1111	6	13,33	11,16	1344	67
Skin/ Hair	24	11,43	0,63	1389	7	15,56	11,16	1152	58
Teeth	3	1,43	0,63	11100	1	2,22	11,16	8073	404
Trembling	0	0	0,63	n.a.	1	2,22	11,16	8073	404
Immunology	<i>n</i> = 16				<i>n</i> = 27				
Basal Immunglobulins	9	56,25	0,09	1975	15	55,56	7,89	456	23
B-/T-cell markers	6	37,5	0,09	2963	12	44,44	7,89	570	29
TGGE	1	6,25	0,09	17778	0	0	7,89	n.a.	n.a.
Nociception	<i>n</i> = 15				<i>n</i> = 3				
Fast	6	40	0,08	3125	1	33,33	0,88	6819	341
Slow	8	53,33	0,08	2344	2	66,67	0,88	3409	170
Jump	1	6,67	0,08	18741	0	0	0,88	n.a.	n.a.
Mitochondrial	<i>n</i> = 0				<i>n</i> = 1				
Lactate	0	0	0,00	n.a.	1	100	0,29	6897	345
Hemostasis	<i>n</i> = 5				<i>n</i> = 7				
High clotting time	2	40	0,09	2778	5	71,43	1,75	1600	80
Low clotting time	3	60	0,09	1852	2	28,57	1,75	4000	200

The period for mutant recovery for a specific phenotype category can be easily estimated with the help of the following simple equations by using the numbers of the table:

For dominant phenotypes $y = ((1/x) * (1/m * k)) + 4$ (one-step breeding with 4 months)
 For recessive phenotype $y = ((1/x) * (1/m * k)) + 10$ (two-step breeding with 10 months)

m : mutant recovery rate for a screen
 k : screen-specific rate for a phenotype category
 x : number of F1 or G3 generated per month
 y : average period to recover a mutant phenotype (with a specific phenotype category)

When applying the equations to the numbers mentioned above for a specific phenotype category the graph shows the dependency of the average period in months until mutant recovery can be statistically expected dependent from the breeding colony size. Additionally, a *cage factor* for both breeding schemes can be calculated to obtain the absolute cage numbers needed, which can be summarized as follows:

Assumptions:

- The cage factor include the cage number for all breeding steps: ENU breeding, F1 and G3 generation
- 5 offspring per litter with equal distribution of 50% male and female offspring
- 5 animals per type II cage
- 20 G3 per micro-pedigree

For F1 breeding:

1) 100 F1 /month	20 cages
2) (100/5) ENU breeding cages	20 cages
Total:	40 cages

Cage factor F1 breeding scheme: 40 cages / 100 F1 = 0,4

For G3 breeding:

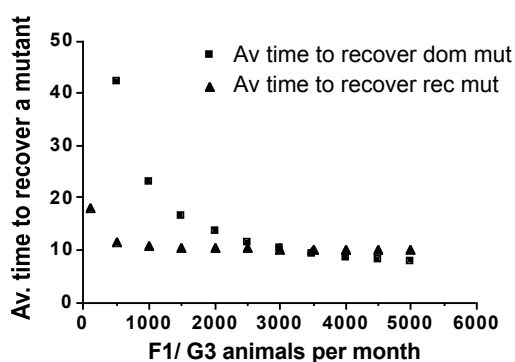
1) 100 G3/ month (from 5 micro-pedigrees)	20 cages
2) F1 males x wt female	2 cages (animals will be separated)
3) F1 male x 4 G4 females	4 cages (single rotation breeding in weekly intervals)
4) 20 G3 offspring	4 cages
5) (5 m+ 5 f F1 offspring/ 5) ENU breeding cages/ month	2 cages
Total:	52 cages

Cage factor for G3 breeding scheme: 52 cages/ 100 G3 = 0,52

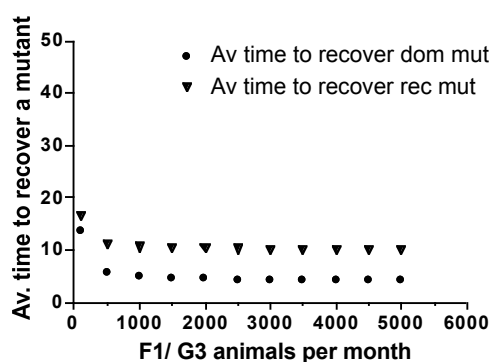
Example 1

Example 2

Period to mutant recovery dependent from colony size for kidney screen



Period of mutant recovery dependent from colony size for BCC screen



Example 1: The recovery rate within the CLC screen for kidney parameters in the dominant screen is 2.5%, whereas it is 17.31% in the recessive screen; this results in approximately one in 19040 F1 animals in the dominant and every 37.5th micro pedigree or one in 751 G3 animals with kidney dysfunctions implying that more recessive traits are presumably connected to kidney function than dominant traits. With a colony size of 1000 G3 animals per month the average period to recover a kidney phenotype is about 10 months. . The number of cages can be calculated with cage factor of 0,4 for the dominant and with 0,52 for the recessive breeding scheme, as described above, resulting in a cage capacity of 400 cages. However, due to the shorter period for the dominant breeding scheme, there is a break-even point at a colony size of 3500 F1/ G3 animals per month, which, nevertheless, will be not affordable for the majority of animal facilities and projects since for a presumed F1 production of, for example, 3500 F1 per month a needed cage capacity of 1400 cages; accordingly, for a presumed G3 production of 200 per month a needed cage capacity of 1820 cages.

Example 2: The recovery rate within the CLC screen for abnormal blood cell count in the dominant screen is 50%, whereas it is 21.15% in the recessive screen; this results approximately in one phenotype among 952 F1 animals in the dominant and every 30.8th recessive family or one in 614 G3 animals with abnormal blood cell count. In this example, it can be concluded that a screen for dominant blood cell count phenotypes is presumably much efficient and faster than a recessive one. With a colony size of 1000 F1 per month the average period to recover a blood cell count phenotype is about 6 months and a cage capacity of 400 cages is needed.

Both examples demonstrated a very theoretical view on potential recovery rates of specific phenotype categories regarding time lines and cage capacities. However, the presented data based on the numbers of this large-scale project can serve as a tool to choose the appropriate breeding strategy, to roughly estimate the scale of a screening project and its feasibility.

6.2.4 Impact of the ENU regime on the strategy

To date, a threshold dose response of ENU concentration and SLT mutation rates had been discussed (Favor, 1998; Favor, 1999). Aim of the retrospective comparison of ENU regimes was to investigate whether there is a preferential ENU regime being advantageous for either one of the strategies. T12 and T16 were not further considered for a comparison since both regimes were only included one time each for the recruitment of MP founders, and from the T31 ENU batches no single MP founder was recruited for the recessive screen. For this reason, only T38 and T39 were considered for further statistical analysis. At the very beginning of the recessive screen, T39 had been used (batch ID19-24) to generate F1 founders, but soon resulting in a high proportion of confirmation crosses of G3 animals across all groups that turned out to be sterile (personal communication H. Fuchs). It had been assumed that due to a higher mutation load multiple

mutations had been induced and might have affected the variants' fertility since ENU is known to deplete germ stem cells (Weber et al., 2000), or induced a higher embryonic lethality. For this reason, a lower ENU regime T38 (batch ID 26-41) had been chosen to continue. It has to be noticed in addition, a number of building reconstructions had been conducted during this phase of the project. Since rodents are known to react sensitively to noise with stress and fetus resorption this factor could have contribute to the decreasing breeding performance. The T39 ENU regime displayed a higher mean MRR in both strategies, which was also statistically confirmed and in concordance with the threshold dose response correlation of ENU concentration and SLT mutation rates (Favor, 1999; Favor et al., 1988; Favor et al., 1990; Hitotsumachi et al., 1985; Russell et al., 1982) Moreover, analysis of sterility periods between T38 and T39 did not show any significant difference, whereas analysis of lifespan of treated males showed a significantly longer life period for animals treated with T39, which is even contradictive to the hypothesis of a disadvantageous effect of a higher ENU concentration. Although the mutant recovery rate is higher with T39, it has to be considered that the relative high standard deviation makes it much more difficult to calculate the appropriate size of a breeding colony, and therefore, T38 should be preferably applied for both strategies.

6.3 Characterization of abnormal limb mutants

This thesis demonstrated that the forward genetics approach by using ENU mutagenesis successfully isolated mouse mutants that do serve as animal models for human inherited diseases and profoundly contribute to the dissection of gene function. Five mutant lines with dysmorphological abnormalities at the limbs were selected for further phenotypic and molecular characterization to show proof of principle and demonstrate the advantages of this approach. The selected mutant lines are ALI3, ALI9, ALI12, ALI19 and ALI037.

6.3.1 ALI3/ ALI9/ ALI12/ ALI19 mutations affect the *Sonic hedgehog* pathway

The limbs have an essential function in all vertebrates, and in humans limb anomalies occur in approximately one in a thousand newborns (Manouvrier-Hanu et al., 1999). For a period of time, limb malformations were classified either on a purely clinical description (Temtamy and McKusick, 1978) or later in relation to embryological patterning defects (Winter and Tickle, 1993). Since more than two decades, knowledge about the genetic bases of many limb malformations has continuously increased, and their classification has developed towards the underlying genetic defects along the three axes of a limb, the determination of limb/ digit identity, and morphogenesis.

Four ENU induced mutant lines ALI3/ ALI9/ ALI12/ ALI19 were isolated in the dominant screen with similar phenotypes displaying preaxial polydactyly at the hind limbs. After subjected to allelism test, the result already gave an indication of the putative signaling pathway and the group

of genes involved. The severe phenotypes of the double heterozygous embryos resemble to the phenotypes of all four single homozygous ALI3/ ALI9/ ALI12/ ALI19 mutant embryos with small variations, as shown in **Table 8**, and strongly resemble to mutants of genes belonging to the sonic hedgehog pathway (Shh) such as the *Ptch* knockout mouse. In mammals, the *Shh* pathway is involved in patterning of the anterior-posterior axis in limbs, the neural tube, gut, and somites. In limb development, *Shh* expression is confined to the zone of polarizing activity (ZPA), representing the posterior region of the limb bud, by a joint action of *Alx4* and *Gli3*. The canonical pathway begins with the Patched-Smoothed (Ptch-Smo) receptor complex, in which *Ptch* is thought to prevent *Smo* from functioning. When *Shh* binds to *Ptch*, this repression is released, allowing *Smo* to signal and leading to dissociation of a complex comprising of Fused (Fu), suppressor of Fused (Su (fu)) and full length *Gli3*. The dissociation leads to a truncation of *Gli3*, and when entering the nucleus it functions as a transcriptional repressor (Niswander, 2003). *Gli3* is known to possess a transcriptional repressive activity adjacent to the 5'-end followed by five, conserved tandem C2H2 zinc finger DNA-binding domains. A proteolytic cleavage site followed by a microtubule interaction site separates the repressive part from its co-activator *CBP* (CREB binding protein) binding site and two adjacent independent transactivation sites next to the carboxyterminal end. The homozygous mouse mutant of *Gli3* allele Extra toes (Xt) exhibits hemimelia, polysyndactyly, and loss of digit identity related to ectopic expression of Shh and *Ptch* in the anterior part of the limb bud and anterior deregulation of 5' *Hoxd* gene expression (Zuniga and Zeller, 1999) thus resembling to ALI3, ALI9, ALI12 and ALI19 phenotypes. Due to this fact, the affected genes were assumed to belong either to the *Shh*-signaling pathway or even represent allelic variations of the same gene. Phenotypic variations between double heterozygotes and single homozygotes or across the homozygotes, for example as for homozygous ALI12 embryos, led to the conclusion that the induced mutations might have different effects to the same secreted protein within the Shh pathway implicating allelic variations of a gene but not to the same functional activity.

6.3.2 ALI3/ ALI9/ ALI12/ ALI19 as new animal models for Greig syndrome and Pallister-Hall syndrome

Molecular characterization of the ALI3/ ALI9/ ALI12/ ALI19 mutations could confirm the assumption from the allelism test for non-complementation and linkage analysis leading to mouse chromosome 13; all four induced mutations were located in the *Gli3* gene.

In ALI3, the point mutation was determined in exon 11 at position nt1779 of the transcript and characterized as a base pair exchange from T to A that leads to an amino acid exchange from histidine to arginine in the zinc finger domain of *Gli3*. As known from the C2H2 zinc finger family, histidine and cysteine are the essential amino acids occurring repeatedly in a specific order to form finger-shaped structures in which two cysteines and two histidines correspondingly bound

zinc. Therefore, it can be hypothesized that an amino acid exchange at one histidine alters the tertiary structure of a zinc finger motif to a certain extent resulting in a loss of a zinc and thus in a reduction of DNA binding capacity. Within the zinc finger domain, the amino acid exchange is localized towards to the 3' end of the domain assuming that at least three of five functional zinc fingers still exist but mediating DNA binding less effectively. Because the repression domain of *Gli3* is localized upstream of the DNA binding domain the repressive activity of *Gli3* was presumably retained. Regarding the penetrance, the preaxial polydactyly phenotype in ALI3 was reduced to approximately 60% (data not shown) this would underline the assumption that DNA binding and transcriptional activity of *Gli3* was not completely abolished. Further detailed investigations are needed to analyze the structure of the remaining protein and its binding capacity. In Western blot analysis it can be demonstrated whether the quantity of truncated *Gli3* is altered in ALI3 comparing to wild type. In addition, reduced transcription activity would have to be confirmed for example by a reporter assay using an expression vector carrying the same mutation.

In ALI9, the mutation was characterized as a transversion from T to C at transcriptional position nt 1668+2 exactly at the boundary of exon/intron 9 located in the zinc finger domain of *Gli3*. In higher eukaryotes, highly conserved sequences can be found at the very beginning (GT) and end (AG) in introns. They generally cannot be altered without affecting the splicing process and are required for exact intron removal from the primary RNA transcript. Therefore, the ALI9 mutation is very likely to affect the splicing process thus causing a reading frame shift, and a non-sense of its message. Within the zinc finger domain, the mutation is localized in the middle of the domain implicating that upstream at least two or three zinc fingers are presumably still functional. Transcription factors are known that use three zinc fingers to recognize specific DNA sequences (Pavletich and Pabo, 1993). Further consequences of the ALI9 mutation were not further investigated on transcript- and protein level, and it can be therefore only hypothesized that, in case of a reading frame shift and subsequent translation, the resulting protein loses a part of its functional zinc finger domain and thus reduces its DNA binding capacity. Even though the splicing defect would be in frame it is very likely that the zinc finger domain would be truncated and less efficient.

In ALI12, the mutation was identified in exon 8 of *Gli3* as a transversion from C to T at transcript position nt 1522, which leads to an amino acid exchange from glutamine to a premature stop codon. Nearby, the mutation of ALI19 was identified as a transition from A to T in exon 8 of *Gli3* at transcript position nt1483, which leads to an amino acid exchange from lysine to a premature stop codon. Both mutations might lead to truncated transcripts and proteins, which were not further investigated by RT-PCR and Western blot analysis. With regard to the localization, both mutations were induced at the 5' region of the zinc finger domain implicating that, if at all, possibly only one zinc finger motif still exist so that DNA binding is completely abolished.

In humans, *GLI3* is associated to a number of autosomal dominant disorders. The Greig cephalosynpolydactyly syndrome (GCPS; MIM 175700) is a rare autosomal disorder affecting limb and craniofacial development. GCPS-affected individuals are characterized by post- and preaxial polydactyly of hands and feet, macrocephaly and craniofacial malformations. Haploinsufficiency of *GLI3* leads to loss or alteration of the zinc finger region, and therefore, presumable deprivation of any transcriptional activity (Wild et al., 1997). ALI12 and ALI19 represent new models for GCPS with the advantage of a pure genetic background that would allow a systematic dissection of phenotypic variations of the syndrome revealing modifying genes or single nucleotide polymorphisms (SNPs) that modulate the phenotype. The Pallister-Hall syndrome (PHS; MIM 146510) is characterized by multiple malformations and limb anomalies including central polydactyly, syndactyly and has been attributed to *GLI3* deletions at the 3' end of the zinc finger domain shifting the reading frame and resulting in a premature stop codon. The resulting protein represents a truncated *GLI3* with remaining repressive activity (Kang et al., 1997). With regard to similar molecular consequences, ALI3 and ALI9 represent new animal models for PHS. A third *GLI3* mutation has been identified in postaxial polydactyly type A (MIM 174200). A frame shift producing a premature stop codon leads to a truncated *GLI3* conserving its DNA binding site, as well as the sites for proteolytic binding and microtubule binding (Radhakrishna et al., 1997).

With the characterization of the mutant lines ALI3, ALI9, ALI12, and ALI19 a new allelic series of *Gli3* could be isolated that can contribute to the dissection of the pathomechanism of GCPS and PHS. The impact and importance of allelic series was formerly demonstrated by Kalff-Suske and colleagues who reported on 15 novel *GLI3* point mutations in human patients leading to GCPS (Kalff-Suske et al., 1999) thus revealing two additional independent trans-activating domains at the C-terminal of *GLI3*. In order to obtain a better understanding about the genotype-phenotype correlation of the transition from GCPS to PHS and to postaxial polydactyly type A additional mutants carrying a new set of point mutations are needed. To date, the bottleneck of gene function studies in the mouse was the molecular characterization by positional cloning or candidate gene approach. But in the last couple of years, technological development of mutation detection i.e. by mass spectrometry in a large scale, strongly improved so that the same investigations could be performed much faster and easier in mutant mouse models. With human patients the availability and accessibility of material is in most cases restricted and the genetic heterogeneity much higher, which leads to difficulties in well defined phenotypic characterization. Interestingly, the ALI3/ALI9/ALI12/ALI19 mutations affect the zinc finger region of *Gli3* implicating that zinc finger domains seemed to be especially sensitive to mutations induced by ENU. Therefore, one could benefit from the obvious existence of specific genomic hot spots for ENU action as in the case of *Gli3*, or presumably for zinc finger proteins in general, to enhance the isolation of allelic series. In general, knowledge about the structural conditions of chromosomal DNA and its

sensitivity for ENU action can be beneficial in positional cloning of ENU-induced mutations by allowing prioritization of candidate genes based on their inherent features (Barbaric et al., 2007).

6.3.3 The effect on downstream targets of ALI3/ ALI9/ ALI12/ ALI19 mutations

5'Hoxd genes were shown to be downstream targets of Gli3, and their expression were broadly activated across the early limb bud of *Gli3*^{-/-} embryos (Zuniga and Zeller, 1999). In addition, *Gli3* and *Hoxd12* interact genetically and physically, and thereby modulating *Gli3* repressor function (Chen et al., 2004) by converting the truncated *Gli3* repressor form into an activator of its targets. This is a proposed model in which *Gli3*-responsive target promoter activity is dependent, in part, on the ratio of *Gli3* to total *Hoxd* expression at a given site, which regulates *Shh* activity in a positive feedback loop (Knezevic et al., 1997; Zakany and Duboule, 1999). It can be hypothesized that in all four *Gli3* mutants, the reduced repressive activity of *Gli3* might lead to an over-expression of *Hoxd12* that, when binding the repressive form of *Gli3*, convert the repressive *Gli3* into an activator. This is also supported by some phenotypic features of *Tg-Hoxd12* that resemble to the homozygous ALI3 and ALI9 mutants including polydactyly at fore and hind limbs, loss of digit identity and tibial hemimelia (Knezevic et al., 1997). Final evidence can be obtained by further investigations of expression levels of the *Shh*-pathway and the 5'Hoxd members by whole mount *in situ* hybridisation and real time-PCR.

6.3.4 ALI037 mutation revealed a putative new regulatory domain of *Plzf*

The ALI037 mutant line was isolated in the recessive screen with dysmorphological abnormalities in the pelvic girdle and the appendicular skeleton of the hind limbs. In the course of phenotypic characterization, a progressive loss of spermatogonial stem cells was additionally observed in male mutant mice. Linkage analysis of the ALI037 mutation showed a clear association to mouse chromosome 9 between the SNP markers *rsWI_WGS_9_65027538* (66.83 Mbp) and *rsWI_WGS_9_32840501* (33.4 Mbp). The most promising candidate genes with regard to the phenotypic null alleles were *Scamp5* located at 57.6 Mbp and *Zbtb16/Plzf/Zfp145* located at 48.86 Mbp. In fact, molecular characterization of the ALI037 mutation revealed a C to T base pair exchange in exon 7 at position nt2292 on transcript level of the gene *Zbtb16*, or *Zfp145* encoding *Plzf*. The *Plzf* (promyelocytic leukaemia zinc finger) gene was initially associated with acute promyelocytic leukemia (APL) when fused to retinoic acid receptor alpha (RAR α) by chromosomal translocation (Chen et al., 1993). *Plzf* is a DNA-binding nuclear phosphoprotein (Reid et al., 1995). The zinc-finger domain at the C- terminus mediates DNA binding (Li et al., 1997) (Sitterlin et al., 1997), whereas the BTB/POZ domain at the N-terminus mediates self-association and transcriptional repression (Bardwell and Treisman, 1994; Dong et al., 1996). *Plzf* function as a transcriptional repressor through its ability to recruit nuclear co-repressors such as SMRT, N-CoR, *Sin3*, and *histone deacetylases (HDAC)* class I/II via the BTB/POZ domain to the transcriptional complex (David et al., 1998; Grignani et al., 1998; Lemercier et al., 2002). Thus,

HDAC activity leads to nucleosome activity and transcriptional repression. Barna and colleagues generated a *Plzf* null mutation in mice (Barna et al., 2000) that display patterning defects the hind limbs and axial skeleton accompanied by homeotic transformations of anterior skeletal elements in the limb into posterior structures. In addition, male *Plzf* knockouts displayed reduced fertility due to progressive loss of spermatogonia with age associated with increasing apoptosis rate and loss of tubule structure (Costoya et al., 2004). Interestingly, the adult ALI037 mutant phenotype resembled most features of the *Plzf* null-mutant phenotype, which finally led to the highest priority candidate gene.

The most striking aspect of the ALI037 mutation is the nature, the localisation of the induced mutation and its consequences on the phenotype. The mutation in ALI037 is a base pair exchange located downstream of the zinc finger domain at the C-terminal of *Plzf*, which resulted in an amino acid exchange from Thr609 to Met. The C-terminus downstream of the zinc finger domain of *Plzf* is a highly conserved region among the vertebrates as shown in the homology sequence analysis. But a specific function of this short C-terminal domain was not known so far. Nonetheless, the high degree of conservation of the C-terminal sequence among the vertebrates may give an indication for a potential novel regulatory domain of *Plzf* beside the BTB/POZ domain. According to the results obtained so far different regulatory mechanisms for the *Plzf* C-terminal can be hypothesized, including a) affecting the tertiary structure of the DNA-binding zinc finger domain, or b) regulation of the repressive activity of *Plzf* through its phosphorylation status.

With regard to the whole mount in situ hybridisation analysis a different expression pattern of the 5' *Hoxd* cluster was observed in E11.5 ALI037 mutant embryos compared to *Plzf*^{-/-} embryos; *Plzf* repression on *Hoxd11* transcription was deregulated in ALI037 embryos compared to wild types whereas regulation of other 5' *Hoxd* family members seemed to be retained. In E11.5 *Plzf*^{-/-} knockout embryos the expression pattern of all 5' *Hoxd* genes were deregulated and were all anteriorized in the developing limb (Barna et al., 2000). It can be speculated that the mutation in the C-terminus differentially deregulates binding 5' *Hoxd* promoters. The induced mutation that resulted in the amino acid exchange Thr609 to Met might affect the tertiary structure of *Plzf*, and due to the vicinity of the mutation to the zinc finger domain it strongly reduces its ability to bind DNA and almost abolishes the repressive activity on *Hoxd11* but not other members of the 5' *Hoxd* cluster. The central role of a functional DNA-binding zinc finger domain is well known for the majority of transcription factors regulating gene expression in all biological processes by directly binding specific DNA sequences in the promoter region of target genes. For *Plzf*, this is underlined by another allele, the *luxoid* (*lu*) mutation, which carries a spontaneous point mutation resulting in a premature stop codon (Buaas et al., 2004; Green, 1961). Since the mutation was localized upstream of the zinc finger domain DNA binding is prevented. Interestingly, the *luxoid* mutant showed similar limb/ skeletal abnormalities and male infertility as the null allele and ALI037. Evidence for the differentially deregulation of DNA binding on 5' *Hoxd* promoters in ALI037 can

be given by performing reporter assays with E 11.5 wild type and mutant limb cell cultures to test the 5' *Hoxd* cluster promoter activities.

Regulation of *Plzf* activity through its phosphorylation status is not yet known but cannot be excluded considering that NetPhos2.0, a tool for the prediction of phosphorylation sites in proteins (<http://www.cbs.dtu.dk/services/NetPhos/>), predicted in total 37 potential *PKC* phosphorylation sites (Ser: 26, Thr: 8, and Tyr: 3) for *Plzf*. In the C-terminal domain of interest, Thr609 was the only phosphorylation site predicted and scored above the threshold of 0.5. Another speculation how the induced mutation affects its transcriptional activity is the deregulation of *Plzf* through the phosphorylation status of the C-terminal end. The dephosphorylated C-terminus of the mutated *Plzf* might favour the inactivation of transcriptional repression for *Hoxd11*, whereas phosphorylation might induce transcriptional inactivation. Evidence for this speculation can be obtained experimentally by reporter assays using wild type and mutant embryonic limb cell cultures to test the 5'*Hoxd* promoter activities in the absence and presence of an inhibitor of *Protein kinase C*.

However, the C-terminal region of *Plzf* seemed to have an essential role in the function of this transcription factor. Since nothing else is known about this putative new regulatory domain further functional analysis would be needed on different levels. In cell culture, one could investigate *in vitro* function using reporter assays testing expression vectors with different *Plzf* C-terminal mutations. For the investigation of a domain for a putative new binding site a yeast two hybrid screen using specifically the C-terminus as bait could reveal new interaction partners. In addition, phenotypic analysis of transgenic or knock-in mouse lines carrying the new mutations with regard to limb development and germ cell differentiation could give new insights into the *in vivo* function.

6.3.5 ALI037 is a hypomorphic allele with a null effect

Although a differential repressive activity of *Plzf* on 5'*Hoxd* expression was observed in E11.5 ALI037 mutant embryos, most strikingly, almost all aspects of phenotypic alterations in adult *Plzf*^{-/-} knockout could also be observed in adult homozygous ALI037 mutants including the patterning defects of skeletal elements in the hind limbs, the axial skeleton as well as the progressive loss of spermatogonia in male mutants. In ALI037 male mutants, the intrinsic effect of progressive spermatogonial degeneration with age was demonstrated in IHC on testes cross sections (using *PCNA* and *Cyclin D1* for mitotic spermatogonia and *p27* for Sertoli cells). Little is known about *Plzf* function in male germ cell differentiation. *Plzf* is believed to regulate the epigenetic state of undifferentiated cells, and was showed to co-localize with *Oct4* in undifferentiated spermatogonia (Buaas et al., 2004). Microarray analysis of undifferentiated male germ cells of *Plzf* null-mice before testis generation showed alterations in the expression profile of genes associated with spermatogenesis (Costoya et al., 2004). Costoya and colleagues therefore concluded that *Plzf* is required to regulate self-renewal and maintenance of the stem cell pool.

Due to these facts, it has also to be considered that the ALI037 mutation might induce a temporally deregulation of genes, which was not displayed in E 11.5 embryos but with a delayed onset of its repressive activity on other *Hoxd* members and other downstream targets acting in a time window, which is still sensitive for limb/ digit differentiation, germ cell differentiation and stem cell maintenance. This might explain that the induced ALI037 mutation could finally result in a similar range of phenotypic alterations of the *Plzf*^{-/-} knockout. In earlier embryonic stages it was already shown that *Plzf* is expressed in an extremely dynamic pattern with transcripts appearing at E 7.5 in the anterior neuroepithelium and quickly spreading to the entire neuroectoderm until E 10 (Avantaggiato et al., 1995). Final evidence could be given by performing expression analysis of later embryonic stages by WISH, real time-PCR time course experiments (on 5' *Hoxd* expression and genes associated to spermatogenesis) or microarray analysis. In vitro, reporter assays using limb cell cultures of embryonic stages later than E11.5 would reveal the dynamic pattern on 5' *Hoxd* promoter activity. If this could be confirmed, ALI037 would primarily represent a hypomorphic allele of *Plzf* acting as a temporally deregulated null allele with a delayed onset.

A single nucleotide polymorphism in the C3HeB/FeJ background for *Plzf* at this position was most probably excluded due to sequence analysis of a number of inbred strains. However, although ALI037 was continuously bred as an isogenic line for at least five generations, it cannot be excluded yet that another mutation might be causative for the mutant phenotype. There is still a small possibility that the phenotype is based on a mutation in a cis- or trans regulatory element, which can be located several kilobases upstream of *Plzf*. Three main reasons exist that make it necessary to confirm that the detected ALI037 mutation induced by ENU is in fact causative for the mutant phenotype: a) only two other mouse *Plzf* alleles (*Plzf*^{-/-} and *lu*) displaying a similar phenotype have been known and published so far, in addition, b) *Plzf* was always associated to acute promyelocytic leukaemia (APL) if fused to *RAR α* in human, whereas no human patients with limb or fertility phenotypes associated to *Plzf* were described so far, and finally c) very little is known about *Plzf* function and regulation in limb development or self-renewal of spermatogonia (Costoya et al., 2004). There are three possibilities to proof this hypothesis, first, by crossing heterozygous ALI037 mice to other heterozygous *Plzf* mutant alleles (*Plzf* knockout or *lu* mutant) in order to produce compound heterozygotes. If 25% of the offspring display the mutant phenotype, the ALI037 mutation could be proofed as a *Plzf* allele by allelic non-complementation. A non-allelic non-complementation by a regulatory element would not be very likely since due to meiotic recombination the penetrance of the phenotype and the Mendelian ratio would decrease. The second strategy, which would be the clear-cut proof, is the generation of homozygous knock-in mice that carry the same point mutation as ALI037 and display the same mutant phenotype. Ideally, an isogenic line on the same original genetic background (C3HeB/FeJ) and a congenic line on a different genetic background (i.e. C57BL/6J) are generated in parallel to investigate potential modifying effects on the mutant phenotype. The third strategy is the confirmation through

phenotype compensation by performing wild type BAC transgenesis or retroviral expression using mutant somatic cells. If the phenotype would be ameliorated/ compensated by allelic complementation resulting in a wild type phenotype the original mutation would be confirmed.

In short, the characterization of the recessive ALI037 mutation could reveal a putative new regulatory mechanism of a gene and differential regulation of its targets.

6.4 More mouse models for inherited diseases in human

Mouse mutants that model a human inherited disease are most valuable for the elucidation of gene function and their mechanism in pathogenesis. The underlying molecular mechanisms of a large number of genetic diseases are still not known as can be observed in the NCBI database for “Online Mendelian Inheritance of Man” (OMIM) (McKusick, 2007). This was one of the main reasons to present all generated mutant phenotypes of this project in the WWW making them openly accessible to interested scientific groups for further detailed functional analysis. A minor part of mutant lines with skeletal anomalies had been functionally analysed by the Institute of Experimental Genetics. This strategy turned out to be very efficient with regard to knowledge of gene function and their role in the pathogenesis of genetic diseases covering the entire spectrum from i) new alleles of known genes, ii) genes with new functions that were connected to other pathways, and finally iii) to completely novel genes. A series of new alleles of the crystalline protein family had been recovered (Graw et al., 1999; Graw et al., 2001a; Graw et al., 2001b; Graw et al., 2001c; Graw et al., 2001d; Graw et al., 2002a) that are associated to disturbances of eye lens opacity (cataract). With the help of a head turner mutant carrying a point mutation in *Jag1*, as a ligand of *Notch1*, a new and earlier function of Notch signalling in the creation or maintenance of sensory/ non-sensory boundaries in the inner ear (Kiernan et al., 2001) was revealed beside the already known later function of mediating lateral inhibition. Another new functionality of a known gene that was not associated to a disease was revealed in the CRA001 mutant that showed neurodegenerative symptoms of amyotrophic lateral sclerosis (ALS), which was based on the disturbance of retrograde axonal transport caused by a mutation in the dynein link protein (Hafezparast et al., 2003). A series of dark skin phenotypes had been isolated, which mutations represent genes or loci not implicated previously in pigmentation (Fitch et al., 2003; Van Raamsdonk et al., 2004) and thus, delineated a new classification of developmental pathways for pigmentation. By isolating the deaf mutant mouse *Beethoven*, a novel gene, *Tmc1*, was associated to progressive hearing loss (Vreugde et al., 2002), and the mutant phenotype was identified as a mouse model for the human progressive hearing loss. In parallel, a dominant allele of *TMCI* had been revealed that was associated with human non-syndromic progressive hearing loss, DFNA36, thus making *Beethoven* an invaluable model for studying postlingual deafness (Kurima et al., 2002). Since the underlying mechanism of the majority of genetic diseases are based on complex traits the next level of functional studies is the analysis of modifiers and sensitized polygenic traits (Matin and Nadeau, 2001; Nadeau et al., 2000) starting from a known

single mutation. A recent QTL study in the Beethoven mouse model already demonstrated a polygenic basis that can modify the cochlear hair cell degeneration as a model system for the dissection of common complex hearing loss phenotypes in human (Noguchi et al., 2006).

6.5 Outlook and perspectives

In the last couple of years the use of animal models to dissect the underlying mechanisms of clinically relevant diseases have become an increasing impact in functional gene analysis. Different approaches had been developed in order to close the gap between phenotype and genotype using targeted mutagenesis by homologous recombination in ES cells, random mutagenesis using chemicals in germ cells or ES cells (Becker et al., 2006; Chen et al., 2003; Guenet, 2004; Kanatsu-Shinohara et al., 2006; O'Brien and Frankel, 2004; Rastan et al., 2004), or insertional mutagenesis using gene trap vectors (Evans et al., 1997; Zambrowicz et al., 1998) or transposons (Carlson et al., 2003). Since cryopreservation technology and mutation detection has been developed to high-throughput technologies in parallel, genotype-driven approaches using insertional mutagenesis within ES-cells and/or germ cells will soon saturate the genome. Due to the advantage of using molecular tags, automated high-throughput sequencing technology and advanced gene annotation, mutation detection screening of germ or ES-cell banks is not the bottleneck anymore. Every required mutant allele can be then re-derived on request for generating mouse models of any gene and their further functional analysis. Nevertheless, since every mutagenesis technology provides only a specific spectrum of mutations the synopsis of all mutation types, modelling all variations of disease phenotypes, is required. This advantage can be also utilized in the investigation of direct or indirect participants in a molecular network or biological process by performing genetic screens for modifiers or sensitized screens, which would be the next level of gene function analysis of complex traits (Curtis, 2004; Huang et al., 2006; Speca et al., 2006). Therefore ENU mutagenesis remains still unconceivable for modelling the situation in human diseases and the generation of allelic series of disease genes that, in the future of molecular medicine, allow the development and application of individually tailored therapeutic agents.

7 References

- Agarwal, P., Wylie, J. N., Galceran, J., Arkhitko, O., Li, C., Deng, C., Grosschedl, R., and Bruneau, B. G. (2003). *Tbx5* is essential for forelimb bud initiation following patterning of the limb field in the mouse embryo. *Development* *130*, 623-633.
- Agulnik, S. I., Papaioannou, V. E., and Silver, L. M. (1998). Cloning, mapping, and expression analysis of *TBX15*, a new member of the T-Box gene family. *Genomics* *51*, 68-75.
- Ahn, D. G., Kourakis, M. J., Rohde, L. A., Silver, L. M., and Ho, R. K. (2002). T-box gene *tbx5* is essential for formation of the pectoral limb bud. *Nature* *417*, 754-758.
- Aigner, B., Rathkolb, B., Herbach, N., Kemter, E., Schessl, C., Klawns, M., Klempt, M., de Angelis, M. H., Wanke, R., and Wolf, E. (2007a). Screening for increased plasma urea levels in a large-scale ENU mouse mutagenesis project reveals kidney disease models. *Am J Physiol Renal Physiol* *292*, F1560-1567.
- Aigner, B., Rathkolb, B., Mohr, M., Klempt, M., Hrabe de Angelis, M., and Wolf, E. (2007b). Generation of ENU-Induced Mouse Mutants with Hypocholesterolemia: Novel Tools for Dissecting Plasma Lipoprotein Homeostasis. *Lipids* *42*, 731-737.
- Anderson, K. V. (2000). Finding the genes that direct mammalian development : ENU mutagenesis in the mouse. *Trends Genet* *16*, 99-102.
- Avantaggiato, V., Pandolfi, P. P., Ruthardt, M., Hawe, N., Acampora, D., Pelicci, P. G., and Simeone, A. (1995). Developmental analysis of murine Promyelocyte Leukemia Zinc Finger (PLZF) gene expression: implications for the neuromeric model of the forebrain organization. *J Neurosci* *15*, 4927-4942.
- Barbaric, I., Wells, S., Russ, A., and Dear, T. N. (2007). Spectrum of ENU-induced mutations in phenotype-driven and gene-driven screens in the mouse. *Environ Mol Mutagen* *48*, 124-142.
- Bardwell, V. J., and Treisman, R. (1994). The POZ domain: a conserved protein-protein interaction motif. *Genes Dev* *8*, 1664-1677.
- Barna, M., Hawe, N., Niswander, L., and Pandolfi, P. P. (2000). *Plzf* regulates limb and axial skeletal patterning. *Nat Genet* *25*, 166-172.
- Barna, M., Merghoub, T., Costoya, J. A., Ruggero, D., Branford, M., Bergia, A., Samori, B., and Pandolfi, P. P. (2002). *Plzf* mediates transcriptional repression of *HoxD* gene expression through chromatin remodeling. *Dev Cell* *3*, 499-510.
- Becker, S., de Angelis, M. H., and Beckers, J. (2006). Use of chemical mutagenesis in mouse embryonic stem cells. *Methods Mol Biol* *329*, 397-407.
- Beckers, J., Gerard, M., and Duboule, D. (1996). Transgenic analysis of a potential *Hoxd-11* limb regulatory element present in tetrapods and fish. *Dev Biol* *180*, 543-553.
- Beumer, T. L., Kiyokawa, H., Roepers-Gajadien, H. L., van den Bos, L. A., Lock, T. M., Gademan, I. S., Rutgers, D. H., Koff, A., and de Rooij, D. G. (1999). Regulatory role of *p27kip1* in the mouse and human testis. *Endocrinology* *140*, 1834-1840.
- Beumer, T. L., Roepers-Gajadien, H. L., Gademan, I. S., Kal, H. B., and de Rooij, D. G. (2000). Involvement of the D-type cyclins in germ cell proliferation and differentiation in the mouse. *Biol Reprod* *63*, 1893-1898.
- Brenner, S. (1974). The genetics of *Caenorhabditis elegans*. *Genetics* *77*, 71-94.
- Brinkman, R. R., Dube, M. P., Rouleau, G. A., Orr, A. C., and Samuels, M. E. (2006). Human monogenic disorders - a source of novel drug targets. *Nat Rev Genet* *7*, 249-260.
- Brown, S. D., and Balling, R. (2001). Systematic approaches to mouse mutagenesis. *Curr Opin Genet Dev* *11*, 268-273.

- Brown, S. D., and Peters, J. (1996). Combining mutagenesis and genomics in the mouse--closing the phenotype gap. *Trends Genet* *12*, 433-435.
- Buaas, F. W., Kirsh, A. L., Sharma, M., McLean, D. J., Morris, J. L., Griswold, M. D., de Rooij, D. G., and Braun, R. E. (2004). Plzf is required in adult male germ cells for stem cell self-renewal. *Nat Genet* *36*, 647-652.
- Candille, S. I., Van Raamsdonk, C. D., Chen, C., Kuijper, S., Chen-Tsai, Y., Russ, A., Meijlink, F., and Barsh, G. S. (2004). Dorsoventral patterning of the mouse coat by Tbx15. *PLoS Biol* *2*, E3.
- Capdevila, J., and Izpisua Belmonte, J. C. (2001). Patterning mechanisms controlling vertebrate limb development. *Annu Rev Cell Dev Biol* *17*, 87-132.
- Carlson, C. M., Dupuy, A. J., Fritz, S., Roberg-Perez, K. J., Fletcher, C. F., and Largaespada, D. A. (2003). Transposon mutagenesis of the mouse germline. *Genetics* *165*, 243-256.
- Charite, J., McFadden, D. G., and Olson, E. N. (2000). The bHLH transcription factor dHAND controls Sonic hedgehog expression and establishment of the zone of polarizing activity during limb development. *Development* *127*, 2461-2470.
- Charles, D. J., and Pretsch, W. (1987). Linear dose-response relationship of erythrocyte enzyme-activity mutations in offspring of ethylnitrosourea-treated mice. *Mutat Res* *176*, 81-91.
- Chen, Y., Knezevic, V., Ervin, V., Hutson, R., Ward, Y., and Mackem, S. (2004). Direct interaction with Hoxd proteins reverses Gli3-repressor function to promote digit formation downstream of Shh. *Development* *131*, 2339-2347.
- Chen, Y., Vivian, J. L., and Magnuson, T. (2003). Gene-based chemical mutagenesis in mouse embryonic stem cells. *Methods Enzymol* *365*, 406-415.
- Chen, Z., Brand, N. J., Chen, A., Chen, S. J., Tong, J. H., Wang, Z. Y., Waxman, S., and Zelent, A. (1993). Fusion between a novel Kruppel-like zinc finger gene and the retinoic acid receptor-alpha locus due to a variant t(11;17) translocation associated with acute promyelocytic leukaemia. *Embo J* *12*, 1161-1167.
- Chiang, C., Litingtung, Y., Lee, E., Young, K. E., Corden, J. L., Westphal, H., and Beachy, P. A. (1996). Cyclopia and defective axial patterning in mice lacking Sonic hedgehog gene function. *Nature* *383*, 407-413.
- Costoya, J. A., Hobbs, R. M., Barna, M., Cattoretti, G., Manova, K., Sukhwani, M., Orwig, K. E., Wolgemuth, D. J., and Pandolfi, P. P. (2004). Essential role of Plzf in maintenance of spermatogonial stem cells. *Nat Genet* *36*, 653-659.
- Coumoul, X., and Deng, C. X. (2003). Roles of FGF receptors in mammalian development and congenital diseases. *Birth Defects Res C Embryo Today* *69*, 286-304.
- Cuénot, L. (1905). Les races pures et les combinaisons chez les souris. *Arch Zool Exp Gén* *4*, 123-132.
- Curtis, D. J. (2004). Modifier screens in the mouse: time to move forward with reverse genetics. *Proc Natl Acad Sci U S A* *101*, 7209-7210.
- Cygan, J. A., Johnson, R. L., and McMahon, A. P. (1997). Novel regulatory interactions revealed by studies of murine limb pattern in Wnt-7a and En-1 mutants. *Development* *124*, 5021-5032.
- David, G., Alland, L., Hong, S. H., Wong, C. W., DePinho, R. A., and Dejean, A. (1998). Histone deacetylase associated with mSin3A mediates repression by the acute promyelocytic leukemia-associated PLZF protein. *Oncogene* *16*, 2549-2556.
- Davis, A. P., and Capecchi, M. R. (1996). A mutational analysis of the 5' HoxD genes: dissection of genetic interactions during limb development in the mouse. *Development* *122*, 1175-1185.
- Davis, A. P., and Justice, M. J. (1998). An Oak Ridge legacy: the specific locus test and its role in mouse mutagenesis. *Genetics* *148*, 7-12.

- Dealy, C. N., Roth, A., Ferrari, D., Brown, A. M., and Kosher, R. A. (1993). Wnt-5a and Wnt-7a are expressed in the developing chick limb bud in a manner suggesting roles in pattern formation along the proximodistal and dorsoventral axes. *Mech Dev* 43, 175-186.
- Dong, S., Zhu, J., Reid, A., Strutt, P., Guidez, F., Zhong, H. J., Wang, Z. Y., Licht, J., Waxman, S., Chomienne, C., *et al.* (1996). Amino-terminal protein-protein interaction motif (POZ-domain) is responsible for activities of the promyelocytic leukemia zinc finger-retinoic acid receptor-alpha fusion protein. *Proc Natl Acad Sci U S A* 93, 3624-3629.
- Duprez, D. M., Kostakopoulou, K., Francis-West, P. H., Tickle, C., and Brickell, P. M. (1996). Activation of Fgf-4 and HoxD gene expression by BMP-2 expressing cells in the developing chick limb. *Development* 122, 1821-1828.
- Ehling, U. H. (1986). Induction of gene mutations in mice: the multiple endpoint approach. *Prog Clin Biol Res* 209B, 501-510.
- Ehling, U. H., Charles, D. J., Favor, J., Graw, J., Kratochvilova, J., Neuhauser-Klaus, A., and Pretsch, W. (1985). Induction of gene mutations in mice: the multiple endpoint approach. *Mutat Res* 150, 393-401.
- Ehling, U. H., Favor, J., Kratochvilova, J., and Neuhauser-Klaus, A. (1982). Dominant cataract mutations and specific-locus mutations in mice induced by radiation or ethylnitrosourea. *Mutat Res* 92, 181-192.
- Ehling, U. H., and Neuhauser-Klaus, A. (1988). Induction of specific-locus mutations in female mice by 1-ethyl-1-nitrosourea and procarbazine. *Mutat Res* 202, 139-146.
- Evans, M. J., Carlton, M. B., and Russ, A. P. (1997). Gene trapping and functional genomics. *Trends Genet* 13, 370-374.
- Favier, B., and Dolle, P. (1997). Developmental functions of mammalian Hox genes. *Mol Hum Reprod* 3, 115-131.
- Favor, J. (1998). The mutagenic activity of ethylnitrosourea at low doses in spermatogonia of the mouse as assessed by the specific-locus test. *Mutat Res* 405, 221-226.
- Favor, J. (1999). Mechanisms of mutation induction in germ cells of the mouse as assessed by the specific locus test. *Mutat Res* 428, 227-236.
- Favor, J., Neuhauser-Klaus, A., and Ehling, U. H. (1988). The effect of dose fractionation on the frequency of ethylnitrosourea-induced dominant cataract and recessive specific locus mutations in germ cells of the mouse. *Mutat Res* 198, 269-275.
- Favor, J., Neuhauser-Klaus, A., Ehling, U. H., Wulff, A., and van Zeeland, A. A. (1997). The effect of the interval between dose applications on the observed specific-locus mutation rate in the mouse following fractionated treatments of spermatogonia with ethylnitrosourea. *Mutat Res* 374, 193-199.
- Favor, J., Peters, H., Hermann, T., Schmahl, W., Chatterjee, B., Neuhauser-Klaus, A., and Sandulache, R. (2001). Molecular characterization of Pax6(2Neu) through Pax6(10Neu): an extension of the Pax6 allelic series and the identification of two possible hypomorph alleles in the mouse *Mus musculus*. *Genetics* 159, 1689-1700.
- Favor, J., Sund, M., Neuhauser-Klaus, A., and Ehling, U. H. (1990). A dose-response analysis of ethylnitrosourea-induced recessive specific-locus mutations in treated spermatogonia of the mouse. *Mutat Res* 231, 47-54.
- Fernandez-Teran, M., Piedra, M. E., Kathiriya, I. S., Srivastava, D., Rodriguez-Rey, J. C., and Ros, M. A. (2000). Role of dHAND in the anterior-posterior polarization of the limb bud: implications for the Sonic hedgehog pathway. *Development* 127, 2133-2142.
- Fitch, K. R., McGowan, K. A., van Raamsdonk, C. D., Fuchs, H., Lee, D., Puech, A., Herault, Y., Threadgill, D. W., Hrabe de Angelis, M., and Barsh, G. S. (2003). Genetics of dark skin in mice. *Genes Dev* 17, 214-228.
- Fraenkel, E., and Pabo, C. O. (1998). Comparison of X-ray and NMR structures for the Antennapedia homeodomain-DNA complex. *Nat Struct Biol* 5, 692-697.

Francis, P. H., Richardson, M. K., Brickell, P. M., and Tickle, C. (1994). Bone morphogenetic proteins and a signalling pathway that controls patterning in the developing chick limb. *Development* *120*, 209-218.

Garcia-Garcia, M. J., Eggenschwiler, J. T., Caspary, T., Alcorn, H. L., Wyler, M. R., Huangfu, D., Rakeman, A. S., Lee, J. D., Feinberg, E. H., Timmer, J. R., and Anderson, K. V. (2005). Analysis of mouse embryonic patterning and morphogenesis by forward genetics. *Proc Natl Acad Sci U S A* *102*, 5913-5919.

Gehring, W. J. (1993). Exploring the homeobox. *Gene* *135*, 215-221.

Gilbert, S. F. (2000). *Developmental Biology*, 6th Edition, 6th edn (Sunderland, MA, USA: Sinauer Associates, Inc.,).

Graw, J., Jung, M., Loster, J., Klopp, N., Soewarto, D., Fella, C., Fuchs, H., Reis, A., Wolf, E., Balling, R., and Hrabe de Angelis, M. (1999). Mutation in the betaA3/A1-crystallin encoding gene *Cryba1* causes a dominant cataract in the mouse. *Genomics* *62*, 67-73.

Graw, J., Klopp, N., Loster, J., Soewarto, D., Fuchs, H., Becker-Follmann, J., Reis, A., Wolf, E., Balling, R., and Habre de Angelis, M. (2001a). Ethylnitrosourea-induced mutation in mice leads to the expression of a novel protein in the eye and to dominant cataracts. *Genetics* *157*, 1313-1320.

Graw, J., Loster, J., Puk, O., Munster, D., Haubst, N., Soewarto, D., Fuchs, H., Meyer, B., Nurnberg, P., Pretsch, W., *et al.* (2005). Three novel Pax6 alleles in the mouse leading to the same small-eye phenotype caused by different consequences at target promoters. *Invest Ophthalmol Vis Sci* *46*, 4671-4683.

Graw, J., Loster, J., Soewarto, D., Fuchs, H., Meyer, B., Reis, A., Wolf, E., Balling, R., and Hrabe de Angelis, M. (2001b). Characterization of a mutation in the lens-specific MP70 encoding gene of the mouse leading to a dominant cataract. *Exp Eye Res* *73*, 867-876.

Graw, J., Loster, J., Soewarto, D., Fuchs, H., Meyer, B., Reis, A., Wolf, E., Balling, R., and Hrabe de Angelis, M. (2001c). Characterization of a new, dominant V124E mutation in the mouse alphaA-crystallin-encoding gene. *Invest Ophthalmol Vis Sci* *42*, 2909-2915.

Graw, J., Loster, J., Soewarto, D., Fuchs, H., Reis, A., Wolf, E., Balling, R., and Hrabe de Angelis, M. (2001d). *Aey2*, a new mutation in the betaB2-crystallin-encoding gene of the mouse. *Invest Ophthalmol Vis Sci* *42*, 1574-1580.

Graw, J., Loster, J., Soewarto, D., Fuchs, H., Reis, A., Wolf, E., Balling, R., and Hrabe de Angelis, M. (2002a). V76D mutation in a conserved gD-crystallin region leads to dominant cataracts in mice. *Mamm Genome* *13*, 452-455.

Graw, J., Neuhauser-Klaus, A., Loster, J., Klopp, N., and Favor, J. (2002b). Ethylnitrosourea-induced base pair substitution affects splicing of the mouse gammaE-crystallin encoding gene leading to the expression of a hybrid protein and to a cataract. *Genetics* *161*, 1633-1640.

Green, M. C. (1961). The position of luxoid in linkage group II of the mouse. *J Hered* *52*, 297-300.

Grignani, F., De Matteis, S., Nervi, C., Tomassoni, L., Gelmetti, V., Cioce, M., Fanelli, M., Ruthardt, M., Ferrara, F. F., Zamir, I., *et al.* (1998). Fusion proteins of the retinoic acid receptor-alpha recruit histone deacetylase in promyelocytic leukaemia. *Nature* *391*, 815-818.

Guenet, J. L. (2004). Chemical mutagenesis of the mouse genome: an overview. *Genetica* *122*, 9-24.

Hafezparast, M., Klocke, R., Ruhrberg, C., Marquardt, A., Ahmad-Annuar, A., Bowen, S., Lalli, G., Witherden, A. S., Hummerich, H., Nicholson, S., *et al.* (2003). Mutations in dynein link motor neuron degeneration to defects in retrograde transport. *Science* *300*, 808-812.

Haffter, P., Granato, M., Brand, M., Mullins, M. C., Hammerschmidt, M., Kane, D. A., Odenthal, J., van Eeden, F. J., Jiang, Y. J., Heisenberg, C. P., *et al.* (1996). The identification of genes with unique and essential functions in the development of the zebrafish, *Danio rerio*. *Development* *123*, 1-36.

Hall, C. M. (2002). International nosology and classification of constitutional disorders of bone (2001). *Am J Med Genet* *113*, 65-77.

- Harrelson, Z., Kelly, R. G., Goldin, S. N., Gibson-Brown, J. J., Bollag, R. J., Silver, L. M., and Papaioannou, V. E. (2004). Tbx2 is essential for patterning the atrioventricular canal and for morphogenesis of the outflow tract during heart development. *Development* 131, 5041-5052.
- Hitotsumachi, S., Carpenter, D. A., and Russell, W. L. (1985). Dose-repetition increases the mutagenic effectiveness of N-ethyl-N-nitrosourea in mouse spermatogonia. *Proc Natl Acad Sci U S A* 82, 6619-6621.
- Hoebe, K., and Beutler, B. (2008). Forward genetic analysis of TLR-signaling pathways: An evaluation. *Adv Drug Deliv Rev* 60, 824-829.
- Hrabe de Angelis, M., and Balling, R. (1998). Large scale ENU screens in the mouse: genetics meets genomics. *Mutat Res* 400, 25-32.
- Hrabe de Angelis, M. H., Flaswinkel, H., Fuchs, H., Rathkolb, B., Soewarto, D., Marschall, S., Heffner, S., Pargent, W., Wuensch, K., Jung, M., *et al.* (2000). Genome-wide, large-scale production of mutant mice by ENU mutagenesis. *Nat Genet* 25, 444-447.
- Huang, T. T., Naeemuddin, M., Elchuri, S., Yamaguchi, M., Kozy, H. M., Carlson, E. J., and Epstein, C. J. (2006). Genetic modifiers of the phenotype of mice deficient in mitochondrial superoxide dismutase. *Hum Mol Genet* 15, 1187-1194.
- Hui, C. C., and Joyner, A. L. (1993). A mouse model of greig cephalopolysyndactyly syndrome: the extra-toesJ mutation contains an intragenic deletion of the Gli3 gene. *Nat Genet* 3, 241-246.
- Izpisua-Belmonte, J. C., Tickle, C., Dolle, P., Wolpert, L., and Duboule, D. (1991). Expression of the homeobox Hox-4 genes and the specification of position in chick wing development. *Nature* 350, 585-589.
- Justice, M. J., and Bode, V. C. (1988a). Genetic analysis of mouse t haplotypes using mutations induced by ethylnitrosourea mutagenesis: the order of T and qk is inverted in t mutants. *Genetics* 120, 533-543.
- Justice, M. J., and Bode, V. C. (1988b). Three ENU-induced alleles of the murine quaking locus are recessive embryonic lethal mutations. *Genet Res* 51, 95-102.
- Justice, M. J., Carpenter, D. A., Favor, J., Neuhauser-Klaus, A., Hrabe de Angelis, M., Soewarto, D., Moser, A., Cordes, S., Miller, D., Chapman, V., *et al.* (2000). Effects of ENU dosage on mouse strains. *Mamm Genome* 11, 484-488.
- Justice, M. J., Noveroske, J. K., Weber, J. S., Zheng, B., and Bradley, A. (1999). Mouse ENU mutagenesis. *Hum Mol Genet* 8, 1955-1963.
- Kalff-Suske, M., Wild, A., Topp, J., Wessling, M., Jacobsen, E. M., Bornholdt, D., Engel, H., Heuer, H., Aalfs, C. M., Ausems, M. G., *et al.* (1999). Point mutations throughout the GLI3 gene cause Greig cephalopolysyndactyly syndrome. *Hum Mol Genet* 8, 1769-1777.
- Kanatsu-Shinohara, M., Ikawa, M., Takehashi, M., Ogonuki, N., Miki, H., Inoue, K., Kazuki, Y., Lee, J., Toyokuni, S., Oshimura, M., *et al.* (2006). Production of knockout mice by random or targeted mutagenesis in spermatogonial stem cells. *Proc Natl Acad Sci U S A* 103, 8018-8023.
- Kang, S., Graham, J. M., Jr., Olney, A. H., and Biesecker, L. G. (1997). GLI3 frameshift mutations cause autosomal dominant Pallister-Hall syndrome. *Nat Genet* 15, 266-268.
- Kasarskis, A., Manova, K., and Anderson, K. V. (1998). A phenotype-based screen for embryonic lethal mutations in the mouse. *Proc Natl Acad Sci U S A* 95, 7485-7490.
- Kiernan, A. E., Ahituv, N., Fuchs, H., Balling, R., Avraham, K. B., Steel, K. P., and Hrabe de Angelis, M. (2001). The Notch ligand Jagged1 is required for inner ear sensory development. *Proc Natl Acad Sci U S A* 98, 3873-3878.
- Kile, B. T., Hentges, K. E., Clark, A. T., Nakamura, H., Salinger, A. P., Liu, B., Box, N., Stockton, D. W., Johnson, R. L., Behringer, R. R., *et al.* (2003). Functional genetic analysis of mouse chromosome 11. *Nature* 425, 81-86.

- Kispert, A., and Hermann, B. G. (1993). The Brachyury gene encodes a novel DNA binding protein. *Embo J* *12*, 4898-4899.
- Klopp, N., Favor, J., Loster, J., Lutz, R. B., Neuhauser-Klaus, A., Prescott, A., Pretsch, W., Quinlan, R. A., Sandilands, A., Vrensen, G. F., and Graw, J. (1998). Three murine cataract mutants (Cat2) are defective in different gamma-crystallin genes. *Genomics* *52*, 152-158.
- Knezevic, V., De Santo, R., Schughart, K., Huffstadt, U., Chiang, C., Mahon, K. A., and Mackem, S. (1997). Hoxd-12 differentially affects preaxial and postaxial chondrogenic branches in the limb and regulates Sonic hedgehog in a positive feedback loop. *Development* *124*, 4523-4536.
- Kraus, F., Haenig, B., and Kispert, A. (2001). Cloning and expression analysis of the mouse T-box gene Tbx18. *Mech Dev* *100*, 83-86.
- Kurima, K., Peters, L. M., Yang, Y., Riazuddin, S., Ahmed, Z. M., Naz, S., Arnaud, D., Drury, S., Mo, J., Makishima, T., *et al.* (2002). Dominant and recessive deafness caused by mutations of a novel gene, TMC1, required for cochlear hair-cell function. *Nat Genet* *30*, 277-284.
- Lemercier, C., Brocard, M. P., Puvion-Dutilleul, F., Kao, H. Y., Albagli, O., and Khochbin, S. (2002). Class II histone deacetylases are directly recruited by BCL6 transcriptional repressor. *J Biol Chem* *277*, 22045-22052.
- Lewandoski, M., Sun, X., and Martin, G. R. (2000). Fgf8 signalling from the AER is essential for normal limb development. *Nat Genet* *26*, 460-463.
- Li, J. Y., English, M. A., Ball, H. J., Yeyati, P. L., Waxman, S., and Licht, J. D. (1997). Sequence-specific DNA binding and transcriptional regulation by the promyelocytic leukemia zinc finger protein. *J Biol Chem* *272*, 22447-22455.
- Lindahl, T., Sedgwick, B., Sekiguchi, M., and Nakabeppu, Y. (1988). Regulation and expression of the adaptive response to alkylating agents. *Annu Rev Biochem* *57*, 133-157.
- Liu, C., Nakamura, E., Knezevic, V., Hunter, S., Thompson, K., and Mackem, S. (2003). A role for the mesenchymal T-box gene Brachyury in AER formation during limb development. *Development* *130*, 1327-1337.
- Loomis, C. A., Harris, E., Michaud, J., Wurst, W., Hanks, M., and Joyner, A. L. (1996). The mouse Engrailed-1 gene and ventral limb patterning. *Nature* *382*, 360-363.
- Lyon, M. F., and Renshaw, R. (1986). Induction of congenital malformations in the offspring of mutagen treated mice. *Prog Clin Biol Res* *209B*, 449-458.
- Manly, K. F., Cudmore, R. H., Jr., and Meer, J. M. (2001). Map Manager QTX, cross-platform software for genetic mapping. *Mamm Genome* *12*, 930-932.
- Mann, R. S., and Affolter, M. (1998). Hox proteins meet more partners. *Curr Opin Genet Dev* *8*, 423-429.
- Manouvrier-Hanu, S., Holder-Espinasse, M., and Lyonnet, S. (1999). Genetics of limb anomalies in humans. *Trends Genet* *15*, 409-417.
- Marschall, S., Huffstadt, U., Balling, R., and Hrabe de Angelis, M. (1999). Reliable recovery of inbred mouse lines using cryopreserved spermatozoa. *Mamm Genome* *10*, 773-776.
- Martin, G. (2001). Making a vertebrate limb: new players enter from the wings. *Bioessays* *23*, 865-868.
- Masuya, H., Inoue, M., Wada, Y., Shimizu, A., Nagano, J., Kawai, A., Inoue, A., Kagami, T., Hirayama, T., Yamaga, A., *et al.* (2005). Implementation of the modified-SHIRPA protocol for screening of dominant phenotypes in a large-scale ENU mutagenesis program. *Mamm Genome* *16*, 829-837.
- Masuya, H., Nakai, Y., Motegi, H., Niinaya, N., Kida, Y., Kaneko, Y., Aritake, H., Suzuki, N., Ishii, J., Koorikawa, K., *et al.* (2004). Development and implementation of a database system to manage a large-scale mouse ENU-mutagenesis program. *Mamm Genome* *15*, 404-411.

- Matin, A., and Nadeau, J. H. (2001). Sensitized polygenic trait analysis. *Trends Genet* *17*, 727-731.
- McKusick, V. A. (2007). Mendelian Inheritance in Man and its online version, OMIM. *Am J Hum Genet* *80*, 588-604.
- Mohan, S., Baylink, D. J., and Srivastava, A. K. (2008). A chemical mutagenesis screen to identify modifier genes that interact with growth hormone and TGF-beta signaling pathways. *Bone* *42*, 388-395.
- Mohr, M., Klempt, M., Rathkolb, B., de Angelis, M. H., Wolf, E., and Aigner, B. (2004). Hypercholesterolemia in ENU-induced mouse mutants. *J Lipid Res* *45*, 2132-2137.
- Moon, A. M., and Capecchi, M. R. (2000). Fgf8 is required for outgrowth and patterning of the limbs. *Nat Genet* *26*, 455-459.
- Nadeau, J. H., Singer, J. B., Matin, A., and Lander, E. S. (2000). Analysing complex genetic traits with chromosome substitution strains. *Nat Genet* *24*, 221-225.
- Naïche, L. A., and Papaioannou, V. E. (2003). Loss of Tbx4 blocks hindlimb development and affects vascularization and fusion of the allantois. *Development* *130*, 2681-2693.
- Nelson, C. E., Morgan, B. A., Burke, A. C., Laufer, E., DiMambro, E., Murtaugh, L. C., Gonzales, E., Tessarollo, L., Parada, L. F., and Tabin, C. (1996). Analysis of Hox gene expression in the chick limb bud. *Development* *122*, 1449-1466.
- Niswander, L. (2003). Pattern formation: old models out on a limb. *Nat Rev Genet* *4*, 133-143.
- Noguchi, Y., Kurima, K., Makishima, T., de Angelis, M. H., Fuchs, H., Frolenkov, G., Kitamura, K., and Griffith, A. J. (2006). Multiple quantitative trait loci modify cochlear hair cell degeneration in the Beethoven (Tmc1Bth) mouse model of progressive hearing loss DFNA36. *Genetics* *173*, 2111-2119.
- Nolan, P. M., Peters, J., Strivens, M., Rogers, D., Hagan, J., Spurr, N., Gray, I. C., Vizor, L., Brooker, D., Whitehill, E., *et al.* (2000a). A systematic, genome-wide, phenotype-driven mutagenesis programme for gene function studies in the mouse. *Nat Genet* *25*, 440-443.
- Nolan, P. M., Peters, J., Vizor, L., Strivens, M., Washbourne, R., Hough, T., Wells, C., Glenister, P., Thornton, C., Martin, J., *et al.* (2000b). Implementation of a large-scale ENU mutagenesis program: towards increasing the mouse mutant resource. *Mamm Genome* *11*, 500-506.
- Noveroske, J. K., Hardy, R., Dapper, J. D., Vogel, H., and Justice, M. J. (2005). A new ENU-induced allele of mouse quaking causes severe CNS dysmyelination. *Mamm Genome* *16*, 672-682.
- Nusslein-Volhard, C., and Wieschaus, E. (1980). Mutations affecting segment number and polarity in *Drosophila*. *Nature* *287*, 795-801.
- O'Brien, T. P., and Frankel, W. N. (2004). Moving forward with chemical mutagenesis in the mouse. *J Physiol* *554*, 13-21.
- Pargent, W., Heffner, S., Schable, K. F., Soewarto, D., Fuchs, H., and Hrabe de Angelis, M. (2000). MouseNet database: digital management of a large-scale mutagenesis project. *Mamm Genome* *11*, 590-593.
- Parr, B. A., and McMahon, A. P. (1995). Dorsalizing signal Wnt-7a required for normal polarity of D-V and A-P axes of mouse limb. *Nature* *374*, 350-353.
- Parr, B. A., Shea, M. J., Vassileva, G., and McMahon, A. P. (1993). Mouse Wnt genes exhibit discrete domains of expression in the early embryonic CNS and limb buds. *Development* *119*, 247-261.
- Pavletich, N. P., and Pabo, C. O. (1993). Crystal structure of a five-finger GLI-DNA complex: new perspectives on zinc fingers. *Science* *261*, 1701-1707.
- Peters, K. G., Werner, S., Chen, G., and Williams, L. T. (1992). Two FGF receptor genes are differentially expressed in epithelial and mesenchymal tissues during limb formation and organogenesis in the mouse. *Development* *114*, 233-243.

- Popp, R. A., Bailiff, E. G., Skow, L. C., Johnson, F. M., and Lewis, S. E. (1983). Analysis of a mouse alpha-globin gene mutation induced by ethylnitrosourea. *Genetics* *105*, 157-167.
- Pretsch, W., and Charles, D. J. (1984). Detection of dominant enzyme mutants in mice: model studies for mutations in man. *IARC Sci Publ*, 361-369.
- Radhakrishna, U., Wild, A., Grzeschik, K. H., and Antonarakis, S. E. (1997). Mutation in GLI3 in postaxial polydactyly type A. *Nat Genet* *17*, 269-271.
- Rajaraman, S., Davis, W. S., Mahakali-Zama, A., Evans, H. K., Russell, L. B., and Bedell, M. A. (2002a). An allelic series of mutations in the kit ligand gene of mice. I. Identification of point mutations in seven ethylnitrosourea-induced Kitl(Steel) alleles. *Genetics* *162*, 331-340.
- Rajaraman, S., Davis, W. S., Mahakali-Zama, A., Evans, H. K., Russell, L. B., and Bedell, M. A. (2002b). An allelic series of mutations in the Kit ligand gene of mice. II. Effects of ethylnitrosourea-induced Kitl point mutations on survival and peripheral blood cells of Kitl(Steel) mice. *Genetics* *162*, 341-353.
- Rallis, C., Bruneau, B. G., Del Buono, J., Seidman, C. E., Seidman, J. G., Nissim, S., Tabin, C. J., and Logan, M. P. (2003). Tbx5 is required for forelimb bud formation and continued outgrowth. *Development* *130*, 2741-2751.
- Rastan, S., Hough, T., Kierman, A., Hardisty, R., Erven, A., Gray, I. C., Voeling, S., Isaacs, A., Tsai, H., Strivens, M., *et al.* (2004). Towards a mutant map of the mouse--new models of neurological, behavioural, deafness, bone, renal and blood disorders. *Genetica* *122*, 47-49.
- Rathkolb, B., Tran, T. V., Klempt, M., Hrabe de Angelis, M., Wanke, R., Wolf, E., and Aigner, B. (2005). Large-scale albuminuria screen for nephropathy models in chemically induced mouse mutants. *Nephron Exp Nephrol* *100*, e143-149.
- Read, T. S. a. A. P. (2003). *Human molecular genetics, Third Edition, 3rd edn*: Garland Science, New York, NY, USA).
- Reid, A., Gould, A., Brand, N., Cook, M., Strutt, P., Li, J., Licht, J., Waxman, S., Krumlauf, R., and Zelent, A. (1995). Leukemia translocation gene, PLZF, is expressed with a speckled nuclear pattern in early hematopoietic progenitors. *Blood* *86*, 4544-4552.
- Revest, J. M., Spencer-Dene, B., Kerr, K., De Moerlooze, L., Rosewell, I., and Dickson, C. (2001). Fibroblast growth factor receptor 2-IIIb acts upstream of Shh and Fgf4 and is required for limb bud maintenance but not for the induction of Fgf8, Fgf10, Msx1, or Bmp4. *Dev Biol* *231*, 47-62.
- Rinchik, E. M., Carpenter, D. A., and Johnson, D. K. (2002). Functional annotation of mammalian genomic DNA sequence by chemical mutagenesis: a fine-structure genetic mutation map of a 1- to 2-cM segment of mouse chromosome 7 corresponding to human chromosome 11p14-p15. *Proc Natl Acad Sci U S A* *99*, 844-849.
- Rinchik, E. M., Carpenter, D. A., and Selby, P. B. (1990). A strategy for fine-structure functional analysis of a 6- to 11-centimorgan region of mouse chromosome 7 by high-efficiency mutagenesis. *Proc Natl Acad Sci U S A* *87*, 896-900.
- Rogers, D. C., Fisher, E. M., Brown, S. D., Peters, J., Hunter, A. J., and Martin, J. E. (1997). Behavioral and functional analysis of mouse phenotype: SHIRPA, a proposed protocol for comprehensive phenotype assessment. *Mamm Genome* *8*, 711-713.
- Roscioli, T., Kennedy, D., Cui, J., Fonseca, B., Watson, G. F., Pereira, J., Xie, Y. G., and Mowat, D. (2005). Pallister-Hall syndrome: unreported skeletal features of a GLI3 mutation. *Am J Med Genet A* *136*, 390-394.
- Rubio-Aliaga, I., Soewarto, D., Wagner, S., Klasten, M., Fuchs, H., Kalaydjiev, S., Busch, D. H., Klempt, M., Rathkolb, B., Wolf, E., *et al.* (2007). A genetic screen for modifiers of the delta1-dependent notch signaling function in the mouse. *Genetics* *175*, 1451-1463.
- Russell, W. L. (1951). X-ray-induced mutations in mice. *Cold Spring Harb Symp Quant Biol* *16*, 327-336.

- Russell, W. L., Carpenter, D. A., and Hitotsumachi, S. (1988). Effect of X-ray and ethylnitrosourea exposures separated by 24 h on specific-locus mutation frequency in mouse stem-cell spermatogonia. *Mutat Res* 198, 303-307.
- Russell, W. L., Hunsicker, P. R., Raymer, G. D., Steele, M. H., Stelzner, K. F., and Thompson, H. M. (1982). Dose-response curve for ethylnitrosourea-induced specific-locus mutations in mouse spermatogonia. *Proc Natl Acad Sci U S A* 79, 3589-3591.
- Russell, W. L., Kelly, E. M., Hunsicker, P. R., Bangham, J. W., Maddux, S. C., and Phipps, E. L. (1979). Specific-locus test shows ethylnitrosourea to be the most potent mutagen in the mouse. *Proc Natl Acad Sci U S A* 76, 5818-5819.
- Seiler, F., Kamino, K., Emura, M., Mohr, U., and Thomale, J. (1997). Formation and persistence of the miscoding DNA alkylation product O6-ethylguanine in male germ cells of the hamster. *Mutat Res* 385, 205-211.
- Sekine, K., Ohuchi, H., Fujiwara, M., Yamasaki, M., Yoshizawa, T., Sato, T., Yagishita, N., Matsui, D., Koga, Y., Itoh, N., and Kato, S. (1999). Fgf10 is essential for limb and lung formation. *Nat Genet* 21, 138-141.
- Shedlovsky, A., Guenet, J. L., Johnson, L. L., and Dove, W. F. (1986). Induction of recessive lethal mutations in the T/t-H-2 region of the mouse genome by a point mutagen. *Genet Res* 47, 135-142.
- Shedlovsky, A., King, T. R., and Dove, W. F. (1988). Saturation germ line mutagenesis of the murine t region including a lethal allele at the quaking locus. *Proc Natl Acad Sci U S A* 85, 180-184.
- Shedlovsky, A., McDonald, J. D., Symula, D., and Dove, W. F. (1993). Mouse models of human phenylketonuria. *Genetics* 134, 1205-1210.
- Shibuya, T., and Morimoto, K. (1993). A review of the genotoxicity of 1-ethyl-1-nitrosourea. *Mutat Res* 297, 3-38.
- Sidman, R. L., Dickie, M. M., and Appel, S. H. (1964). Mutant Mice (Quaking and Jimpy) with Deficient Myelination in the Central Nervous System. *Science* 144, 309-311.
- Silver, L. M. (1995). *Mouse genetics, Concepts and Applications*.
- Singh, M. K., Petry, M., Haenig, B., Lescher, B., Leitges, M., and Kispert, A. (2005). The T-box transcription factor Tbx15 is required for skeletal development. *Mech Dev* 122, 131-144.
- Sitterlin, D., Tiollais, P., and Transy, C. (1997). The RAR alpha-PLZF chimera associated with Acute Promyelocytic Leukemia has retained a sequence-specific DNA-binding domain. *Oncogene* 14, 1067-1074.
- Soewarto, D., Blanquet, V., and Hrabe de Angelis, M. (2003). Random ENU mutagenesis. *Methods Mol Biol* 209, 249-266.
- Sordino, P., van der Hoeven, F., and Duboule, D. (1995). Hox gene expression in teleost fins and the origin of vertebrate digits. *Nature* 375, 678-681.
- Specia, D. J., Rabbee, N., Chihara, D., Speed, T. P., and Peterson, A. S. (2006). A genetic screen for behavioral mutations that perturb dopaminergic homeostasis in mice. *Genes Brain Behav* 5, 19-28.
- Strivens, M. A., Selley, R. L., Greenaway, S. J., Hewitt, M., Liu, X., Battershill, K., McCormack, S. L., Pickford, K. A., Vizer, L., Nolan, P. M., *et al.* (2000). Informatics for mutagenesis: the design of mutabase—a distributed data recording system for animal husbandry, mutagenesis, and phenotypic analysis. *Mamm Genome* 11, 577-583.
- Sun, X., Mariani, F. V., and Martin, G. R. (2002). Functions of FGF signalling from the apical ectodermal ridge in limb development. *Nature* 418, 501-508.
- Suzuki, T., Takeuchi, J., Koshiba-Takeuchi, K., and Ogura, T. (2004). Tbx Genes Specify Posterior Digit Identity through Shh and BMP Signaling. *Dev Cell* 6, 43-53.

- Takeuchi, J. K., Koshiba-Takeuchi, K., Suzuki, T., Kamimura, M., Ogura, K., and Ogura, T. (2003). Tbx5 and Tbx4 trigger limb initiation through activation of the Wnt/Fgf signaling cascade. *Development* *130*, 2729-2739.
- te Welscher, P., Fernandez-Teran, M., Ros, M. A., and Zeller, R. (2002). Mutual genetic antagonism involving GLI3 and dHAND prepatterns the vertebrate limb bud mesenchyme prior to SHH signaling. *Genes Dev* *16*, 421-426.
- Temtamy, S. A., and McKusick, V. A. (1978). The genetics of hand malformations. *Birth Defects Orig Artic Ser* *14*, i-xviii, 1-619.
- Thaung, C., West, K., Clark, B. J., McKie, L., Morgan, J. E., Arnold, K., Nolan, P. M., Peters, J., Hunter, A. J., Brown, S. D., *et al.* (2002). Novel ENU-induced eye mutations in the mouse: models for human eye disease. *Hum Mol Genet* *11*, 755-767.
- Thomas, K. R., and Capecchi, M. R. (1987). Site-directed mutagenesis by gene targeting in mouse embryo-derived stem cells. *Cell* *51*, 503-512.
- Tickle, C., and Munsterberg, A. (2001). Vertebrate limb development--the early stages in chick and mouse. *Curr Opin Genet Dev* *11*, 476-481.
- van der Hoeven, F., Sordino, P., Fraudeau, N., Izpisua-Belmonte, J. C., and Duboule, D. (1996). Teleost HoxD and HoxA genes: comparison with tetrapods and functional evolution of the HOXD complex. *Mech Dev* *54*, 9-21.
- Van Raamsdonk, C. D., Fitch, K. R., Fuchs, H., de Angelis, M. H., and Barsh, G. S. (2004). Effects of G-protein mutations on skin color. *Nat Genet* *36*, 961-968.
- Venter, J. C., Adams, M. D., Myers, E. W., Li, P. W., Mural, R. J., Sutton, G. G., Smith, H. O., Yandell, M., Evans, C. A., Holt, R. A., *et al.* (2001). The sequence of the human genome. *Science* *291*, 1304-1351.
- Vivian, J. L., Chen, Y., Yee, D., Schneider, E., and Magnuson, T. (2002). An allelic series of mutations in Smad2 and Smad4 identified in a genotype-based screen of N-ethyl-N-nitrosourea-mutagenized mouse embryonic stem cells. *Proc Natl Acad Sci U S A* *99*, 15542-15547.
- Vollrath, D., Jaramillo-Babb, V. L., Clough, M. V., McIntosh, I., Scott, K. M., Lichter, P. R., and Richards, J. E. (1998). Loss-of-function mutations in the LIM-homeodomain gene, LMX1B, in nail-patella syndrome. *Hum Mol Genet* *7*, 1091-1098.
- Vortkamp, A., Gessler, M., and Grzeschik, K. H. (1991). GLI3 zinc-finger gene interrupted by translocations in Greig syndrome families. *Nature* *352*, 539-540.
- Vreugde, S., Erven, A., Kros, C. J., Marcotti, W., Fuchs, H., Kurima, K., Wilcox, E. R., Friedman, T. B., Griffith, A. J., Balling, R., *et al.* (2002). Beethoven, a mouse model for dominant, progressive hearing loss DFNA36. *Nat Genet* *30*, 257-258.
- Wang, C., Pan, Y., and Wang, B. (2007). A hypermorphic mouse Gli3 allele results in a polydactylous limb phenotype. *Dev Dyn* *236*, 769-776.
- Weber, J. S., Salinger, A., and Justice, M. J. (2000). Optimal N-ethyl-N-nitrosourea (ENU) doses for inbred mouse strains. *Genesis* *26*, 230-233.
- Weinstein, B. M., Schier, A. F., Abdelilah, S., Malicki, J., Solnica-Krezel, L., Stemple, D. L., Stainier, D. Y., Zwartkruis, F., Driever, W., and Fishman, M. C. (1996). Hematopoietic mutations in the zebrafish. *Development* *123*, 303-309.
- Wieschaus, E., Nusslein-Volhard, C., and Kluding, H. (1984). Kruppel, a gene whose activity is required early in the zygotic genome for normal embryonic segmentation. *Dev Biol* *104*, 172-186.
- Wild, A., Kalff-Suske, M., Vortkamp, A., Bornholdt, D., Konig, R., and Grzeschik, K. H. (1997). Point mutations in human GLI3 cause Greig syndrome. *Hum Mol Genet* *6*, 1979-1984.

- Wilkinson, D. G., Bhatt, S., and Herrmann, B. G. (1990). Expression pattern of the mouse T gene and its role in mesoderm formation. *Nature* 343, 657-659.
- Winter, R. M., and Tickle, C. (1993). Syndactylies and polydactylies: embryological overview and suggested classification. *Eur J Hum Genet* 1, 96-104.
- Wrobel, K. H., Bickel, D., and Kujat, R. (1996). Immunohistochemical study of seminiferous epithelium in adult bovine testis using monoclonal antibodies against Ki-67 protein and proliferating cell nuclear antigen (PCNA). *Cell Tissue Res* 283, 191-201.
- Xu, X., Weinstein, M., Li, C., and Deng, C. (1999). Fibroblast growth factor receptors (FGFRs) and their roles in limb development. *Cell Tissue Res* 296, 33-43.
- Xu, X., Weinstein, M., Li, C., Naski, M., Cohen, R. I., Ornitz, D. M., Leder, P., and Deng, C. (1998). Fibroblast growth factor receptor 2 (FGFR2)-mediated reciprocal regulation loop between FGF8 and FGF10 is essential for limb induction. *Development* 125, 753-765.
- Zakany, J., and Duboule, D. (1996). Synpolydactyly in mice with a targeted deficiency in the HoxD complex. *Nature* 384, 69-71.
- Zakany, J., and Duboule, D. (1999). Hox genes in digit development and evolution. *Cell Tissue Res* 296, 19-25.
- Zakany, J., Fromental-Ramain, C., Warot, X., and Duboule, D. (1997). Regulation of number and size of digits by posterior Hox genes: a dose-dependent mechanism with potential evolutionary implications. *Proc Natl Acad Sci U S A* 94, 13695-13700.
- Zakany, J., Kmita, M., and Duboule, D. (2004). A dual role for Hox genes in limb anterior-posterior asymmetry. *Science* 304, 1669-1672.
- Zambrowicz, B. P., Friedrich, G. A., Buxton, E. C., Lilleberg, S. L., Person, C., and Sands, A. T. (1998). Disruption and sequence identification of 2,000 genes in mouse embryonic stem cells. *Nature* 392, 608-611.
- Zarbališ, K., May, S. R., Shen, Y., Ekker, M., Rubenstein, J. L., and Peterson, A. S. (2004). A focused and efficient genetic screening strategy in the mouse: identification of mutations that disrupt cortical development. *PLoS Biol* 2, E219.
- Zuniga, A., and Zeller, R. (1999). Gli3 (Xt) and formin (ld) participate in the positioning of the polarising region and control of posterior limb-bud identity. *Development* 126, 13-21.

8 Appendix Published Literature

The outcome of the first part of this PhD work resulted in the following publications:

Graw, J., Jung, M., Loster, J., Klopp, N., Soewarto, D., Fella, C., Fuchs, H., Reis, A., Wolf, E., Balling, R., and Hrabe de Angelis, M. (1999). Mutation in the betaA3/A1-crystallin encoding gene *Cryba1* causes a dominant cataract in the mouse. *Genomics* 62, 67-73.

Flaswinkel, H., Alessandrini, F., Rathkolb, B., Decker, T., Kremmer, E., Servatius, A., Jakob, T., Soewarto, D., Marschall, S., Fella, C., et al. (2000). Identification of immunological relevant phenotypes in ENU mutagenized mice. *Mamm Genome* 11, 526-527.

Hrabe de Angelis, M. H., Flaswinkel, H., Fuchs, H., Rathkolb, B., Soewarto, D., Marschall, S., Heffner, S., Pargent, W., Wuensch, K., Jung, M., et al. (2000). Genome-wide, large-scale production of mutant mice by ENU mutagenesis. *Nat Genet* 25, 444-447.

Justice, M. J., Carpenter, D. A., Favor, J., Neuhauser-Klaus, A., Hrabe de Angelis, M., Soewarto, D., Moser, A., Cordes, S., Miller, D., Chapman, V., et al. (2000). Effects of ENU dosage on mouse strains. *Mamm Genome* 11, 484-488.

Pargent, W., Heffner, S., Schable, K. F., Soewarto, D., Fuchs, H., and Hrabe de Angelis, M. (2000). MouseNet database: digital management of a large-scale mutagenesis project. *Mamm Genome* 11, 590-593.

Rathkolb, B., Decker, T., Fuchs, E., Soewarto, D., Fella, C., Heffner, S., Pargent, W., Wanke, R., Balling, R., Hrabe de Angelis, M., et al. (2000). The clinical-chemical screen in the Munich ENU Mouse Mutagenesis Project: screening for clinically relevant phenotypes. *Mamm Genome* 11, 543-546.

Schindewolf, C., Lobenwein, K., Trinczek, K., Gomolka, M., Soewarto, D., Fella, C., Pargent, W., Singh, N., Jung, T., and Hrabe de Angelis, M. (2000). Comet assay as a tool to screen for mouse models with inherited radiation sensitivity. *Mamm Genome* 11, 552-554.

Soewarto, D., Fella, C., Teubner, A., Rathkolb, B., Pargent, W., Heffner, S., Marschall, S., Wolf, E., Balling, R., and Hrabe de Angelis, M. (2000). The large-scale Munich ENU-mouse-mutagenesis screen. *Mamm Genome* 11, 507-510.

Graw, J., Klopp, N., Loster, J., Soewarto, D., Fuchs, H., Becker-Follmann, J., Reis, A., Wolf, E., Balling, R., and Hrabe de Angelis, M. (2001). Ethylnitrosourea-induced mutation in mice leads to the expression of a novel protein in the eye and to dominant cataracts. *Genetics* 157, 1313-1320.

Graw, J., Loster, J., Soewarto, D., Fuchs, H., Meyer, B., Reis, A., Wolf, E., Balling, R., and de Angelis, M. H. (2001). Characterization of a new, dominant V124E mutation in the mouse alphaA-crystallin-encoding gene. *Invest Ophthalmol Vis Sci* 42, 2909-2915.

Graw, J., Loster, J., Soewarto, D., Fuchs, H., Meyer, B., Reis, A., Wolf, E., Balling, R., and Hrabe de Angelis, M. (2001). Characterization of a mutation in the lens-specific MP70 encoding gene of the mouse leading to a dominant cataract. *Exp Eye Res* 73, 867-876.

Graw, J., Loster, J., Soewarto, D., Fuchs, H., Reis, A., Wolf, E., Balling, R., and Hrabe de Angelis, M. (2001). *Aey2*, a new mutation in the betaB2-crystallin-encoding gene of the mouse. *Invest Ophthalmol Vis Sci* 42, 1574-1580.

Graw, J., Loster, J., Soewarto, D., Fuchs, H., Reis, A., Wolf, E., Balling, R., and Hrabe de Angelis, M. (2002). V76D mutation in a conserved gD-crystallin region leads to dominant cataracts in mice. *Mamm Genome* 13, 452-455.

Soewarto, D., Blanquet, V., and Hrabe de Angelis, M. (2003). Random ENU mutagenesis. *Methods Mol Biol* 209, 249-266.

Dalke, C., Loster, J., Fuchs, H., Gailus-Durner, V., Soewarto, D., Favor, J., Neuhauser-Klaus, A., Pretsch, W., Gekeler, F., Shinoda, K., et al. (2004). Electroretinography as a screening method for mutations causing retinal dysfunction in mice. *Invest Ophthalmol Vis Sci* 45, 601-609.

- Graw, J., Loster, J., Puk, O., Munster, D., Haubst, N., Soewarto, D., Fuchs, H., Meyer, B., Nurnberg, P., Pretsch, W., et al. (2005). Three novel Pax6 alleles in the mouse leading to the same small-eye phenotype caused by different consequences at target promoters. *Invest Ophthalmol Vis Sci* 46, 4671-4683.
- Jakob, T., Kollisch, G. V., Howaldt, M., Bewersdorff, M., Rathkolb, B., Muller, M. L., Sandholzer, N., Nitschke, L., Schiemann, M., Mempel, M., et al. (2007). Novel mouse mutants with primary cellular immunodeficiencies generated by genome-wide mutagenesis. *J Allergy Clin Immunol*.
- Rubio-Aliaga, I., Soewarto, D., Wagner, S., Klawns, M., Fuchs, H., Kalaydjiev, S., Busch, D. H., Klempt, M., Rathkolb, B., Wolf, E., et al. (2007). A genetic screen for modifiers of the delta1-dependent notch signaling function in the mouse. *Genetics* 175, 1451-1463.
- Abe, K., Wechs, S., Kalaydjiev, S., Franz, T. J., Busch, D. H., Fuchs, H., Soewarto, D., Behrendt, H., Wagner, S., Jakob, T., and Hrabe de Angelis, M. (2008). Novel lymphocyte-independent mechanisms to initiate inflammatory arthritis via bone marrow-derived cells of Ali18 mutant mice. *Rheumatology (Oxford)* 47, 292-300.
- Pawlak, C. R., Sanchis-Segura, C., Soewarto, D., Wagner, S., Hrabe de Angelis, M., and Spanagel, R. (2008). A phenotype-driven ENU mutagenesis screen for the identification of dominant mutations involved in alcohol consumption. *Mamm Genome* 19, 77-84.

Persönliche Daten/ Personal Data

Name	Dian Agustina Anna Michel, geb. Soewarto
Adresse	Borstellstr. 16, 12167 Berlin
Telefon	030 398 341 90 oder 0179 949 37 39 (Mobil)
Email	dian.michel@charite.de
Geboren	17. August 1968
Geburtsort	Peking, VR China
Staatsangehörigkeit	Deutsch
Familienstand	verheiratet

Ausbildung / Education

2005-2009	Promotion an der Technischen Universität München, Lehrstuhl für Experimentelle Genetik; Thema: Implementation and optimization of a large-scale ENU mouse mutagenesis screen and characterisation of five ENU-induced limb mutant lines.
1994-1996	Studium an der Technischen Fakultät der Universität Bielefeld, Fachrichtung: Naturwissenschaftliche Informatik
1987-1994	Studium an der Fakultät Biologie der Universität Bielefeld, Fachrichtung: Zellbiologie, Zytogenetik Diplomarbeit am Lehrstuhl für Mikrobiologie und Gentechnologie, AG Eichenlaub-Ritter „Untersuchungen zur Zellzyklussteuerung und Chromosomenverteilung in Oozyten der Maus“, Gesamturteil: sehr gut
1987	Abitur am Gymnasium Brackwede, Bielefeld

Beruflicher Werdegang / Career

Jul 2008 -	Wissenschaftliche Koordinatorin des Molekularen Krebsforschungszentrums der Charité – Universitätsmedizin Berlin
Feb 2006 – Jun 2008	Koordinatorin des Marie Curie Early Stage Research Training Programms CARDIOVASC, Charité – Universitätsmedizin Berlin, Center for Cardiovascular Research (CCR)
März 2000 – Jan 2006	Wissenschaftliche Angestellte GSF Neuherberg, Institut für Experimentelle Genetik, (Direktor: Prof. M. Hrabé de Angelis) Teilprojektleitung im ENU-Maus-Mutageneseprojekt NGFN, Plattform 5 und DHGP Leitung der Core Facility GSF
Nov 1996 – Feb 2000	Wissenschaftliche Angestellte bei der Gesellschaft für Umwelt und Gesundheit (GSF) Neuherberg, Institut für Säugetiergenetik (Direktor: Prof. R. Balling)
Sep 1994 - Okt 1996	Kaufmännische Sachbearbeiterin Bertelsmann Distribution, Gütersloh-Verl